Ministry of Higher Education and Scientific Research

Kasdi Merbah University – Ouargla

Faculty of Applied Sciences   جامعة قاصدي مرباح ـ ورقلة

Preparation and characterization of activated carbon from date palm fibers: application as adsorbents and super capacity

Author: **Supervisor:**

Djehad BENTARFA   **Pr M^ed Lamine SEKIRIFA**

A thesis submitted in the fulfilment of the requirements for the degree of Doctor of philosophy in the:

Biogeochemistry Laboratory of Desert Environments

Department of Chemical Engineering

Option : Processus and industrial systems

Mr : KORICHI	*Mourad*	*Pr*	*President*	*UKMO*
Mr : SEKIRIFA	*Mohamed Lamine*	*Pr*	*Supervisor*	*UKMO*
Mr : ZERROUKI	*Djamal*	*Pr*	*Examine*	*UKMO*
Mr :SELLAMI	*Mohamed Hassen*	*Pr*	*Examine*	*UKMO*
Mr : BENOUNIS	*Messaoud*	*Pr*	*Examine*	*Khenchela university*
Mr : BELKHALFA	*Hakim*	*Senior researcher*	*Examine*	*CRAPC Ouargla*

2021/2022

Gratitude

The time has come to put an end to this work and all these years of research carried out at the "Biochemistry Laboratory of Desert Environments" in Kasdi Merbah University.

I have the honor to say a big thank you to my teacher **Mr. SEKIRIFA Mohamed Lamine** for the trust he has always shown to me and for his perpetual encouragement.

I would like to thank **Mr. KORICHI Mourad** for the honor he has done by agreeing to chair the jury for this thesis. And I present a deep appreciation to **Mr. Mr. ZERROUKI Djamal, Mr. SELLAMI Mohamed Hassen, Mr. BENOUNIS Messaoud, Mr. BELKHALFA Hakim** who agreed to review my work.

I also, would like to express my deepest gratitude to Director **Mr. BELKHALFA Hakim** (Research Center Physico - Chemical Analysis), and all its employees, for providing me with all the possibilities to complete my work.

And I give a big thanks to Professor **Ammar H. Al-Dujaili** and TEMMAR Abderrezzak for proofreading.

Finally, in the last lines, I would like to thank my parents, my husband, my brothers, and sisters, providing advice and encouragement that always give me moral support. Without them, I would not be where I am and what I am. Thank you all.

Djehad Bentarfa

Dedication

إذا كان لبحثي قيمة فإن هناك كثيرين ممَّن شاركوني في ذلك..

طريق البحث العلمي كان شاقًّا وصعبًا..

ولكن هناك من كانوا عونًا من الناحية المعنويَّة

المُكرَّمان والمُحمولان على الأعناق، اللذان قدَّما لي يد العون في مسيرتي دون مُقابل...

إلى أبويَّ الجليلين...

إلى من بــــها أعلو، وعليها أرتكز، إلى القــــلب المعطاء

أُمِّي الحبيبة : تمار خديجة

لن تكفي جُمل الشُّكر، وحتى لو بلغت ملء الأرض والسماء، أن تُعبِّر عن فضل أمي.

أُمِّي الحنون، التي جعلتني أتمسَّك بالأمل وأتجاوز الصعاب بكل ثبات..

حفظكِ الله لنا، وجعلكِ ذخرًا لنا، وقلبًا نابضًا أستلهم منه طاقتي الإيجابية..

إلى من شجعني على المثابرة طوال عمري، إلى الرجل الأبرز في حياتي

أبي المُبجَّل: محمد بن طرفة

لن تستطيع كلماتي أن تصف مدى شعوري بالامتنان لصاحب الصدر الرحب والدي.

صاحب الكلم الطيب، والقلب العطوف...

أطال الله في عُمرك، وسلَّمك من جميع الأسقام..

إلى شريك الحياة، ومن كان خيرَ مُعين..إلى من شاركني السرَّاء والضراء، ولم أره عابسا يومًا، أقرب الناس إلى نفسي.

زوجي المخلص و المُوقَّر : بن طرفة عبد الكريم

إلى من أتشوَّق لأن أرى مستقبله المشرق بإذن الله....... إلي فلذة كبدي ونور حياتي، روحي وقُرَّة عيني ونبض فؤادي.

إبني الغالي: معاذ

إلى من بذلوا جهدًا في مساعدتي وكانوا خيرَ سندٍ، الذين لم يبخلوا عليَّ بالجُهد الوفير..

إخــوتي وأخواتي: إسلام، مريم، إيمان، إكرام، شفاء، العيد، إناس.

أصدقائي وأهلي المُبجَّلون الذين أُكِنُّ لهم كل الاحترام، الذين يُشاركونني الفرح والحزن على الدّوام..

أساتذتي الكرام أصحاب الفكر المُستنير...

إلى كل هؤلاء: أهديكم خلاصة جُهدي العلمي، الذي أسأل الله تعالى أن يتقبله خالصًا....

Djehad Bentarfa

Abstract

Date palm fibers (Ghars) from Ouargla-Algeria were invested in this work to prepare activated carbon by physical activation using CO_2 under different parameters pyrolysis temperature, pyrolysis time, and sample size.

Activated carbon has been characterized using the Physical characterization (Burn-off, Gas adsorption method (N_2 adsorption-desorption), and Scanning Electron Microscope (SEM), X-ray diffraction and fluorescence microanalysis), Chemical characterization (Studies on point of charge, Study of surface functional group, and FT-IR analysis). In Adsorption tests the effect of mass, initial concentration, time, and temperature on the adsorption capacity of Phenol and Methylene Blue on activated carbon were studied, the adsorption model, Langmuir and Freundlich's isotherms were adopted. To study the adsorption kinetics, a pseudo-first-order model, a second-order model, and a thermodynamic adsorption plot were applied. The results can be summarized as follows the largest surface area 313.4 $m^2.g^{-1}$ with pore diameter 1.93 nm had a high amount of adsorption of N_2, while the smallest surface area 166.29 $m^2.g^{-1}$ with pore diameter 2.11 nm. The highest adsorption capacity was recorded of 11.96, 2.82 $mg.g^{-1}$ for adsorption of Phenol and MB. XRD showed activated carbon samples have an amorphous structure more than a crystalline structure, while XRF indicate that The raw fiber and the activated carbon samples consist of the common elements such as calcium (Ca), Iron (Fe), Copper (Cu). The pHzpc and Boehm titration also showed the richness of negative charges and their strongly acidic character respectively of ACs. From FTIR study of both RF's and ACF's was found the common functional groups are: C= C acetone, C-H of (CH_3band) alkane, C-O ether, C-O-C, aromatic C-H.

The supercapacitors for energy storage were prepared using the prepared activated carbon and was successful. while were characterized using the following techniques: Cyclic voltammetry, Charge-discharge galvanostatic, Scanning Electron Microscope (SEM). The Higher specific capacitance was observed at 91.64 $F.g^{-1}$ while the lower specific capacitance was of 29.05 $F.g^{-1}$, and the maximum specific energy and specific power were produced with values of 45.82 $Wh.kg^{-1}$ and 1800 $W.kg^{-1}$, respectively.

Keywords : Adsorption, activated carbon, date palm fiber, electrochemical sensors, physical activation, chemical activation.

Résumé

Fibres de palmier dattier variété (Ghars) de Ouargla-Algeria a été investi dans ce travail pour préparer du charbon actif par activation physique à l'aide de CO_2 sous différents paramètres de température de pyrolyse, de temps de pyrolyse et de taille d'échantillon.

Le charbon actif a été caractérisé en utilisant la Caractérisation Physique (Burn-off, Méthode d'adsorption de gaz (N_2 adsorption-désorption) et Microscope Electronique à Balayage (MEB), et Diffraction et fluorescence des rayons X), Caractérisation Chimique (Etudes sur le point de charge, Etude du groupe fonctionnel de surface, et FT-IR Analyse). Dans les tests d'adsorption, l'effet de la masse, de la concentration initiale, du temps et de la température sur la capacité d'adsorption du Phénol et du Bleu de méthylène sur charbon actif a été étudié. Les modèle d'adsorption, les isothermes de Langmuir et Freundlich ont été adoptés. Pour étudier la cinétique d'adsorption, un modèle de pseudo-premier ordre, un modèle de second ordre et un graphique d'adsorption thermodynamique ont été appliqués.

Les résultats peuvent être résumés comme suit, la plus grande surface spécifique 313,4 $m^2.g^{-1}$ avec un diamètre de pores de 1,93 nm avait une quantité élevée d'adsorption de N_2, tandis que la plus petite surface spécifique 166,29 $m^2.g^{-1}$ avec un diamètre de pores de 2,11 nm. La capacité d'adsorption la plus élevée a été enregistrée de 11,96, 2,82 $mg.g^{-1}$ pour l'adsorption du Phénol et du MB respectivement. XRD a montré que les échantillons de charbon actif ont une structure amorphe plus qu'une structure cristalline, tandis que XRF indique que la fibre brute et les échantillons de charbon actif sont constitués d'éléments communs tels que le calcium (Ca), le fer (Fe), le cuivre (Cu). Le pH_{zpc} et Boehm titrage ont également montré la richesse en charges négatives et un fort caractère acide respectivement des ACs. D'après l'étude FT-IR des RF et des ACF, les groupes fonctionnels communs sont les suivants : C = C acétone, C-H de (CH3band) alcane, C-O éther, C-O-C, C-H aromatique.

Les supercondensateurs pour le stockage d'énergie ont été préparés à l'aide du charbon actif préparé et ont été couronnés de succès. Tandis qu'ont été caractérisés à l'aide des techniques suivantes : voltamétrie cyclique, charge-décharge galvanostatique, microscope électronique à balayage (MEB). La capacité spécifique supérieure a été notée de 91,64 $F.g^{-1}$ tandis que la CS inférieure était de 29,05 $F.g^{-1}$, et l'énergie

spécifique maximale et la puissance spécifique ont été produites avec des valeurs de 45,82 Wh.kg^{-1} et 1800 W.kg^{-1}, respectivement .

Mots-clés : Adsorption, charbon actif, fibre de palmiers dattiers, capteurs électrochimique, activation physique, activation chimique.

الملخص

تم استثمار ألياف نخيل التمر (غرس) من ورقلة-الجزائر في هذا العمل لتحضير الكربون المنشط عن طريق التنشيط الفيزيائي باستخدام ثاني أكسيد الكربون في معايير مختلفة لدرجة حرارة الانحلال الحراري ، وزمن الانحلال الحراري ، وحجم العينة.

تم توصيف الكربون المنشط باستخدام التوصيف الفيزيائي (الإحتراق ، طريقة إمتزاز الغازات (إمتزاز النيتروجين) ، المجهر الإلكتروني الماسح، و حيود الأشعة السينية و وميض الأشعة السينية) ، التوصيف الكيميائي (تحديد الرقم الهيدروجيني عند نقطة الصفر ، دراسة المجموعة الوظيفية السطحية ، و تحليل بالأشعة الفوق الحمراء)، في إختبارات الإمتزاز تمت دراسة تأثير الكتلة والتركيز الأولي والوقت ودرجة الحرارة على قدرة إدمصاص الفينول والميثيلين الأزرق على الكربون المنشط، وتم إعتماد نموذج الإمتزاز ، متساوي الحرارة لانجموير وفرندليش. لدراسة حركية الإمتزاز ، تم تطبيق نموذج زائف من الدرجة الأولى ، ونموذج زائف من الدرجة الثانية ، ومخطط إمتزاز ديناميكية الحراري.

يمكن تلخيص النتائج على النحو التالي: أكبر مساحة سطحية 313.4 متر مربع لكل غرام بقطر مسامي 1.93 نانومتر كان بها كمية عالية من إدمصاص النيتروجين، بينما أصغر مساحة سطحية 166.29 متر مربع لكل غرام بقطر مسامي 2.11 نانومتر. تم تسجيل أعلى قدرة على الامتصاص من 11.96 ، 2.82 ملي غرام لكل غرام من الممتز لإدمصاص الفينول والميثيلين الأزرق. أظهر حيود الأشعة السينية أن عينات الكربون المنشط لها بنية غير متبلورة أكثر من هيكل بلوري ، بينما يشير وميض الأشعة السينية إلى أن الألياف الخام وعينات الكربون المنشط تتكون من عناصر مشتركة مثل الكالسيوم والحديد والنحاس. أظهرت نتائج تحديد الرقم الهيدروجيني عند نقطة الصفر و معايرة بوهام أيضًا ثراء الشحنات السالبة وخاصية حمضية قوية لعينات الفحم المنشط على التوالي. من دراسة الأشعة الفوق الحمراء لكل من الليف الخام و عينات الكربون المنشط تم العثور على المجموعات الوظيفية المشتركة التالية : أسيتون C = C، C-H من (CH3band) ألكان ، C-O إيثر ، C-O-C، عطري C-H .

تم تحضير المكثفات الفائقة لتخزين الطاقة باستخدام الكربون المنشط المحضر وكانت ناجحة. بينما تم توصيفها باستخدام التقنيات التالية: قياس الفولتميتر الدوري ، الجلفانوستاتيك لتفريغ الشحنات، المسح المجهري الإلكتروني. لوحظ أن القدرة النوعية الأعلى كانت 91.64 فرادي لكل غرام بينما كانت القدرة النوعية الأدنى 29.05 فرادي لكل غرام، وتم إنتاج الطاقة النوعية القصوى والقوة النوعية بقيم 45.82 واط ساعي لكل كيلو غرام و 1800 واط لكل كيلو غرام، على التوالي.

الكلمات المفتاحية: الإمتزاز ، الكربون المنشط ، ألياف النخيل ، مستشعرات الكهروكيميائية ، التنشيط الفيزيائي ، التنشيط الكيميائي.

Contents

Contents

Contents

List of images

List of figures

List of tables

List of symbols and abbreviations

Symboles	Means	Unit
AC	Alternating Current	A
ACF	Activated Carbon Fiber	-
ACFH	Activated Carbon Fiber after acidicfication	-
ACs	Activated Carbons	-
BET	Brunauer–Emmett–Teller	-
BJH	Barrett, Joyner, and Halenda	-
C	Concentration	$mg.l^{-1}$
CAP	Activated Carbon Powder	-
C_e	Concentration at equilibrium	$mg.l^{-1}$
CI	The crystallinity index	%
C_o	Concentration at initial	$mg.l^{-1}$
C_s	The specific capacity	
C_t	Concentration at time t.	$mg.l^{-1}$
CV	The cyclic voltammetry	-
d	The interreticular distance between the diffracting planes	m
DC	Direct current	A
D_p	Pore diameter	nm
D-R	Dubinin–Radushkevick	-
E_0	Activation energy	$kj.mol^{-1}$
E_D	The energy density	$Wh.kg^{-1}$
EDLC	Electric double layer capacitor	-
FT-IR	Fourier Transform Infrared	-
GAC	Grain Activated Carbon	-
GCD	Galvanostatic charge/discharge	-
H_J	Differential heat	cal
H_L	Latent heat of evaporation	cal
I	Current	A
IUPAC	International Union of Pure and Applied Chemistry	-
K_1	The pseudo first-order rate constant	$l.min^{-1}$
K_2	The second order model rate constant	$g.mg^{-1}.min^{-1}$
K_D	The equilibrium constant	$l.g^{-1}$
k_f	The Freundlich constant	$[(mg.g^{-1})\,(l.mg^{-1})^{1/n}]$
K_{id}	The intra-particle diffusion rate constant	$mg.g^{-1}.h^{-1/2}$
k_l	The Langmuir equilibrium constant	$l.mg^{-1}$
L	The size of the micropores	nm
m	The mass	g
M	The molecular mass	$g.mol^{-1}$
m_f	The Final Mass	g
m_i	The Initial Mass	g
MWCNT	Multi-walled carbon nanotubes	-
n	The Freundlich constant	-
N_{CSF}	The amount of functional groups on carbon surface	$meq.mg^{-1}$
N_{eq}	The number equivalent reacted	meq
P	Relative pressure	atm
P_D	The power density	$W.kg^{-1}$
pH	Potential of Hydrogen	-
pH_f	pH final	-
pH_i	pH initial	-
pH_{PZC}	pH at point of zero charges	-
P_m	The equilibrium pressure	atm
P_o	The saturated vapor pressure	atm
q_e	The amounts of the adsorbent adsorbed at equilibrium	$mg.g^{-1}$
Q_{gaz}	The adsorbed quantity of gaz	$mg.g^{-1}$
q_{max}	The maximum adsorption capacity	$mg.g^{-1}$

Q_{max}	The maximum adsorbed quantity	$mg.g^{-1}$
q_t	The amounts of the adsorbent adsorbed at time t	$mg.g^{-1}$
R	Gas Constant	$J.mol^{-1}.K^{-1}$
R%	The ratio of removal of phenol	-
R^2	The value of correlation coefficients	-
RF	Raw fiber	-
R_L	indicative of the isotherm shape	-
RS	Series Resistance	-
S_{BET}	The BET specific surface areas	$m^2.g^{-1}$
SE1	Secondary electron detector	-
SEM	Scanning electron microscope	-
S_{ext}	External surface	$m^2.g^{-1}$
S_{micro}	The microporous surface	$m^2.g^{-1}$
t	Time	s
T	Temperature	°C (K)
t_d	The discharge time	s
UV-Vis	Ultraviolet-visible	-
V	volume	l
V_{acidic}	The volume of acidic function group	$meq.g^{-1}$
V_{ads}	The volume quantities of adsorbed gas	l
V_{basic}	The volume of basic function group	$meq.g^{-1}$
$V_{carboxylic}$	The volume of carboxylic function group	$meq.g^{-1}$
$V_{lactone}$	The volume of lactone function group	$meq.g^{-1}$
V_m	The volume mono molecular layer	$cm^3.g^{-1}$
V_{mes}	The mesopore volume	$cm^3.g^{-1}$
V_{mic}	The micropore volume	$cm^3.g^{-1}$
$V_{phenolic}$	The volume of phenolic function group	$meq.g^{-1}$
V_{tot}	Total volume	$cm^3.g^{-1}$
W_0	The micropore volume	$cm^3.g^{-1}$
XRD	X-ray Diffraction	-
XRF	X-ray fluorescence	-
Z	number equivalent	eq
β	constant	$mol^2.kJ^{-2}$
ΔG°	standard free energy	$kJ.mol^{-1}$
ΔH°	standard enthalpy	$kJ.mol^{-1}$
ΔS°	standard entropy	$kJ.mol^{-1}$
ε	The potential energy	-
θ	The angle between the incident beam and the diffracting planes	°
λ	The wavelength of the incident beam	A°
$λ_{max}$	The wavelength	nm
ρ	The density of the pure liquid	$g.cm^{-3}$
$σ_0$	The surface occupied by a molecule	m^2

General Introduction

GENERAL INTRODUCTION, OBJECTIVES, AND THESIS OUTLINE.

In this chapter, a brief introduction is explained about the world's needs for energy on the one hand, and the protection of the environment on the other hand, the reasons for choosing date palm fibers for preparing activated carbon as a solution.

The main objective and specific objectives are listed, and finally, the thesis outline is presented.

General Introduction

Energy is the basis of well-being, prosperity, economy, and the condition of development in societies. Population growth, industrial development, and economic growth are increasing the demand for energy. The increasing demand leads to environmental challenges such as global warming and climate change, the health effects of air pollution, and the risk of soil and water pollution (Dehghani-Sanij, Tharumalingam, Dusseault, & Fraser, 2019). So meeting energy needs and protecting the environment should be parallel.

Therefore, Urbanization is a crucial pollution source, particularly in developing countries and particularly for groundwater, as a result of under-managed solid waste disposal and poorly managed sanitation infrastructure (Rim Baccar Ep Yangui, Montserrat Sarrà Adroguer, Paqui Blánquez Cano, & Bouzid., 2014).

Individuals, large industries ... everyone contributes in their somehow to environmental pollution, This phenomenon results from the rejection of waste and emission of polluting gas, toxic substances, because of industrial pollution, urban pollution, or agricultural pollution leading to strong negative effects on biodiversity and freshwater ecosystems, also threatening essential ecosystem services (Djidel, 2011; Rim Baccar Ep Yangui et al., 2014; UNESCO, 2020).

Knowledge of the most causes of environmental pollution proves to be essential today insofar as their impacts will be felt on a worldwide scale. Several techniques are accustomed to remove pollutants from industrial effluents. But the value which is being paid or is paid within the near future is going to be too high. (Crini, Lichtfouse, Wilson, & Morin-Crini, 2018).

Adsorption is one of the foremost used techniques for this elimination. Activated carbon is the most ordinarily used adsorbent, but it remains very expensive and also requires regeneration. The research was directed toward treatment processes using less costly natural materials, specifically plant waste.

Is it possible to store energy and protect the environment at the same time by using activated carbon at a cheap cost without harming the environment?

The research is directed towards treatment processes using less expensive natural materials, specifically from plant waste. The preparation of activated carbon from

vegetable waste is very interesting from an economic point of view because we benefit from simple transformations, from a direct application of these starting materials.

Date palm (Phoenix dactylifera L.) trees collectively of mankind's oldest cultivated plants belong to the family of Palmae (Arecaceae). Recently, the worldwide production of palm fruits is continuously increasing which indicates the importance of the Phoenix dactylifera trees. The quantity of date palms existing within the world is estimated at quite 100 million palm trees. Its spatial distribution highlights that Asia is in the first position with 60 million date palms; while Africa is in the second position with 32.5 million date palms (Al-Oqla & Sapuan, 2014).

Algeria, is one of the largest countries in Africa and in the Arab world, is among the leading countries in the cultivation and production of many types of palms dates. It is the world's fourth-largest date producer with a total of more than 20 million palm trees (710,000 metric tons), The production in Algeria is mainly concentrated in the southeastern part of the country (Biskra, El Oued, and Ouargla), which is responsible for 76 % of national production, While, Ouargla is ranked third (Bouguedoura, Bennaceur, Babahani, & Benziouche, 2015; Boumediri et al., 2019).

Based on botanical descriptions, about 1,000 cultivars of date palms can be found in Algeria and the analysis of their production by category shows that the variety of Ghars palm tree represents up to 10% of the total production in Algeria (Al-Oqla & Sapuan, 2014; Boumediri et al., 2019; Mimouni, Siboukeur, & Bayoussef, 2014).

However, as reported in (Boumediri et al., 2019) the tree of date palm generates a large amount of by-products, such as (a) the leaves: petiole, rachis, leaflets; (b) the trunk; (c) the products obtained from the bunches (fruit bunch branch of palm, date seeds) without proper utilization (as a residue) an amount estimated to more than 800,000 tons of residues are produced per year in Algeria. This huge residue amount isn't taken advantage of because it is often frequently discarded by burning or is considered as animal feed or waste and it has been seldom utilized in handicrafts such as basketry, crates, ropes, and traditional construction.

Fibers of date palm Phoenix dactylifera L, called (Fibrillum) are considered as one of the most available natural fiber types worldwide. which comes from the bark surface called "Fibrillum", This biomass waste is of potential interest to support industrial

sustainability by producing alternative cheap eco-friendly materials (Al-Oqla & Sapuan, 2014; Owaid, Al-Saeedi, & Al-Assaffii, 2014).

The abundant and easy availability of agricultural by-products makes it a good source of raw materials for the production of alternating current. And generally inexpensive and their effective use is desirable, these by-products have attracted the interest of many researchers for two main purposes: environmental protection and economic exploitation. The by-products of the date palm (Phoenix dactylifera L.) (Leaves, trunk, pits, pedicels, etc.), formerly widely used in various uses in the Saharan regions (construction, feeding cattle, etc.), have limited use while they are not often thrown away (Alwared, Al-Hubboubi, & Dawood, 2016).

The efficient utilization of natural sources certainly has a positive impact on our environment. In fact, the development of agro-waste reinforced composites is a prominent solution for the utilization of such waste as renewable sources (Dixit & Yadav, 2019).

Activated Carbons (ACs) are high surface area and porous carbon has been widely used as an adsorbent for separation, purification, decolorization, and deodorization of vegetable oils and fats, water purification and pollution treatment, air, and gas purification, and super condensate production to store energy. ACs can be synthesized by two methods, chemical and physical activation (Al-Swaidan & Ahmad, 2011). The use of fibers surrounding the stem of date palm trees has not been reported in the literature especially the date palm fiber variety (Ghars) from Ouargla - Algeria region.

The main objective of this study is to prepare the best adsorbents at a cheap cost from this resource and exploit them in the above-mentioned important concerns, environmental protection (purification of water, gases, etc.), and the preparation of supercapacitors for energy storage.

We have chosen the most common date variety (Ghars). our objectives are:

- ✓ Study in-depth the transformation of date palm fibers into activated charcoal under an inert atmosphere (pyrolysis),
- ✓ Study the effect of the various operating parameters on the quality of the coals prepared (particle size, duration of pyrolysis, the temperature of pyrolysis, the flow rate of activation gas, etc.),

✓ Characterize the obtained activated carbon, before and after treatment.

✓ Studying the adsorption of phenol and methylene blue (considered to be the most dangerous pollutants) on activated carbon.

✓ Carry out an application: elaboration of electrochemical sensors carbon based material

The manuscript thus has two main parts:

- The first illustrates a bibliographical collection on the subject.

- The second (experimental) part is devoted to the fundamental aspect of this work, namely the characterization of our adsorption precursors and the application mentioned above.

Reference of the Introduction

Al-Oqla, F. M., & Sapuan, S. M. (2014). Natural fiber reinforced polymer composites in industrial applications: feasibility of date palm fibers for sustainable automotive industry. *Journal of Cleaner Production, 66*, 347-354.

Al-Swaidan, H. M., & Ahmad, A. (2011, 2011). *Synthesis and characterization of activated carbon from Saudi Arabian dates tree's fronds wastes*.

Alwared, A. I., Al-Hubboubi, S. K. A., & Dawood, D. S. (2016). Effect of Date Palm Leaf Fiber on Mechanical Properties of Concrete. *Association of Arab Universities Journal of Engineering Sciences, 23*(2), 49-66.

Bouguedoura, N., Bennaceur, M., Babahani, S., & Benziouche, S. E. (2015). Date palm status and perspective in Algeria. In *Date palm genetic resources and utilization* (Vol. 1, pp. 125-168): Springer.

Boumediri, H., Bezazi, A., Del Pino, G. G., Haddad, A., Scarpa, F., & Dufresne, A. (2019). Extraction and characterization of vascular bundle and fiber strand from date palm rachis as potential bio-reinforcement in composite. *Carbohydrate polymers, 222*, 114997. doi:https://doi.org/10.1016/j.carbpol.2019.114997

Crini, G., Lichtfouse, E., Wilson, L. D., & Morin-Crini, N. (2018). Adsorption-oriented processes using conventional and non-conventional adsorbents for wastewater treatment. *Green adsorbents for pollutant removal, 18*, 23-71. doi:https://doi.org/10.1007/978-3-319-92111-2_2

Dixit, S., & Yadav, V. L. (2019). Synthesis of green thermally resistant composite: A review. *Indian Journal of Chemical Technology (IJCT), 26*(6), 494-503.

Djidel, T. (2011). *Etude de la préparation d'un charbon actif a partir des grain d'olives et application sur des rejets industriels.* Université des Sciences et de la Technologie Med-BOUDIAF d'Oran,

Mimouni, Y., Siboukeur, O., & Bayoussef, Z. (2014). Fructose-rich syrup from Ghars cultivar dates (Phoenix dactylifera L.). *Emirates Journal of Food and Agriculture*, 963-969.

Owaid, M. N., Al-Saeedi, S. S., & Al-Assaffii, I. A. A. (2014). Impact palm date fibers (fibrillum) and sawdust extract on mycelial growth rate of four species of Pleurotus. *Tikrit Journal for Agricultural Sciences, 14*, 1-7.

Rim Baccar Ep Yangui, Montserrat Sarrà Adroguer, Paqui Blánquez Cano, & Bouzid., J. (2014). *Removal of water pollutants by adsorption on activated carbon prepared from olive-waste cakes and by biological treatment using ligninolytic fungi.* Universitat Autònoma de Barcelona,

UNESCO. (2020). World: World Water Development Report 2020 - Water and Climate Change.

Chapter I.   Bibliographic Overview

I.   Adsorption

The term "adsorption" was coined for the first time in 1881 by the German physicist Heinrich Kayser (1853–1940). In chemistry, adsorption is a surface phenomenon by which atoms, ions, or molecules (adsorbates) attach themselves to a solid surface (adsorbent) from a gas, liquid, or solid solution phase selectively, this process creates a film of the adsorbate on the surface of the adsorbent. In the case of an adsorbed atom, we speak of adatom, The sites where the adsorbate molecules attach are called active sites, This phenomenon should not be confused with absorption in which a fluid or the component of a solid solution is absorbed into the volume of another liquid or solid phase (Djidel, 2011; Rouquerol, Rouquerol, & Sing, 1999).

Adsorption could be a physicochemical phenomenon, this process is therefore based on the interaction of the adsorbate with a surface, which can involve various more or less intense processes such as Van der Waals interactions, dipolar interactions, or covalent or ionic chemical bonds. The reverse phenomenon, whereby molecules adsorbed on a surface detach from it, especially under the action of an increase in temperature, or a decrease in pressure, is called desorption (Crini et al., 2018; Djidel, 2011; Dubinin, 1947).

Adsorption is present in many natural, physical, biological and chemical systems (processes) and is widely used in industrial applications such as heterogeneous catalysts, activated charcoal, the capture of pollutants, gas separation, catalysis, and/or potentially detoxification process on an industrial scale, is utilized to purify, detoxify, decolorize, freshen up, separate, and concentrate to permit removal and to recover the harmful products from liquid solutions and gas mixtures, etc. It is also the basis of many methods of characterization of solids such as the measurement of specific surfaces or the study of porosity. In industrial mechanics, it plays a fundamental role in lubrication and brazing processes.(Boehm, 1966; Crini et al., 2018).

I.1. Different types of adsorption

Depending on the nature of the interactions which bind the adsorbate to the surface of the adsorbent, it is a consequence of surface energy, the adsorption can be generally classified into two families: physisorption (characteristic of weak van der Waals forces

or electrostatic attraction) or chemisorption (characteristic of covalent bonding) (Djidel, 2011; Rouquerol et al., 1999).

Physical adsorption (or physisorption) involves weak interactions such as Van Der Waals attraction forces and forces due to electrostatic polarization interactions. The strength of the bonds created can be estimated by the adsorption energy which is between 5 and 50 kJ.mol-1 which is considered to be weak. These interactions are not very specific and reversible and desorption can be total, is usually exothermic, and generally occurs as a multilayer. Physical adsorption is rapid and generally limited by diffusion phenomena, Physisorption systems generally attain equilibrium fairly rapidly, but equilibration is additionally slow if the transport process is that the rate-determining (Djidel, 2011; Rouquerol et al., 1999; Sekirifa, 2013).

✓ Van der Waals-type interaction forces:

They originate from the attractions appearing between the instantaneous and induced dipoles when the molecules located on the solid adsorption sites come together. These forces are always present and can be dispersive (London), or repulsive (Pauli) (Soubeyrand, 2012).

✓ The electrostatic interaction forces:

These forces result from the possible polarization of the adsorbent material via dipolar or quadrupolar interactions with the adsorbable. These polar interactions are significant for adsorbents with an ionic structure. The interaction between the adsorbent and the adsorbed molecule will depend on the match between the properties of the two entities (polar or not), the molar mass as well as the shape of the molecule (Soubeyrand, 2012).

Chemical adsorption (or chemisorption) involves high binding energies, such as covalent, ionic, or metallic bonds between the adsorbed chemical species and the adsorbent. It is accompanied by a profound modification of the distribution of the electronic charges of the adsorbed molecules, these bonds are much stronger than physical interactions, and the energy of adsorption is greater than 100-500 kJ.mol^{-1}. It is often irreversible (or difficult to reverse). Since it requires the formation of interactions of high energy and at a short distance, chemisorption causes the formation of a monomolecular layer. The system won't have sufficient thermal energy to realize thermodynamic equilibrium (Djidel, 2011; Rouquerol et al., 1999; Sekirifa, 2013).

TableI-1: Typical characteristics of physical adsorption and chemisorption processes (Foo & Hameed, 2010).

Parameter	Physical adsorption	Chemisorption
Binding type	Van der Waals (electrostatic)	Ionic or covalent
Binding energy	Low	Strong
Reversibility	Easy	Difficult
Adsorption heat ($Kj.mol^{-1}$)	5 to 50	100 to 500
Adsorption enthalpy	Low (<2 or 3 times latent heat of evaporation)	High (>2 or 3 times latent heat of evaporation)
Specificity	Non specific	Highly specific
Adsorption site/Layer type	Monolayer or multilayer /Poly-molecular	Monolayer only /Mono-molecular
Nature of adsorption	No dissociation of adsorption species	May involve dissociation
Temperature range	Only significant at relatively low temperature	Possible over a wide range of temperature
Kinetics of adsorption	Rapid, non-activated, reversible	Activated, may slow and reversible
Electron transfer	No electron transfer although polarization of sorbate may occur	Electron transfer leading to bond formation between sorbate and surface
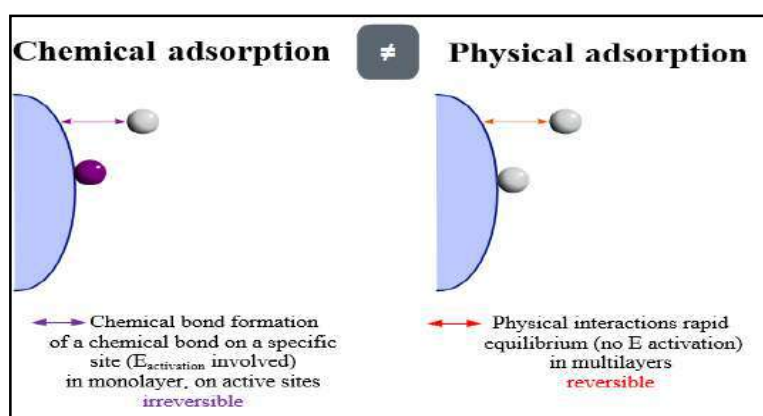
Image I-1: representation of physical adsorption and chemical adsorption (Poudres, 2018).

I.2. Adsorption mechanism

Knowledge of the adsorption kinetics is of considerable practical interest for the optimal use of an adsorbent in an industrial operation based on adsorption phenomena, as well as for knowing the factors leading to the fastest possible kinetics (Abdallah, 2018; Bechki & Lounas, 2019).

The adsorption phenomenon, controlled by the diffusion of molecules, reaches equilibrium relatively quickly (a few seconds to a few minutes), but, can be prolonged over very long times for the micro-porous adsorbents because of the slowing down of the diffusion of the molecules in these structures of dimensions close to the diameter of the molecules of the fluid, The transfer of a liquid phase containing the adsorbate to a solid phase with solute retention at the surface of the

adsorbent takes place in several steps (Abdallah, 2018; Bechki & Lounas, 2019). It is generally accepted that the dynamic process of adsorption, both in the gas phase and in the liquid phase for that matter, can be divided into three stages:

- **Step 01:** External mass transfer (external diffusion) which corresponds to the transfer of the solute (molecules of the liquid phase) from within the solution to the external surface of the particles.

- **Step 02:** Internal mass transfer in the pores (internal diffusion), involving the penetration of the adsorbate into the porous system of the adsorbent.

- **Step 03:** Adsorption proper, Surface diffusion for some adsorbents, this last step is considered extremely fast in the case of gases, and slow in the case of liquids, there may also be a contribution from the diffusion of the molecules adsorbed along the surfaces pores on the scale of a grain of adsorbent (Abdallah, 2018; Bechki & Lounas, 2019).
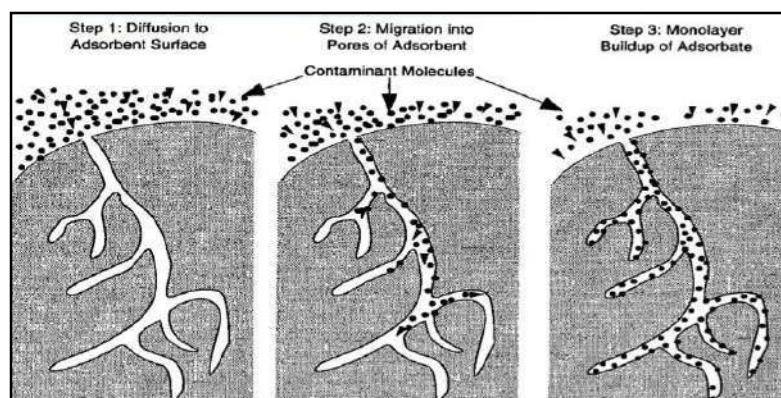
Image I-2: Diagram of adsorbate transport mechanism with in a grain (1-external diffusion, 2- internal diffusion (in the pores), 3- surface diffusion)

I.3. Factors influencing adsorption

The adsorption balance between an adsorbent and an absorbate depends on many main factors that are:

a) **Concentration:** For low concentrations of dissolved product, it is generally observed that the absorption rate as a function of the concentration of dissolved substance follows Freundlich's law. This law no longer applies at high concentrations, it is then observed that frequently that with the increase in concentration, the absorption passes by a maximum, then decreases to become negative (Abdallah, 2018; Djidel, 2011).

b) **Temperature:** Adsorption is an exothermic process and therefore its progress must be favored by lowering the temperature

c) **Adsorption speed:** While the physical adsorption of gases or vapors by solid adsorbents is extremely fast, the liquid phase adsorption is much slower. The viscosity of the solution must be a factor acting on the speed of adsorption, and it is likely that by decreasing the viscosity we increase the speed (Belaid, 2017; Djidel, 2011).

d) **PH and pH$_{PZC}$:** The effect of pH can be described on the basis of the zero point pH$_{PZC}$ charge corresponding to the net adsorbent charge is zero. According to Al - Degs et al the pH$_{PZC}$ is an index of the surface capacity (either positively or negatively charged), controlled by the pH of the surrounding solution. When a solution of pH <pH$_{PZC}$, the adsorbent (activated carbon) will react as a positive surface and as a negative surface when the solution pH> pH$_{PZC}$ (Belaid, 2017; Djidel, 2011).

e) **Nature of the adsorbent:** Polarity, pore-volume, specific surface area, porosity, and surface functions all of this are the characteristics of the adsorbent

The adsorbents depended on a liquid medium act first of all by their external surface. Certain adsorbents have a specific action characterized according to the polarity of the external surface because the latter has an affinity with water or alcohol. Polar adsorbents are "hydrophilic", on the other hand, non-polar adsorbents are generally said to be "hydrophobic". Polymeric adsorbents and carbon adsorbents are examples of non-polar adsorbents that have less affinity for water (Boulkrah, 2008; Djidel, 2011).

The adsorption is proportional to the specific surface, the adsorption kinetics depend on the size of the outer surface of the particles, it is fundamental for the use of activated carbon, Porosity is related to the distribution of pore size. It reflects the internal structure of microporous adsorbents (Belaid, 2017; Boulkrah, 2008).

f) **The nature of the adsorbate:** polarity, solubility, and molecular weight; the Physico-chemical parameters of the environment; Temperature and pH.

The adsorption of a substance increases as its concentration in the solution increases. However, this increase is not proportional because it occurs slowly.

For it to have good adsorption it must have an affinity between the solid and the solute. In general, polar solids preferentially adsorb other polar bodies. On the other hand, non-polar solids preferentially adsorb non-polar substances (Djidel, 2011).

If the dimensions of the pores of the adsorbent are smaller than the diameters of the molecules of the adsorbate, the adsorption of this compound does not take place even if the surface of the adsorbent has a high affinity for this compound (Belaid, 2017; Djidel, 2011).

I.4. Adsorption isotherm

I.4.1. Gas-solid adsorption

The adsorption isotherm of equation $V_{ads} = f(p/p_0)$ is obtained by measuring the volume quantities of adsorbed gas V_{ads} for increasing values of the relative pressure represented by p/p_0, p being the equilibrium pressure and p_0 the saturated vapor pressure of the gas at the temperature considered (Belaid, 2017; Leinekugel-le-Cocq, 2004).

Six types of isotherms are listed by IUPAC (International Union of Pure and Applied Chemistry) (Rouquerol et al., 1999; Kenneth S. W. Sing, 1985). This classification includes most of the isotherms studied in the literature Image I-3, each type of isotherm obtained already allows qualitative conclusions to be drawn on the interactions between the adsorbate and the adsorbent (Koller, 2001).

Image I-3: Types of isotherms listed by IUPAC

- **The type I**: Isotherm corresponds to adsorption on microporous solids (pore radius <2nm) or the limit with no porosity. This isotherm reflects a relatively strong interaction between the adsorbate and the adsorbent, a monolayer adsorption corresponding to the filling of micropores with saturation when the available volume is completely

filled. It is fully reversible over the entire pressure range (Belaid, 2017; Leinekugel-le-Cocq, 2004).

This isothermal classified in three forms represented in Image I-4 of quantity of adsorbed gas Q as a function of p/p_0:

Image I-4: The subtypes of type I

- (I_a): a microporosity exclusively with a distribution of narrow d_W/d_L pores, therefore once the micropores are filled, adsorption stops.

- (I_b): represents the adsorption of carbon with a more heterogeneous micropore distribution than for (I_a).

- (I_c): the adsorbent has a wide distribution of microporosity and a well-developed mesoporosity.

The increase in the adsorbed quantity Q_{gaz}, from Q_{max} corresponds to the multilayer adsorption on the external surface (Sekirifa, 2013).

- **The type II**: Isotherm is characteristic of adsorption to mesoporous or macroporous surfaces (with an average diameter greater than 20 nm). The filling is done in multilayer. This isotherm is reversible over the entire pressure range.

- **The rarer type III**: Isotherm derives from the previous one with a completely non-existent first part (most often for macroporous samples). Multilayers are formed at low pressures due to the strong interactions between the adsorbate and the adsorbent. This is the case with the adsorption of water on hydrophobic surfaces (eg: graphite or activated carbon containing little oxygen) (Koller, 2001; Leinekugel-le-Cocq, 2004; Sekirifa, 2013).

- **Type IV**: Isotherms for mesoporous samples (2 nm <pore<50 nm). There is formation of monolayers and multilayers. They present a hysteresis loop generally associated with the filling of mesopores by capillary condensation.

- Can result from the combination of a type I (strong but limited adsorption) and type V isotherm (Koller, 2001; Leinekugel-le-Cocq, 2004; Sekirifa, 2013).

- **Type VI**: Isotherms exhibit steps characteristic of multilayer adsorption on a very homogeneous (highly uniform) non-porous surface (Soubeyrand, 2012).

- **Type V**: Isotherms for mesoporous samples also reflect a strong interaction between adsorbate and adsorbent.

- As with type III isotherms, multilayers are formed at low pressures. In addition, the existence of a hysteresis (Defined below) during desorption reflects the presence of mesopores in which the vapor condenses to form a strongly curved meniscus (Koller, 2001; Leinekugel-le-Cocq, 2004; Sekirifa, 2013).

❖ **The phenomenon of hysteresis loops (desorption)**

Hysteresis (or hysteresis) is a Greek word and meaning "after" or "later", it is the property of a system that tends to remain in a certain state when the external cause which produced the change of state ceased. When a porous solid is exposed to a gas vapor, the vapor condenses in the pores, forming a liquid as a dense state (Marsh & Reinoso, 2006).

This phenomenon, known as capillary condensation, occurs at the gas pressure lower than the saturated vapor pressure at the given temperature. As the temperature increases, the effect of capillary condensation disappears, however, the critical temperature of capillary condensation is lower than the critical bulk temperature. Capillary condensation indicates a shift in the apparent gas-liquid balance characterized by a typical step in adsorption isotherms is associated with pronounced hysteresis. Adsorption-desorption isotherms form a reproducible hysteresis loop, the shape of which depends on the structure and nature of the pore distribution (Koller, 2001).

Hysteresis has been observed in adsorption isotherms for a number of gas-solid systems and in general, is attributed to the adsorption of mesoporous materials with capillary condensation, the presence of pores opening at the surface of the solid explains the irregularities of physisorption when the pressure of the gas increases. The delay observed during desorption is interpreted by the existence of pores in the form of bottles. Four typical hysteresis loops have been selected (Liu, Zakharova, Adeyilola, & Zeng, 2021):
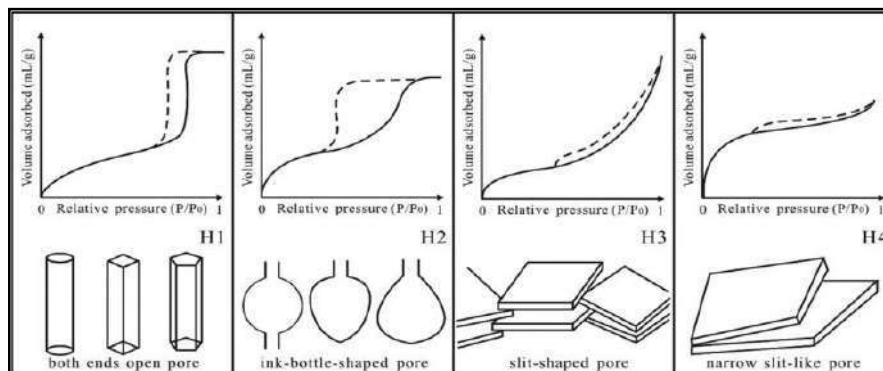
Image I-5: Hysteresis loop types and their corresponding pore shapes.

- H$_1$ type loop for samples with a very narrow distribution of uniformly sized mesopores.

- H$_2$-type loop for samples with a more complex pore structure consisting of tightly bonded networks of pores of different sizes and shapes (often with a bottleneck). This may be the case with pores associated with spherical particles.

- Loop type H$_3$ for samples composed of aggregates of flat particles or containing slit pores.

- H$_4$-type loop for samples also composed of slit pores but whose pore size distribution is mainly in the microporous region (Belaid, 2017; Koller, 2001; Marsh & Reinoso, 2006; Rouquerol et al., 1999).

I.4.2. Liquid-solid adsorption

Experimentally, according to Giles (Giles, Smith, & Huitson, 1974), isotherms have been classified into four main types and presented in figure 2.6: S (Sigmoid), L (Langmuir), H (High affinity) and C (constant partition):

• The solvent adsorbs at the same sites as the solute. This implies the existence of an adsorption competition between the solvent and the solute.

• The number of sites capable of receiving solute molecules on the surface of the solid decreases as the amount adsorbed increases.

• The orientation of molecules on the surface. We can cite the case where the molecules are adsorbed vertically or horizontally on the surface.

• Finally, the attractive or repulsive interactions between the adsorbed molecules are manifested in a notable way in the phenomenon of adsorption (Marsh & Reinoso, 2006).

Class S: The isotherms of this class have, at low concentration, an upward facing concavity. The adsorbed molecules promote the subsequent adsorption of other molecules (cooperative adsorption). This is due to molecules attracting by Van Der Waals
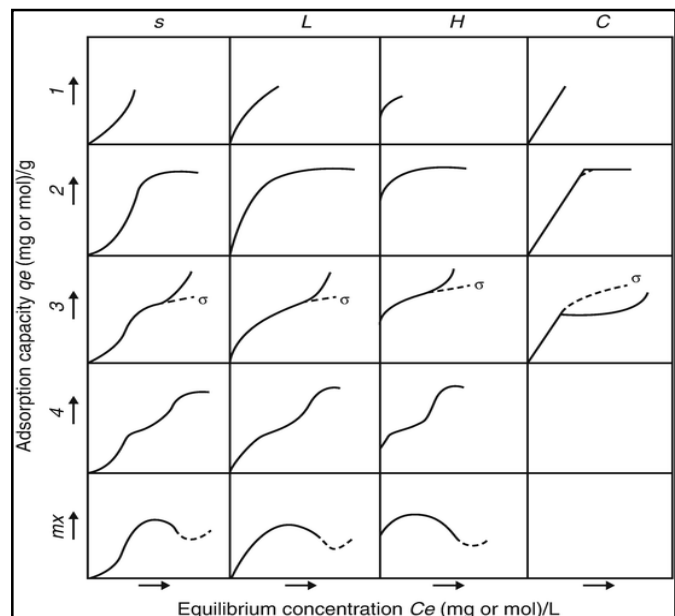
Image I-6: Types of isotherms according to Giles

14

forces (Belaid, 2017; Koller, 2001; Rim Baccar Ep Yangui et al., 2014).

Class L: Class L isotherms exhibit a low concentration in solution, a downward concavity which reflects a decrease in free sites as the adsorption progresses. This phenomenon occurs when the forces of attraction between the adsorbed molecules are weak. It is often observed when molecules are adsorbed horizontally, which minimizes their lateral attraction. It can also appear when molecules are adsorbed vertically and when the competition for adsorption between solvent and solute is weak. In this case, the adsorption of the isolated molecules is strong enough to make the side interactions negligible (Belaid, 2017; Koller, 2001; Rim Baccar Ep Yangui et al., 2014).

Class H: The initial part of the isotherm is almost vertical; the adsorbed quantity appears significant at almost zero concentration of the solute in the solution. This phenomenon occurs when the interactions between the adsorbed molecules and the surface of the solid are very strong. The H-class isotherm is also observed during the adsorption of micelles or polymers formed from solute molecules (Belaid, 2017; Koller, 2001; Rim Baccar Ep Yangui et al., 2014).

Class C: Isotherms of this class are characterized by a constant partition between the solution and the substrate up to a plateau. Linearity shows that the number of free sites remains constant during adsorption. This means that the sites are created during adsorption. This implies that the isotherms of this class are obtained when the solute molecules are able to modify the texture of the substrate by opening pores which had not been opened previously by the solvent (Belaid, 2017; Koller, 2001; Rim Baccar Ep Yangui et al., 2014).

I.5. Adsorption models

To understand the adsorption mechanism many empirical relations have appeared connecting the amount adsorbed with principal variable such as concentration and temperature. there are many adsorption models but we have explained the four traditional adsorption isotherm models, relating to adsorption equilibrium, such as Freundlich, Langmuir, Temkin and Dubinin-Radushkevich (D-R) isotherm model (Rim Baccar Ep Yangui et al., 2014).

I.5.1. The Freundlich model

The model is based on adsorption on heterogeneous surfaces and is a widely met isotherm (''L'' or ''H'' isotherms). The first model is empirical by (Van Bemmelen in 1888, and Freundlich in 1906) (Rim Baccar Ep Yangui et al., 2014) and the model which is known to be satisfactory for low concentrations is expressed by the equation 1(Boudrahem et al., 2019; Sekirifa & Hadj-Mahammed, 2005):

$$q_e = K_F C_e^{1/n} \quad ....Eq\ 1$$

The equation may be linearized by taking the logarithm of both sides. When log (qe) is plotted against log (Ce), we will have a straight line with a slope of 1/n and an intercept of log (KF).

Where q_e is the equilibrium sorption concentration of solute per gram of adsorbent (mg.g^{-1}); C_e is the equilibrium aqueous concentration of the solute (mg.l^{-1}); K_F [(mg. g^{-1}) (l.mg^{-1})$^{1/n}$] and n are Freundlich constants which are related to the adsorption capacity and the intensity of adsorption. A value of n between 2 and 10 shows good adsorption (Djidel, 2011; Trifi, 2012).

I.5.2. The Langmuir model

The Langmuir adsorption is valid for monolayer adsorption. It is a very common model and is based on reaction hypotheses (Langmuir, 1918). The solid is assumed to have a limited adsorption capacity q_{max}. All the adsorption sites (are assumed to be identical, each site retains one molecule of the given compound, and all sites are energetically independent of the adsorbed quantity) (Rim Baccar Ep Yangui et al., 2014) (Sekirifa & Hadj-Mahammed, 2005).

The Langmuir isotherms model is described by the equation (Eq 2):

$$q_e = \frac{q_{max} K_L C_e}{1 + K_L C_e} \quad ....Eq\ 2$$

Where q_{max} and K_L represented the maximum adsorption capacity and the Langmuir constant, respectively. The essential characteristics of a Langmuir isotherm can be expressed in terms of dimensionless constant separation factor R_L defined as:

$$R_L = \frac{1}{1 + K_L C_0} \quad ....Eq\ 3$$

Where C_0 is the initial concentration. R_L values less than unit y confirm the

favorable uptake of the sorbent (Djidel, 2011; Trifi, 2012).

I.5.3. The Temkin model

This isotherm contains a factor that explicitly takes into account of adsorbent-adsorbate interactions. The Temkin isotherm can be expressed by the following equation 4:

$$q_e = \frac{RT}{b} ln(AC_e) \quad ....Eq\ 4$$

Where R T/b= B (J mol^{-1}), which is the Temkin constant related to heat of sorption whereas A (l.g^{-1}) is the equilibrium binding constant corresponding to the maximum binding energy. R (8.31 4 J.mol^{-1}.K^{-1}) is the universal gas constant and T (K) is the absolute solution temperature (Rim Baccar Ep Yangui et al., 2014; Trifi, 2012).

I.5.4. Dubinin-Radushkevich (D-R) isotherm

The Dubinin-Radushkevich (D-R) isotherm model is applied to distinguish between physical and chemical adsorption (Rim Baccar Ep Yangui et al., 2014). The D-R equation is given as follows:

$$q_e = q_m exp(-\beta \varepsilon^2) \quad ....Eq\ 5$$

With:

$$\varepsilon = RT\ ln(1 + \frac{1}{C_e}) \quad ....Eq\ 6$$

Where q$_m$ is the maximum amount adsorbed and can be called the adsorption capacity, β is a constant related to the adsorption energy (mol^2.kJ^{-2}), ε is the potential energy of the surface, R is the gas constant (kJ.mol^{-1}.K^{-1}) and T is the absolute temperature. The constant B gives the free energy E (kJ.mol^{-1}) of the transfer of 1 mol of solute from infinity to the surface of adsorbent, and can be computed using the following relationship:

$$E = \frac{1}{\sqrt{2B}} \quad ....Eq\ 7$$

I.6. Adsorption kinetics

The study of adsorption from a kinetic perspective can lead to a better understanding of the mechanism of the process. The kinetic studies describe the rate of adsorption and this rate controls the equilibrium time. These kinetic models are useful for the de sign and optimization of effluent treatment models. Pseudo first order, pseudo second order,

Elovich and Intra-particle diffusion kinetic models were adopted in this work (Rim Baccar Ep Yangui et al., 2014).

I.6.1. Pseudo-First and pseudo-second order Kinetic Models

The modeling of kinetics of adsorption was investigated by two common models, namely, the pseudo-first order model and pseudo-second order model, in the linear form, are expressed by equations 8 and 9, respectively:

$$log(q_e - q_t) = log\, q_e - K_1 t \quad ....Eq\ 8$$

$$\frac{t}{q_t} = \frac{1}{k_2 q_e} + \frac{1}{q_e} t \quad ....Eq\ 9$$

Where q_e and q_t are the amounts of the adsorbent adsorbed at equilibrium and at time t, respectively, and are expressed in mg.g^{-1}, K_1 and K_2 are the pseudo first-order and the second order model rate constant expressed in l.min^{-1} and g.mg^{-1}.min^{-1} respectively (Rim Baccar Ep Yangui et al., 2014).

I.6.2. Elovich equation

The Elovich equation is another rate equation in which the absorbing surface is heterogeneous (Chien & Clayton, 1980). It is generally expressed as given as follows:

$$q_t = \frac{1}{b} ln(ab) + \frac{1}{b} ln\, t \quad ....Eq\ 10$$

Where a (mg.g^{-1}.h^{-1}) is the initial sorption rate and b (mg.g^{-1}) is related to the extent of surface coverage and activation energy for chemisorption. The parameters (1/b) and (1/b) ln(ab) can be obtained from the slope and intercept of the linear plot of q_t versus ln(t). The value of 1/b is indicative of the number of sies available for adsorption, while the (1/b) ln(ab) value is the adsorption quantity when ln(t) is equal to zero (Tan, Ahmad, & Hameed, 2009).

I.6.3. Intra-particle Diffusion Model

Intra-particle diffusion model based on the theory proposed by Weber and Morris was tested to identify the diffusion mechanism (Shaarani & Hameed, 2010). According to this theory:

$$q_t = K_{id} t^{1/2} + C \quad ....Eq\ 11$$

Where C is the intercept and k_{id} (mg.g^{-1}.h$^{-1/2}$) is the intra-particle diffusion rate constant, which can be evaluated from the slope of the linear plot of q_t versus $t^{1/2}$. If intra-particle diffusion is a rate controlling step, then the plots should be linear and pass

through the origin. In most cases these plots give general features of three stages; initial curved portion, followed by an intermediate linear portion and a plateau. The initial portion due to external mass transfer, the intermediate li near part is due to intra-particle diffusion and the plateau to the equilibrium stage where intra-particle diffusion s tarts to slow down due to extremely low solute concentrations in the solution (Daifullah, Yakout, & Elreefy, 2007; Rim Baccar Ep Yangui et al., 2014).

I.6.4. Thermodynamic adsorption

The temperature has great effect on the adsorption. The equilibrium constant K_D of the adsorption process, expressed in $l.g^{-1}$, can be used to estimate the thermodynamic parameters due to their dependence on temperature. The changes in standard free energy ($\Delta G°$), enthalpy ($\Delta H°$) and entropy ($\Delta S°$) of adsorption process were determined using the following equations 12, 13 and 14:

$$K_D = \frac{q_e}{C_e} \;........Eq\;12$$

$$\Delta G° = -RT\;ln\,K_D \;........Eq\;13$$

$$ln\,K_D = \frac{\Delta S°}{R} - \frac{\Delta H°}{RT} \;.........Eq\;14$$

A Van't Hoff plot of $ln\,K_D$ as a function of $1/T$ yields to a straight line. The $\Delta H°$ and $\Delta S°$ parameters were calculated from the slope and intercept of the plot, respectively (Rim Baccar Ep Yangui et al., 2014).

II.   Adsorbents

The adsorbents most used industrially are micro-porous solids, generally synthetic: « active carbon, carbon molecular sieve, activated alumina, silica gel, zeolites…». The particularly high adsorption capacities of these materials are partly linked to their highly developed porous structures and their large specific surfaces (Djidel, 2011).

Adsorbents can be usually classified into five categories:

- **natural materials** such as sawdust, wood, fuller's earth or bauxite;
- **natural materials treated** to develop their structures and properties such as activated carbons, activated alumina or silica gel;
- **manufactured materials** such as polymeric resins, zeolites, or alumina-silicates;
- **agricultural solid wastes and industrial by-products** such as date pits, fly ash, or red mud;
- **bio-sorbents** such as chitosan, fungi, or bacterial biomass (Crini et al., 2018).

19

All the solids acting as adsorbents are characterized by the microporous structure which gives them a very large active surface per unit mass. The adsorbents used in practice are either organic (plant or animal) or mineral in nature. They are used as-is or after an activation treatment aimed at increasing porosity (Koller, 2001).

The most used adsorbents are:
- Silica gel
- Activated alumina
- Molecular sieves
- Zeolites

The most widely used adsorbent in industrial applications is activated carbon.

II.1.   Activated carbon

Activated carbon is the most widely used adsorbent in industry. It is considered by the US Environmental Protection Agency as one of the best technologies for "environmental control". It is made from carbonaceous materials such as coals, petroleum coke, coconut, peat…, used mainly in granular and powdered forms, but can also be produced in textile form by controlled carbonization and activation of textile fibers (Koller, 2001; Marsh & Reinoso, 2006).

The specific properties of activated carbon are linked to its specific surface which, unlike that of the main other adsorbents, has a low selectivity (ability to separate two compounds) compared to other adsorbents due to its wide distribution of pore sizes, is non-polar or weakly polar, which allows it to preferentially the adsorption of large quantities of organic or non-polar compounds, even in the presence of water. This explains its preferred use for the adsorption of organic products in water and wet gas treatment processes (Djidel, 2011).

In order to increase its adsorptive properties, after initial treatment and shaping, there is a carbonization step at 400 - 500 °C to remove the bulk of volatile materials, then an activation step (physical or chemical), physical activation by gasification such as CO_2, water vapor, combustion gases are used, the activated carbon produced by this process is mainly used in the adsorption of gases and vapors. while the chemical activation by different activation agents such as phosphoric acid, zinc chloride, sulfur sulfide, potassium…etc, generally leads to powdered activated carbon, used especially in water treatments. The activated carbon has a specific surface area of the order of 300

to 1000 $m^2.g^{-1}$ with pores of 10 to 60 Å, a low apparent density (0.5 kg per liter), and above all two main properties: an adsorbing power and a catalytic power (Koller, 2001).

It can thus be used for gas separation/purification operations without prior dehumidification, unlike most other adsorbents. The adsorbate/adsorbent binding energy is generally lower for activated carbon than for the other adsorbents, Thus, we do not need a lot of energy in the regeneration phase (Djidel, 2011).

Carbon adsorbents have a porous carbon structure, which contains small amounts of different heteroatoms such as oxygen and hydrogen. Some activated carbons also contain variable amounts of mineral matter (ash content) depending on the nature of the raw material used as precursor. The porous structure is perhaps the main physical property that characterizes activated carbons. This is formed by pores of different sizes which according to IUPAC recommendations (Kenneth S. W. Sing, 1985) can be classified into three major groups (Menéndez-Díaza & Martín-Gullón, 2006).

- Micropores with a pore width of less than 2 μm.
- Mesopores with widths from 2.0 to 50 μm.
- Macropores with a pore width larger than 50 μm.
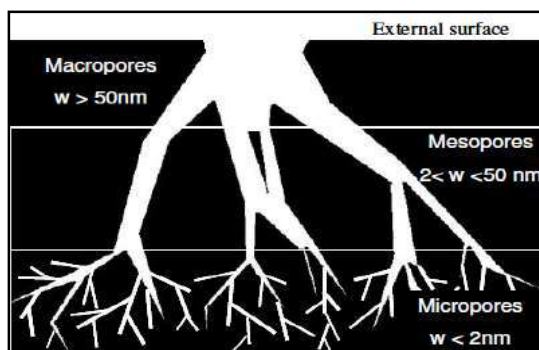
Image I-7: Pore classification

Furthermore, the presence or absence of surface groups, formed by heteroatoms (atoms different to the carbon atom), that may bond themselves to the carbon atoms at the edges of the basal planes gives rise to carbons with different chemical properties. The physical and chemical properties are of great importance for the behavior of carbon adsorbents (Marsh & Reinoso, 2006; Menéndez-Díaza & Martín-Gullón, 2006).

II.1.1. Type of activated carbon

Activated carbon is generally available in two forms: powder and granulated.

TableI-2: Type of activated carbon

Type of activated carbon	Description	Utilization	Advantages	Inventions
ACP	• Takes the form of grains • 95-100% diameter ≤ 0.177 mm.	• Used in combination with a clarifying treatment. • Continuously added with water to be treated with flocculating agents.	• 3 times cheaper than granular activated carbon. • Additional quantities can be added • Adsorption is rapid • A large part of the contact surface is directly available.	• Can't be regenerated • It is difficult to remove the last traces of impurities without adding a very large amount of powdered activated carbon. • Its applicable concentration is limited.
GAC	• The shape: either in granulated or extruded form • represented by sizes such as 8x20, 20x40, or 8x30 for liquid phase applications and by 4x6, 4x8 or 4x10 for vapor phase applications	• Used in different types in the water treatment system for the reduction of residual chlorinated oxidants and a very low elimination of certain disinfection by-products used to remove turbidity and to dissolve organic compounds, odor, stains, dyes. • Used for the removal of organic micro pollutants and organic matter in the form of dissolved carbon. • used in filtration for finishing treatments	• The lifespan of granulated activated carbon depends on the reduction of the material • Organic and smoothing of pesticide points. • The choice of the type of activated carbon is also decisive on the efficiency of elimination. • Granulated activated carbon has the capacity to absorb some of almost all vapors. • It has a high adsorption capacity for organic substances, in particular solvents. • It retains a large number of chemicals at the same time. It works well in a wide range of temperature and humidity. • It is inert and can be used safely. • It is readily available and inexpensive.	• Limited lifespan. • Prefiltration: requiring pretreatment in most cases. • Cost: The need to regularly replace spent carbon makes granulated activated carbon more expensive than stripping for high concentrations of contaminants. • Hazardous waste: it can be disposed of as hazardous waste, which would increase cost and liability.

II.1.2. Manufacture of active carbon

Activated carbon obtained from biomass or agricultural by-products, which cost less than activated carbon from fossil materials, can be made from many substances with a high carbon content such as grain husks, corn waste, and nutshells. At present, the growing demand for adsorbent materials for environmental protection processes is prompting additional research into the production of active carbon from materials that are not conventional, specifically from plant waste, because to the various studies have shown, activated carbon obtained from vegetable waste is very interesting from an economic point of view (Djidel, 2011).

❖ A plant cell wall is made up essentially of four components: cellulose, hemicellulose, lignin, and pectin (Elena-Fernandez, 2002).

➢ Cellulose is a linear polymeric structure composed of glucose residues (between 300 and 3000) linked by β (1 → 4) glucosidic bonds. Several cellulose molecules come together in clumps and we obtain structures called "micelles". The micelles

will group together in a parallel fashion and are linked transversely by hydrogen bonds to form the "microfibrils" (Elena-Fernandez, 2002).

➢ The hemicellulose and the pectins are perpendicular to these microfibers and arrange themselves forming a network, it is made up of approximately 50 units of simple sugars, where the major component is xylan, linked by β $(1 \rightarrow 4)$ glucosidic bonds. It is linked to cellulose by hydrogen bonds located on the surface of microfibers. Pectins and hemicellulose are cross-linked, resulting in a network on the wall of plant cells (Djidel, 2011; Elena-Fernandez, 2002).

➢ To define the fourth component, lignin, it should be known that the cell wall of plant cells is divided into three secondary walls close to the cell which are called S1, S2, and S3 made up mainly of cellulose, hemicellulose, and a proportion of lignin of less than 20%. The difference between the three secondary walls is due to the difference in direction of the cellulose fibrils (Djidel, 2011; Elena-Fernandez, 2002).

After the secondary walls, the primary wall is made up of hemicellulose, pectins, and approximately 50% lignin.

Finally, we arrive at the middle lamella which contains about 70% lignin. The latter is a water-insoluble polymer formed from phenolic radicals. Lignin is a support material especially abundant in wood, where it is also found in significant proportions in the primary and secondary walls (Djidel, 2011; Elena-Fernandez, 2002).

Each of the components described here is found in plants in a specific proportion. Thus, the proportion of cellulose, hemicellulose, and lignin can to some extent determine the properties of activated carbon obtained from given plant material (Djidel, 2011; Elena-Fernandez, 2002).
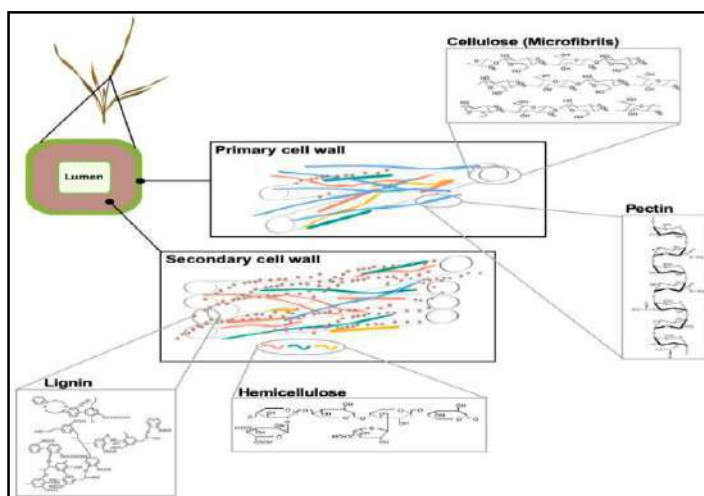
Image I-8: The components of a plant cell wall.

❖ Generally, the preparations of activated carbon involve two stages, mainly pyrolysis and activation process (Vargas et al., 2011), it can be chemical activation or physical activation.

It has been shown by Tang and Bacon that cellulose, hemicellulose, and lignin undergo thermal decomposition in a well-defined temperature range, we can assume that the thermal decomposition of plants is the result of the separate decomposition of each of its components (Elena-Fernandez, 2002) .

II.1.2.1. Pyrolysis process

Pyrolysis is the process in which a sample is subjected to high temperatures (400-1000°C) under an inert atmosphere, as to obtain a solid carbon product, as well as volatile compounds (liquid and gaseous) such as carbon monoxide, hydrogen, methane and other hydrocarbons, including result is a solid residue with high carbon content, with a rudimentary microporosity which can then be developed in the activation process, Pyrolysis also leads to an initial opening of the carbon structure of the precursor (Djidel, 2011; Elena-Fernandez, 2002).

The main parameters determining the quality, properties and yield of the pyrolysate are represented by a series of external factors that influence the pyrolysis process as well as others that depend solely on the nature of the raw material used.

➢ External variables (specific to all pyrolyses)
- Heating rate ($°C.min^{-1}$);
- Thermal decomposition of chemical components (°C);
- Final temperature (°C);

➢ Internal variables (specific to the material)
• Thermal conductivity ($J.m^{-1}.s^{-1}.°C^{-1}$): particle size;
• Residence time (h or min);
• Preliminary treatments carried out in the original material;

The product of pyrolysis is strongly influenced by the rate of heating and the final temperature. In general, at low heating rates, a few volatile compounds are obtained and the original structure is retained to a certain extent. The opposite is observed as the heating rate increases.

The final temperature determines the loss of mass ([Byrne & Nagle, 1997](#)) and the appearance of the carbon surface. The volume of the product then has a maximum microporosity at a fixed temperature, but different for each material.

There is a pyrolysis temperature for each material from which the yield (below) remains constant:

$$efficiency\ (\%) = \frac{mass_{final}}{mass_{initial}} \times 100 \quad ....Eq\ 15$$

The minimum residence time required corresponds to the duration of temperature equalization between the interior and the exterior of the particle in question.

The aim of a pre-treatment of the material is to obtain carbon with different thermal characteristics, different functional groups on the surface, or lower ash content ([Elena-Fernandez, 2002](#)).

II.1.2.2. Activation process

Activation is a process in which charred particles are exposed to an activating agent at high temperature under a vertical or a horizontal furnace, activation increases the volume and, to some extent, enlarges the pores created during the pyrolysis process. The nature of the raw material as well as the pyrolysis conditions predetermine the structure and the width of the pores.

➢ **Physical Activation**

Physical activation consists of a high temperature (750 -1000 °C) oxidation of the carbonate by a gaseous oxidizing agent. The gases used, alone or as a mixture, weakly oxidizing, are water vapor and carbon dioxide CO_2. The temperature level plays an important role in the activation process. In fact, at low temperature, the oxidation kinetics are low and the activation leads to a homogeneous pore size distribution throughout the volume of the material. When the temperature increases, the reaction rate increases faster than the diffusion of the oxidizing gas. The process is therefore limited by the transport of the oxidizing gas within the material, which leads to a loss of homogeneity of the porosity ([Atheba, 2009](#); [Djidel, 2011](#)).

$$CA + CO \Longrightarrow 2CO \quad ......1$$

$$2\ CA + H_2O \Longrightarrow CO + H_2 \quad ....2$$
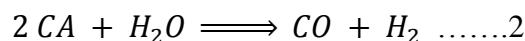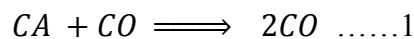
➢ **Chemical Activation**

It is an alternative process that involves a chemical agent (base or acid) such as sulfuric acid H_2SO_4, phosphoric acid H_3PO_4, Potassium hydroxide, and so forth…promoting dehydration, then a structural reorganization at lower temperatures than in the physical activation process. The precursor is impregnated with the chemical agent in order to improve the development of a porous structure following heat treatment.

A disadvantage of chemical activation is the incorporation of impurities in the carbon during the impregnation, which can affect the chemical properties. The chemical reagent can be recovered by washing the activated carbon produced.

II.1.3. Structure porous of activated carbon

The pores are classified according to their diameter, into three types of porosity, according to the definition of IUPAC (K. S. W. SING et al., 1985), the porosity is classified in the following way:

- Micropores: $D_p < 2$ nm
- Mesopores: 2 nm $< D_p < 50$ nm
- Macropores: $D_p > 50$ nm

The specific surface directly depends on the porosity: the greater the microporosity, the greater the specific surface. Adsorption on the surface of macropores is often negligible compared to that in micropores and mesopores.

II.1.3.1. Characterization of activated carbon

In this field, three types of characterization are distinguished, namely, physical characterization (Gas adsorption method, scanning electron microscope (SEM), Iodine index, Methylene blue index, Phenol index, the x-ray microanalysis...), chemical characterization (Studies on point of charge, Study of surface functional group, Infrared Spectroscopy (FT-IR) …), as well as characterization using adsorption capacity (Adsorption isotherm, Adsorption kinetics…).

II.1.3.2. Physical characterization

The physical properties are all that is related to the characterization of the specific surface, the dimensions and types of pores by gas adsorption method, the microscopic images as well as the x-ray microanalysis of the activated carbon.

The specific surface available for adsorption into the porous structure of activated carbon can be measured by several methods, the weight of different standard substances such as nitrogen, iodine, molasses, phenol, or methylene blue can be used to measure the specific surface in certain fractions of all pores.

II.1.3.2.1.   Gas adsorption method

Nitrogen adsorption by the Brunauer-Emmett-Teller (BET) model measures the specific surface of activated carbon, it is used as a first indicator of activity level, it is based on the principle that the larger the surface the greater the number of adsorption sites available (Holmes, 1991).

Brunauer-Emmett-Teller method: The BET hypothesis is based on the formation of several layers of adsorbed molecules, thus the molecules are placed on top of each other to give an interfacial zone which can contain several thicknesses of adsorbed molecules. The first layer of adsorbate acts as a substrate for subsequent adsorption and releases a constant differential heat H_J, while for the molecules of all the other layers, the heat of adsorption is equal to the enthalpy of liquefaction H_L (heat the tent).

The Brunauer-Emmett-Teller isotherm (BET) can be used to estimate the specific surface area of an adsorbent or its specific area. The BET isotherm is given by the relation:

$$\frac{P}{V(P^0-P)} = \frac{1}{(CV_m)} + \frac{(C-1)}{(CV_m)} \cdot \frac{P}{P^0} \quad ....Eq\ 16$$

Or:

$$\frac{V}{V_m} = \frac{(C.P)}{(P^0-P)\ [1+(C-1)\frac{P}{P^0}]} \quad ....Eq\ 17$$

Where V is the volume of adsorbed gas, P the pressure of the gas, P^0 the vapor pressure above several layers of adsorbed molecules and V_m the volume necessary to form a complete mono molecular layer on the surface of one gram of solid (Atheba, 2009; Sekirifa, 2013).

C: is the constant given by the expression:

$$C = exp\left(\frac{H_J - H_L}{RT}\right) \ \ldots\ldots\ldots Eq\ 18$$

Where H_J: differential heat (cal).

H_L: latent heat of evaporation (cal).

By plotting $\frac{P}{V(P^0 - P)}$ as a function of $\frac{P}{P^0}$, we must obtain a straight line with slope $\frac{C-1}{CV_m}$ and with an intercept of $\frac{1}{CV_m}$. This is calculated in the application area where $\frac{P}{P^0}$ is between 0.05 and 0.35.

We calculate the volume corresponding to a total recovery V_m, by the relation:

$$V_m = 1/(a + b) \ \ldots\ldots\ldots Eq\ 19$$

Where (a) and (b) are the slope and the intercept

The specific surface Asp can be directly calculated from V_m using the following relation:

$$S_{BET} = \frac{P_m V_m}{RT_m} \times 6.023 \times 10^{23} \times \sigma_0 \ \ldots\ldots\ldots Eq\ 20$$

Where Pm and Tm are the pressure and the temperature of the adsorbed gas, and σ0 the surface occupied by a molecule. σ_0 Can be expressed by the following relation:

$$\sigma_0 = 1.09 \times \left[\frac{M}{(6.023 \times 10^{23} \times \rho)}\right]^{(2/3)} \ \ldots\ldots\ldots Eq\ 21$$

Where M is the molecular mass of the adsorbed gas, ρ the density of the pure liquid at the temperature of the experiment. For example, for nitrogen at −195.8 °C, ρ = 0.808 g.cm^{-3}.

II.1.3.2.2. Iodine index

The iodine index is a measure of the pore volume present for the diameter range 10 to 28 Å. This index refers to the quantity in milligrams of iodine adsorbed by one gram of activated carbon when the concentration at equilibrium. This index is very important for the characterization of activated carbon in that it gives an essential idea of the surface available for small substances (micropores) (Boutadara, Ben Ali, & Kalloum, 2017; Djidel, 2011).

II.1.3.2.3. Methylene blue index

The methylene blue index is the number of milligrams of methylene blue adsorbed by one gram of activated carbon when the equilibrium concentration of methylene blue is 1 mg. l^{-1}. The methylene blue index gives an idea of the area available for micro and mesoporous adsorbents. The surface occupied by a molecule of methylene blue is 130 $Å^2$ (Boutadara et al., 2017; Djidel, 2011).

II.1.3.2.4. Phenol index

The phenol index is the number of milligrams of phenol adsorbed by one gram of activated carbon when the equilibrium concentration of phenol is 1 mg. l^{-1}. Phenol used as a first species to simulate certain toxic chemicals in the study of solid-liquid adsorption, as well as to measure the porosity of activated carbon (Boutadara et al., 2017; Djidel, 2011).

II.1.3.2.5. Scanning Electron Microscope (SEM)

A scanning electron microscope (SEM) is a type of electron microscope that produces images of a sample by scanning the surface with a focused beam of electrons. The electrons interact with atoms in the sample, producing various signals that contain information about the surface topography and composition of the sample. The electron beam is scanned in a raster scan pattern, and the position of the beam is combined with the intensity of the detected signal to produce an image (Marsh & Reinoso, 2006; Nzihou, 2020).

In the most common SEM mode, secondary electrons emitted by atoms excited by the electron beam are detected using a secondary electron detector (Everhart-Thornley detector). The number of secondary electrons that can be detected, and thus the signal intensity, depends, among other things, on specimen topography. SEM micrographs have a large depth of field yielding a characteristic three-dimensional appearance useful for understanding the surface structure of a sample (Marsh & Reinoso, 2006; Nzihou, 2020).

II.1.3.2.6. The X-ray Diffraction and fluorescence microanalysis

X-rays are high-energy electromagnetic radiation. They have energies ranging from about 200 eV to 1 MeV; which puts them between y-rays and ultraviolet (UV) radiation in the electromagnetic spectrum ([Suryanarayana & Norton, 1998](#)).

X-ray microanalysis can produce in situ chemical information from virtually any type of specimen. Generally, operate in a high vacuum and a very dry environment in order to produce the high energy beam of electrons needed for analysis. it is an analytical method that could be utilized far more comprehensively; research aiming not only at the identification of samples but also towards understanding the relationships between their chemical and morphological properties and their source as well as the mechanisms of their formation and dissipation in the environment ([Binette, 2000](#)).

X-ray fluorescence is a non-destructive analytical technique used to determine the elemental composition of materials. XRF analyzers determine the chemistry of a sample by measuring the fluorescent (or secondary) X-ray emitted from a sample when it is excited by a primary X-ray source. Each of the elements present in a sample produces a set of characteristic fluorescent X-rays that is unique for that specific element. XRF analysis determines the elemental composition of a sample but does not provide information about how the various elements are combined together. Such mineralogical information is only available through X-ray diffraction ([Shackley, 2010](#)).

X-ray Diffraction (XRD) can determine the presence and amounts of minerals species in the sample, as well as identify phases. an atom can scatter x-rays, and if many atoms are together then the scattered waves from all the atoms can interfere. If the scattered waves are in phase (coherent), they interfere in a constructive way and we get diffracted beams in specific directions ([Suryanarayana & Norton, 1998](#)). These directions are governed by the wavelength of the incident radiation and the nature of the crystalline sample. Bragg's law, formulated by ([Bragg & Bragg, 1913](#)), relates the wavelength of the x-rays to the spacing of the atomic planes.

To derive Bragg's law, we begin by assuming that each plane of atoms partially reflects the incident wave much like a half-silvered mirror.

The samples are analyzed by X-ray diffraction, using a diffractometer its principle is based on the selective reflection of X-rays by a crystal, using Bragg's law ([Faouzia, 2014](#)):

$$\lambda = 2d \sin \theta \ \text{........ } Eq\ 22$$

where:

λ: The wavelength of the incident beam ($\lambda = 1.54181 A°$)

d: The interreticular distance between the diffracting planes.

θ: The angle between the incident beam and the diffracting planes. The domain of the angle (2θ) is between $10°$ and $80°$.

II.1.3.3. Chemical characterization

The chemical properties are all that is related to determining the functional groups of activated carbon, either by infrared imaging or by using Boehm method, in addition to determining its pH at zero points.

II.1.3.3.1.   Studies on point of charge

The pH_{ZPC} is a value of zero net surface charge (zero electric charge) is a convenient measure of the tendency of the activated carbon surface to become either positively or negatively charged as a function of pH.

For the pH_{ZPC} determination, N_aCl solution is prepared and placed in a closed bottle. The pH is adjusted at different values between 2 and 12 by adding HCl or N_aOH 0.1 mol.l^{-1} solution. A specific mass of the sample is added to the closed bottle and then is set stirring for 24h ([Daoud & Benturki, 2014](#); [Villacanas, Pereira, Orfao, & Figueiredo, 2006](#)), or 48h ([Boudrahem et al., 2019](#); [Reffas et al., 2010](#)) or 5 days ([Belaid, Bebba, Sekirifa, Baameur, & Al-Dujaili, 2017](#); [Bernal, Giraldo, & Moreno-Piraján, 2018](#)) at room temperature before measuring the final pH.

 After the final pH of the solution is measured. Thus, the curve $pH_i - pH_f = f(pH_i)$ is drawn. The point of intersection between this curve and the line of equation x = 0 gives the pH at the zero point charges of the active carbon considered.

31

II.1.3.3.2. Study of surface functional group

Although the previously mentioned properties (specific surface and porosity) play a key role in the adsorption capacity on activated carbon, it is the functional groups present on the surface of activated carbon that mainly influence the absorption capacity (Menéndez-Díaza & Martín-Gullón, 2006). The most commonly identified surface functional groups are oxygen functions, formed when the activated carbon is treated with an oxidizing agent. These treatments create three types of surface oxides: acidic, basic, and neutral. Oxidation processes increase the surface concentration of these chemical groups. The main acidic groups forming part of the surface composition of activated carbon are the carboxyl, lactone, hydroxyl/phenol, carbonyl functions (Djidel, 2011).

The surface functions are determined by the Boehm method (Bamba et al., 2009).

The Boehm method: For the determination of the surface functions of the acid type, we put a specific mass of activated carbon in contact with 0.1 N solution of $NaHCO_3$, Na_2CO_3, NaOH, and HCl, in the case of Na_2CO_3, a half volume of the other reaction bases was used to make the solution in the same equivalence of the base (Kim, Yang, Lim, Kim, & Park, 2012).

The three bases ($NaHCO_3$, Na_2CO_3, or NaOH) allowing us to classify the surface groupings of the acidic groups: $NaHCO_3$ (for carboxylic group (−COOH) neutralization), Na_2CO_3 (for carboxylic and lactonic groups (−COO−) neutralization) and the strongest base NaOH (for the three organic functions "carboxylic, lactonic, and phenolic (−OH) groups") (Nzihou, 2020). As well as the basic functions, neutralize by HCl solution.

The solution is stirred for 72 hours and allowed to settle and then filtered. The titration with a solution of HCl (0.1 N) or NaOH (0.1 N), as appropriate (Bamba et al., 2009), allows each type of function to be quantified using the following formula:

$$N_{CSF} = \frac{N_{eq}}{m} = \frac{C \times V \times Z}{m} \ldots\ldots Eq\ 23$$

With: N_{CSF} (meq.g^{-1}) the amount of functional groups on the surface of the carbon that reacted with the base during the mixing step, N_{eq} (meq) the number equivalent

reacted, C concentration (N), V volume (ml) , Z number equivalent (eq) ([Kim, Yang, Lim, Kim, & Park, 2012](#)).

II.1.3.3.3.   FT-IR analysis

The discovery of the near-infrared region can be attributed to William Herschel for his work presented in April 1800 "Experiments on the Refrangibility of the invisible Rays of the Sun" ([Herschel, 1800](#)), Infrared spectrometry is a destructive analysis method, based on the study of the absorption by the sample of electromagnetic radiation with wavelengths λ, the absorptions in this area form a sort of spectral imprint of the compounds characteristic of the interatomic bonds that compose it ([Coates, 2006](#); [Djidel, 2011](#)).

In the near and middle infrared, the absorption of light originates from the interaction between the radiations of the light source and the chemical bonds, the absorption of radiation in this area causes vibrations and molecular rotations. These vibrations are essentially localized in the functional groups but do not reach the rest of the molecule; such functional groups can thus be identified by their absorption band ([Coates, 2006](#); [Djidel, 2011](#)).

II.1.3.4. Pollutant adsorption

Adsorption experiments of the pollutant are carried out using batch equilibration.

- Solutions of pollutants are prepared in different ranges of concentration.
- Adding these solutions to flasks containing a specific mass of activated carbon sample, are sealed and shaken until equilibrium is reached.
- The conditions are changed according to the type of study, such as mass, time, concentration, temperature...etc.
- The solution is separated from the adsorbent;
- The samples are analyzed by UV-Visible spectrophotometry;
- The percentage removal of pollutants and uptake at equilibrium adsorption on a solid phase is calculated.
- Then the different curves are created for the characterization of the samples in terms of the effect of mass, concentration, time, temperature, etc, and discussion of results ([Bansal & Goyal, 2005](#); [Sun, Meunier, & Baron, 2005](#)).

II.1.4. Activated carbon demand

The demand for activated carbon continues to increase in all areas of gas and liquid processing. Due to the multiple challenges faced in the worrying pollution of the environment around the world that everyone has to face, this will make the demand for activated carbon very important in the future (Koller, 2001).

II.1.5. Application of activated carbon

- water treatment including drinking water; wastewater and groundwater treatment (Ahmed, 2016);
- Gas recovery applications;
- Solvent recovery applications;
- Industrial respirators;
- Elimination of odors (refrigeration);
- Cigarette filters;
- Filter cartridges (air purification, water filters);
- Mineral recovery (gold extraction);
- Activated Carbon Adsorption Applications;
- Food Processing;

- The discoloration of sweet juices and vegetable fats;
- Decolorization of Oils and Fats;
- Sugar Industry;
- Chemical and Pharmaceutical Industries;
- Heavy metals extracted;
- Purification of Electrolytic Baths;
- Refining of Liquid Fuels;
- Recovery of Organic Solvents;
- Nuclear Technology;
- Vacuum Technology;
- Medicinal Applications;
- Gas Storage;
- Air conditioning (Koller, 2001).

Chapter II. Experimental section

I. Introduction

Activated Carbons (ACs) are high surface area and porous material, they have been widely used as an adsorbent for separation, purification, decolorization, and deodorization of vegetable oils and fats, water purification and pollution treatment...etc. ACs can be prepared from many organic materials having a high content of carbon (animal or vegetable materials).

The date palm (scientific name: Phoenix dactilifera) plays a very important economic, social, and ecological role for the people of arid and semi-arid regions. It is directly or indirectly a source of life, through the production of dates and thru the assorted uses of its by-products for the benefit of oasis residents and their herds.

The increasing demand for more sustainable and renewable materials has increased the interest in natural fibers. Natural fibers aren't only environmentally friendly, but they even have high specific properties, due to their lightweight.

In fact, palm trees provide food (fruits, sugars, drinks), certain construction materials (stipe, leaves), and fibers for various uses (clothing, decorative objects, etc.). There are four parts that contain different types of fiber of the date palm, namely, the midribs, spadix stems, leaflets, and mesh (Elseify, Midani, Shihata, & El-Mously, 2019).

Algeria is one of the most important dates-producing countries in the world. The number of date palm trees is estimated to be more than 20 million. The high number of date palm results in huge quantities of by-products of annual pruning, what makes it one of the foremost available sources of natural fibers. This has little economic value and is sometimes disposed of as waste or burnt and this could be harmful to the environment. The plenty and easy availability of agricultural by-products make them good sources as the raw materials for AC production. Lastly, these agricultural by-products are usually low-cost and their effective use is desirable.

In this work, we've prepared activated carbon by the physical activation of Ouargla-Algeria date palm fiber from the mesh using carbon dioxide. While many techniques have been used for the characterization of activated carbons.

II. Sample preparation

a) **Materials:** A crusher (ACHTUNG-WARTING), a sifter FRITSH, a vertical oven (Réf. BGVA12-300b de CARBOLITE, R-U), an oven.

b) **Products:** Raw material (Date palm fiber), Distilled water, CO_2, N_2.

Date palm fiber: The date palm tree, a member of the palm tree family (phoenix dactylifera), normally exists in the Middle East, the Canary Islands, Northern Africa, Pakistan, India, and the United States (California).

There are more than 100 million date palm trees in the world and each tree can live for more than 100 years. The perfect use of fibers surrounding the stem of date palm trees as reinforcement in polymeric materials has been reported in few studies 93-100. The palm tree stem is covered with a mesh made of single fibers. These fibers create a natural woven mat of crossed fibers of different diameters. Traditionally the mat is removed from the trees and cleaned to make ropes and baskets in many parts of the world. However, these applications account for a small percentage of the total potential world production (Al-Kaabi, Al-Khanbashi, & Hammami, 2004; Dixit & Yadav, 2019).

Image II-1: Date palm tree

➢ **Vernacular names:**
- Arab: Nakhla.
- Greek: Phoenix.
- English: Date.
- Italian: Datter.
- Hindu: Khajur, Pinda

c) **Methods**

➢ **Precursor used and sampling**

In order to promote local by-products, we used as a precursor date palm fiber from the mesh part of Ouargla region (South East Algeria), we chose the palm tree of Ghars variety.

> ➢ **The pretreatment**

Palm waste, namely date palm fiber Ghars, was obtained from an oasis of date palms in Ouargla, Algeria, the fibers was washed with distilled water to remove all dirt and dust in its original particle size followed by filtration and then dried at room temperature 105 °C. After drying, they were crushed Annexe 1 and sieved Annexe 2. The fractions between two sets (250µm <d <500µm) and (45µm <d <125µm).

Image II-2: The steps of the pretreatment

> ➢ **The pyrolysis procedure**

The pyrolysis was performed at 500°C for two hours under N_2 flow 250 mL.min^{-1} and heating rate of 5°C.min^{-1} during a vertical furnace (Ref. BGVA12-300B, CARBOLITE), 75 g of crushed data palm fiber are introduced during a cylindrical quartz cell with an internal diameter of 40 mm including a frit disc at half-height (Sekirifa, 2013).

1: Gas inlet (nitrogen or CO_2);
2: Residue recovery system (such as gas) at the outlet);
3: Quartz cell (sample holder);
4: Vertical tube furnace (M. L. Sekirifa et al., 2013).
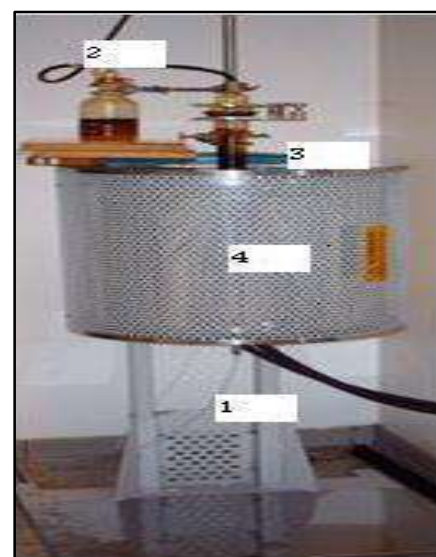
Image II-3: vertical furnace
(Ref. BGVA12-300B,

> ➢ **The activation procedure**

The resulting pyrolysis date palm fiber samples were activated at 600°C for 2 hours using the same assembly. The carbon dioxide flow rate was maintained at 250 mL.min^{-}

[1] and heating rate of $5°C.min^{-1}$. The pyrolysis and activation conditions of the samples are shown in table II-1.

Table II-1 : The pyrolysis and activation conditions of the ACs.

| Raw materials | Granularities | Samples | Pyrolysis conditions | | | | Activation condition |
			Temperature (°C)	Duration (hour)	Flow rate (N_2) (ml.min^{-1})	heating rate (°C.min^{-1})	
RF$_1$	(250µm<d<500 µm)	ACF$_1$	600	2			600°C, 2 h, 250 ml.min^{-1} (CO_2), 5°C. min^{-1}
		ACF$_2$	500	2			
RF$_2$	(45µm<D<125 µm)	ACF$_3$	500	1	250	5	
		ACF$_4$	500	2			
		ACF$_5$	500	3			

III. Characterization

Activated carbons are uniquely complex in terms of the size, shape, and variability of their porosity. Their complete characterization, accordingly, is a major challenge to the surface chemist. The techniques of adsorption from gaseous and liquid phases, kinetics and energetics, assessments of surface polarities, and X-ray and neutron scattering need to be combined to provide a complete characterization, we tried to examine most of the methodologies (Villacanas et al., 2006).

The main techniques and devices used for the characterization of samples are the following:

Table II-2: The main techniques and devices used

The technique	The device	Objective
BET Surface Area Analysis	The ASAP 2010 (Micromeritics)	The porous structure
Electron microscopy technique	Scanning Electron Microscopy (SEM)	Morphology
Zero point of charges (pH$_{ZPC}$)	pH meter	Indicates the acid or basic character
Boehm titration:	pH meter	Surface chemistry characterization (acidity–basicity)
Fourier transform infrared spectroscopy (FT-IR)	Infrared spectroscopy (CARY 600)	Identification of the functional groups
The adsorbing capacity	UV-Visible (cary 100)	Evaluation of the adsorption capacity

III.1. Physical characterization

This part summarizes the physical structural characteristic (The BET, the external and micropore surface, meso, micro, and total pore volume, and the image microscopic) of the activated carbon samples and their relationship and influence to each other using different techniques such as the burn-off, the N_2 adsorption-desorption, and the Scanning electron microscope.

III.1.1. Burn-off of activated carbon fiber

The burn-off for the ACF derived from date palm fiber Ghars was analyzed to determine the effect of activation time on pore development. It was calculated on the basis of the following equation:

$$Burn - off\,(\%) = \frac{m_i - m_f}{m_i} \times 100\% \qquad ....Eq\ 24$$

Where mi and mf are the initial and final mass (g) of ACF, respectively.

It can be seen from Table II-3 that the burn-off for ACF_1, ACF_2, ACF_3, ACF_4 and ACF_5 samples are 82.38, 95.73, 93.7, 93.54 and 92.96 wt %, respectively. With the decrease in pyrolysis temperature from 600°C for ACF_1 to 500°C for ACF_2, the burn-off increased from 82.38 to 95.73 wt %. The values of burn-off for ACF_3, ACF_4 and ACF_5 decreased from 93.7 to 93.54 and 92.96 wt %, respectively, as duration time increased from 1 h to 3 h. In addition, the values of burn-off of ACF_2 and ACF_4 decrease from 95.73 to 93.54 wt%, respectively, as the granularity decrease from (250µm<d<500µm) to (45µm<d<125µm).

These results suggested that the lower the temperature and duration of pyrolysis and the larger the sample size, the burn-off increase. The rise in burn-off suggested the elimination of more volatile organic species that eventually improved the ACF's pore growth (Mohamed L. Sekirifa et al., 2013). Porosity enhancement may increase the surface area of the ACF and thus affect the ability of adsorption. It is apparent that despite lower yield, high burn-off is the vital aim to produce highly porous ACF for the effective adsorption process (Ooi, Cheah, Sim, Pung, & Yeoh, 2017).

Table II-3: Characteristics of activated carbon.

Characteristics of activated carbon

Activated carbons	Burn-off (%)	The specific surface area (m²·g⁻¹)							Total pore volume (cm³·g⁻¹)				Pore diameter (nm)			$\frac{S_{micro}}{S_{BET}}$	$\frac{V_{micro}}{V_t}$
		Single point	BET	Langmuir	t-plot		BJH		Single point	t-plot	BJH		D_p	BJH			
					S_{micro}	S_{EXT}	Adsorption cumulative	desorption cumulative	V_t	V_{micro}	Adsorption cumulative	desorption cumulative	BET	Adsorption cumulative	desorption cumulative		
ACF$_1$	82.38	288.46	278.22	368.04	241.22	36.99	15.43	0.208	0.13	0.11	0.01676	0.00341	1.92	4.346	65.58	0.87	0.84
ACF$_2$	95.73	325.65	313.40	414.75	275.47	37.94	15.46	0.923	0.15	0.13	0.02863	0.01743	1.93	7.406	75.48	0.88	0.85
ACF$_3$	93.70	172.07	166.29	220.72	136.56	29.73	15.01	7.795	0.09	0.06	0.03144	0.02116	2.11	8.376	10.86	0.82	0.72
ACF$_4$	93.54	175.07	168.13	222.40	154.25	13.88	18.84	14.051	0.08	0.07	0.04	0.03268	1.89	8.494	9.30	0.92	0.90
ACF$_5$	92.96	212.89	205.53	272.49	170.26	35.26	3.93	1.356	0.11	0.08	0.02699	0.02619	2.10	27.46	77.23	0.83	0.73

Table II-4: The D-R parameters

Properties	Methods	ACF$_1$	ACF$_2$	ACF$_3$	ACF$_4$	ACF$_5$
W$_0$ (cm³·g⁻¹)		0.11	0.12	0.07	0.07	0.08
L (nm)	D–R plot	0.88	0.77	1.11	0.64	1.03
E$_0$ (kj·mol⁻¹)		23.64	25.43	21.11	28.19	21.85

III.1.2.   Gas adsorption method (N_2 adsorption-desorption)

The activated carbon samples were prepared at the optimized conditions in order to get the best characteristics for the date palm fibers Ghars. The optimized conditions for the CO_2 activation are an activation temperature and time of 600°C, 2 h respectively, and a CO_2 flow and heating rate of 250 ml.min^{-1}, 5°C.min^{-1}respectively, with the change in the conditions of pyrolysis to determine the extent of its impact. The N_2 adsorption-desorption isotherms obtained with the different activated carbons at 77K experiment was performed to characterize the pore structure of the ACF samples.

The textural of activated carbons was characterized by using N_2 adsorption-desorption isotherms measurements at liquid nitrogen temperature (77 K) using the ASAP 2010 (Micromeritics).

The BET specific surface areas (S_{BET}) were calculated by using the BET method (Brunauer, Emmett, & Teller, 1938) assuming that the surface area occupied by nitrogen molecule was 0.162 nm^2. The total pore volume was estimated on the basis of the liquid volume of nitrogen adsorbed at a relative pressure of $p/p_o = 0.97$. The micropore volume (pores < 2 nm) L(nm) was determined according to the Dubinin-Rad ushkevich equation (Dubinin, 1947). The microporous surface (S_{micro}) and external surface (S_{ext}), as well as the micropore volume (V_{mic}) was evaluated by the t-plot method. BJH method (Barrett, Joyner, and Halenda) is a procedure for calculating pore size distributions from experimental isotherms using the Kelvin model of pore filling (Bamba et al., 2009). The mesopore volume (V_{mes}) was obtained by deducting the micropore volume from the total pore volume. The average pore diameters were estimated from the BET surface area and total pore volume ($D_p = 4V_{tot}/S_{BET}$) assuming an open-ended cylindrical pore model without pore networks (Boudrahem et al., 2019).

Details of the texture properties of the carbon materials produced are summarized in Table II-3. The surface area and pore volume of activated carbon prepared of the optimum condition was 313.40 m^2.g^{-1} and 0.15 cm^3.g^{-1}, respectively for the sample ACF$_2$. The specific surface area of ACF's has been observed by the BET method. The BET surfaces areas for ACF$_1$, ACF$_2$, ACF$_3$, ACF$_4$ and ACF$_5$ samples are 278.22, 313.40, 166.29, 168.13 and 205.53 (m^2.g^{-1}) respectively. The BET surface area

increased with the decrease in the pyrolysis temperature and the increase in the duration of pyrolysis and the granularity of samples.
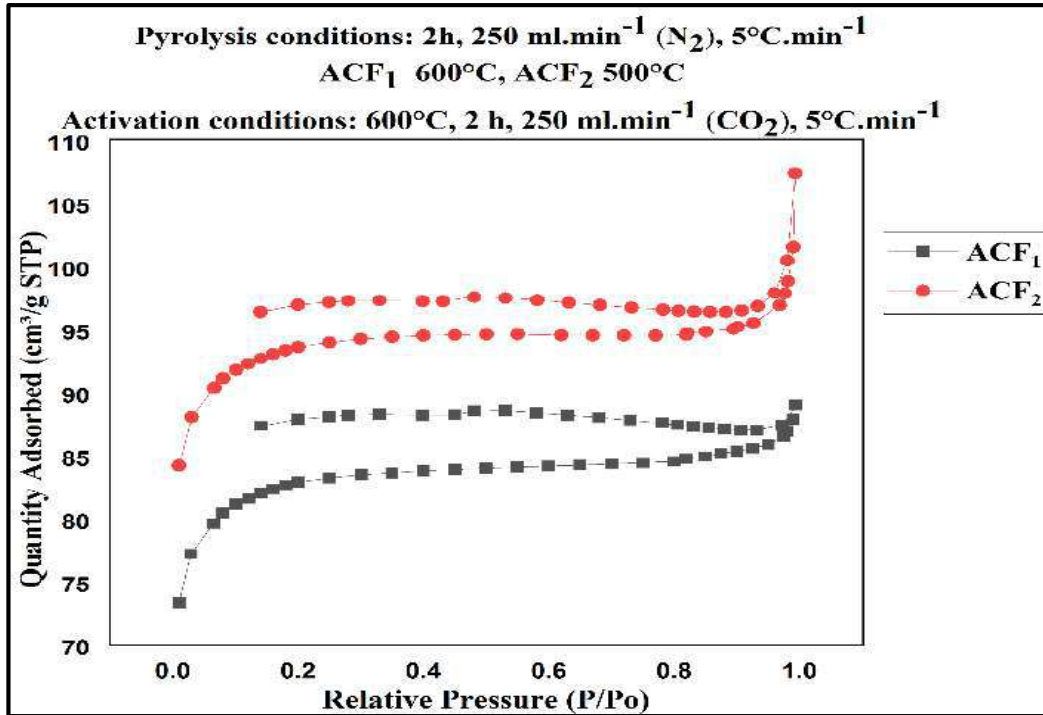

Figure II-2: Isothermal adsorption of N_2 at 77 K on activated carbon (Effect of the pyrolysis temperature on the quantity adsorbed)
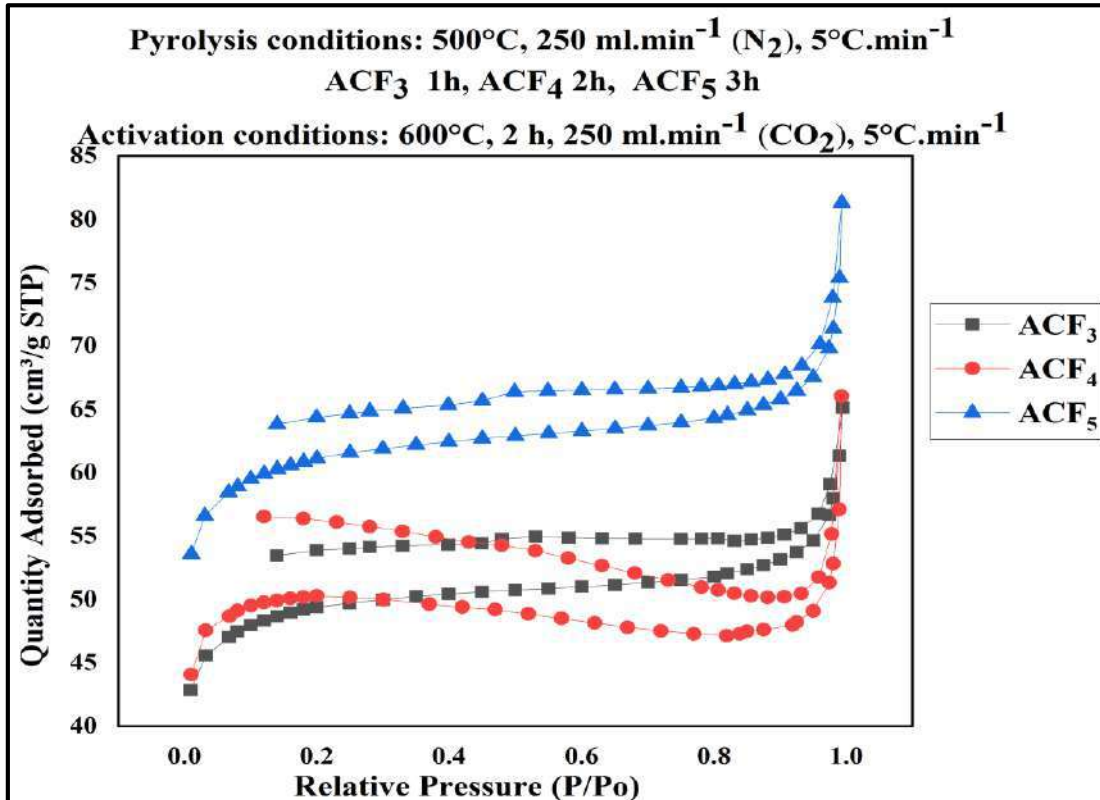
Figure II-1: Isothermal adsorption of N_2 at 77K on activated carbon (Effect of the duration of pyrolysis on the quantity adsorbed)

42
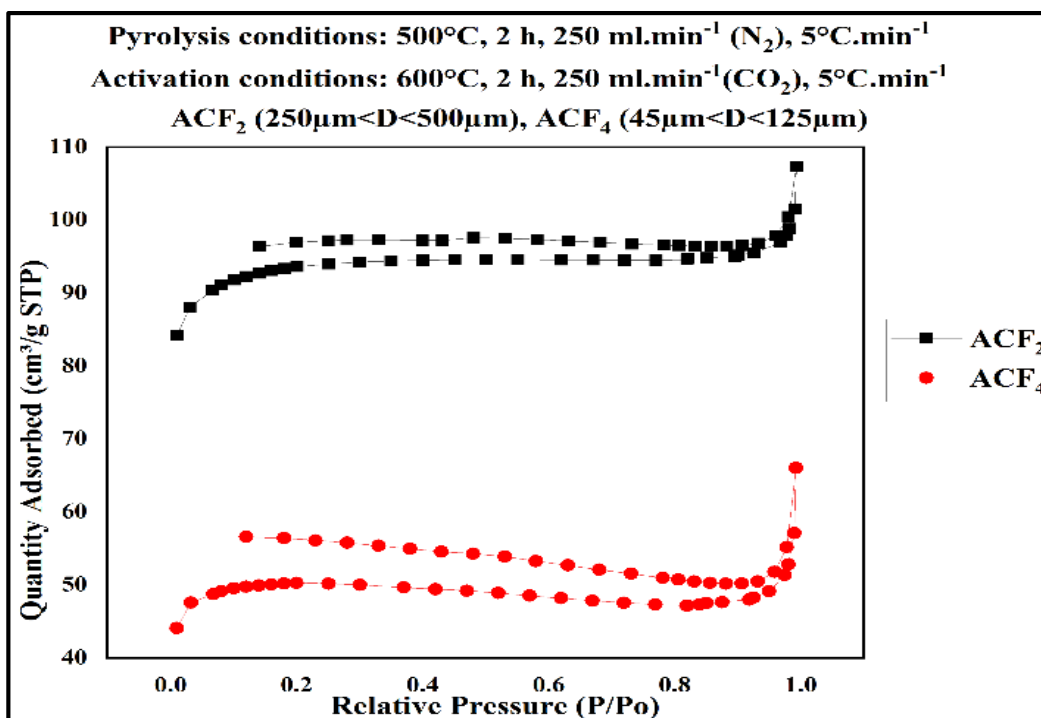
Figure II-3: Isothermal adsorption of N_2 at 77 K on activated carbon (Effect of particle size on the quantity adsorbed)

In order to further clarify the effect of different conditions, we have combined the curves of the N_2 adsorption-desorption isotherm that have a change in the factor, whether pyrolysis temperature, pyrolysis time, or sample size, so we have three different figures II-1, II-2, and II-3 with different effect conditions, Those figures show the effect of the pyrolysis temperature, the effect of particle size, the effect of the duration of pyrolysis on the quantity adsorbed, respectively, we observe that the increase in the volume of nitrogen adsorbed is related to the changing in the pyrolysis temperature, the particle size, and the duration of pyrolysis; Because through the figures we notice that the lower the pyrolysis temperature, and the greater the duration of pyrolysis, and the larger the particle size, the quantity of adsorbed increase. All isotherms of the activated carbons series present dense micropore structures (dimensions < 2 nm), which belong to type I according to IUPAC classification (K. S. W. SING et al., 1985), This isotherm reflects a relatively strong interaction between the adsorbate and the adsorbent, a monolayer adsorption corresponding to the filling of micropores with saturation when the available volume is completely filled. It is fully reversible over the entire pressure range (Belaid, 2017; Leinekugel-le-Cocq, 2004).

The presence of small hysteresis (H4) shape in the desorption curve indicated the presence of mesoporosity associated with a small contribution of the mesopore and the

possible occurrence of a capillary condensation phenomenon. In addition, it was suggested that the carbon products contained mostly microspores (Belaid et al., 2017), The nitrogen uptake amount for the ACF samples increased rapidly up to a relative pressure (P/Po) of 0.2 before a plateau was achieved, the amount of nitrogen uptake for the ACF_2 sample is much higher than those for the other ACF samples. The result suggested that the ACF_2 sample contained relatively larger amount of micropores compared to other ACF samples.
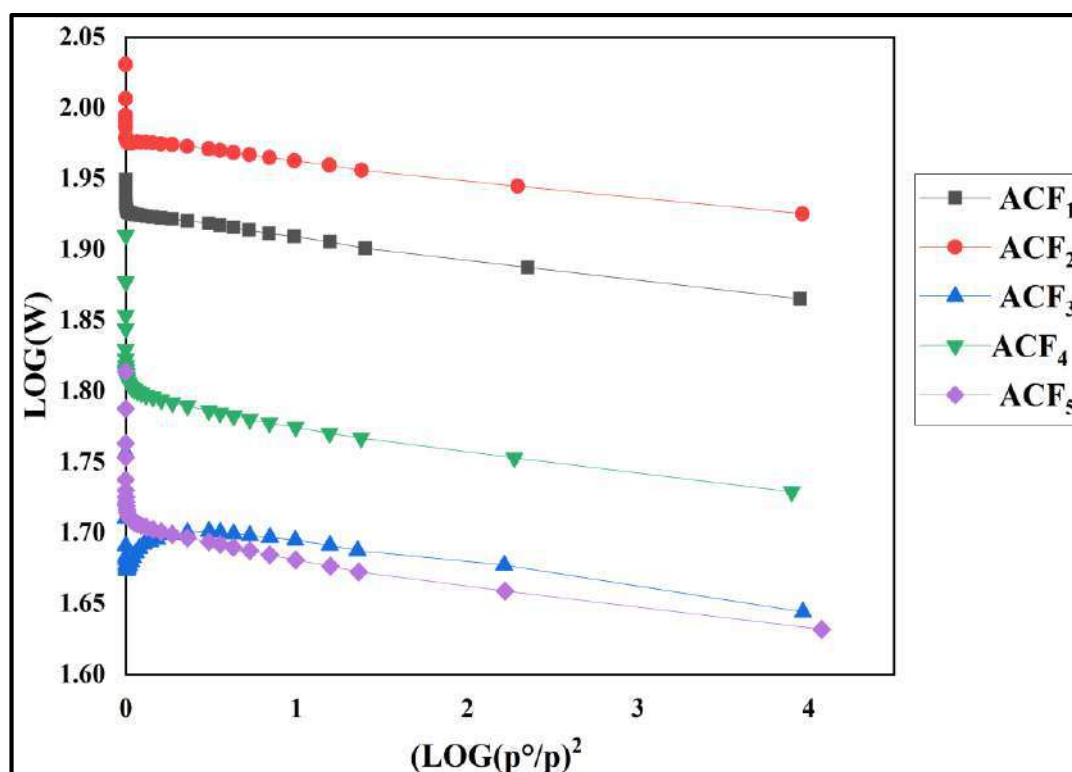
Figure II-4: the D-R isothermal equilibrium model.

D–R data of the isotherms of nitrogen adsorption of all AC are shown in Figure II-4. The texture parameters of the D-R isothermal equilibrium model are summarized in Table II-4. The micropore size (L) of the samples ACF_1, ACF_2, ACF_3, ACF_4 and ACF_5 was 0.88, 0.77, 1.11, 0.64, 1.03 nm and the mean activation energy was 24 kJ mol^{-1} corresponding to chemisorption.

Figure II-5 showed the material's pore size distribution data, those data indicate that due to the sharp increase in pore size distribution values for pore diameters less than 2 nm, all activated carbons are microporous materials, which indicates that most pores have existed in the range of 2-50 nm. This result is confirmed in the microporous and

mesoporous volumes, corresponding to 81% of the average microporosity, compared with 19% of the average mesoporosity.
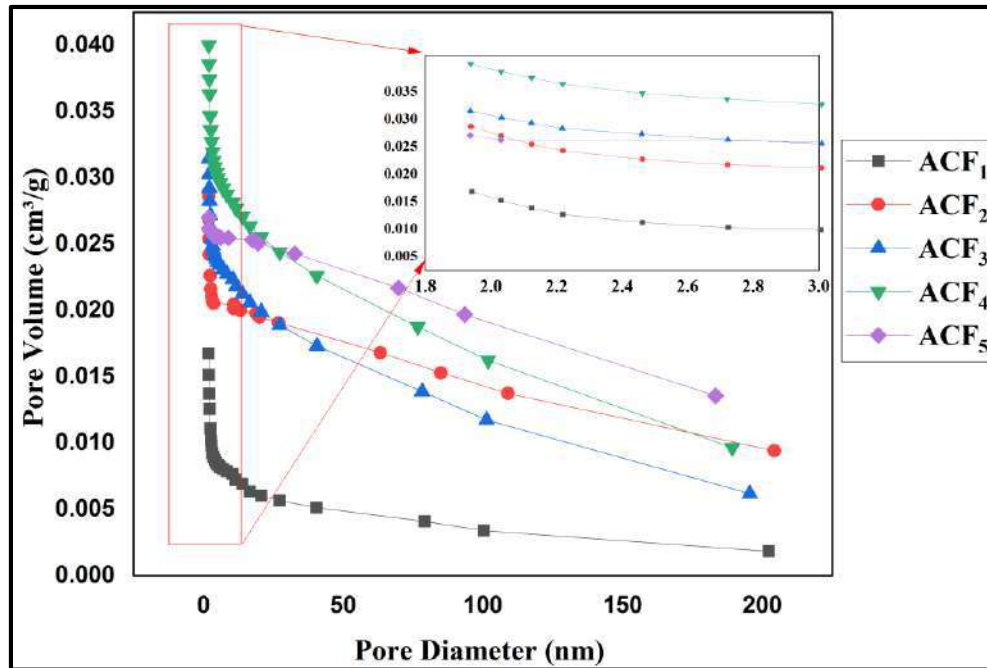
Figure II-5: Pore size distribuions.

III.1.3.   Scanning Electron Microscope (SEM)

The micrographs were obtained with a SEM (EVO ZEISS 15) equipped with a secondary electron detector (SE1). Micrographs were obtained under an acceleration voltage of 20 KV with a 1.00 Kx magnification to estimate the surface pore structure of the ACs.

Image II-4 show SEM micrographs of the ensemble of both types of raw fiber, RF_1 and RF_2 and all type of AC ACF_1, ACF_2, ACF_3, ACF_4 and ACF_5, respectively. Image II-4 (a) and Image II-4 (d) show the disparity between RF_1 and RF_2 respectively, that is due to the particle size which is clearly seen in the micrograph picture, in addition what show the fibers are cylindrical with their non-smooth outer surface and filled with some artificial impurities (sand and dust) and residual lignin (Alhijazi, Zeeshan, Safaei, Asmael, & Qin, 2020). The micrographs clearly demonstrate that, since there is a clear difference in the microstructure of these ACs, the difference in granularity affects the resulting AC.

45
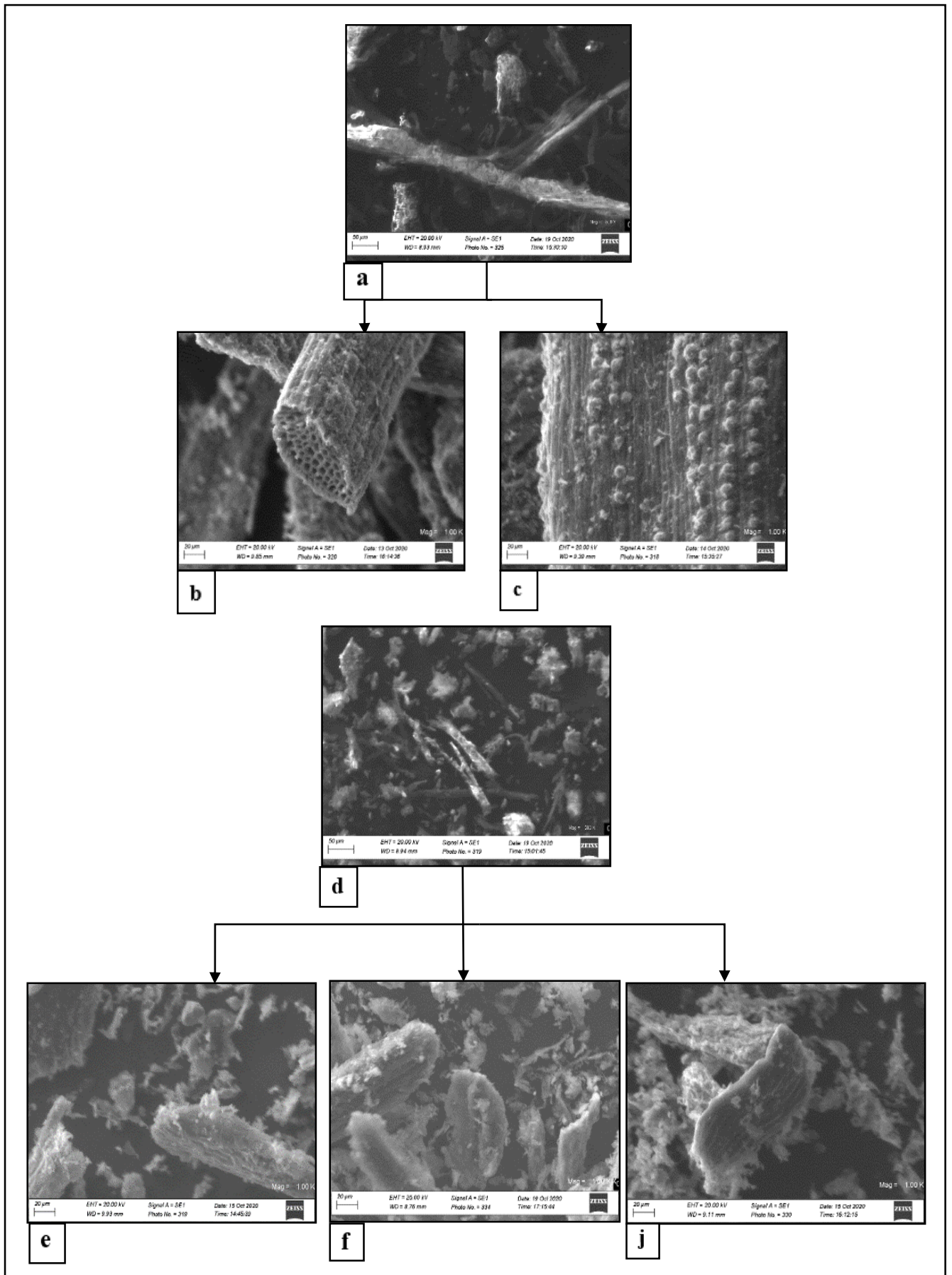
Image II-4: SEM micrographs of (a) RF_1, (b) ACF_1, (c) ACF_2, (d) RF_2, (e) ACF_3, (f) ACF_4 and (j) ACF_5

Image II-4 (b) show a cross-section for ACF_1, where the microstructural observation showed that the surface area was elliptical, almost circular in shape, and ACF_1 shows a series of multicellular fibers with central voids (lumen) in each. The multicellular fibers (individual fibers) are compactly arranged to form a technical fiber whose shape is roughly cylindrical with a smaller diameter in the range of 1-7 μm, aligned and bound together by lignin, pectin and other non-cellulosic materials (Alhijazi et al., 2020).

The surface (longitudinal direction) SEM micrograph for ACF_2 and ACF_4 is shown in the Image II-4 (c) and f. On the surface of both ACs, the presence of certain impurities randomly distributed is observed. The fiber structure is oriented in the direction of the fiber axis, stacked and compacted in the form of microfibers so that they appear in layers (Boumediri et al., 2019).

However, in Image II-4 (e) and Image II-4 (j) for the samples ACF_3 and ACF_5 respectively the SEM images showed the ACs structure in the form of nanometer hills on the surface allowing active sites to be formed in order to enhance the process of adsorption, the SEM images did not vary significantly between them and had almost the same morphology.

The images of SEM micrographs of both raw materials and samples of AC showed that porosity and broad surface area for adsorption were produced by carbonization through pyrolysis and activation processes, thus aligned with the literature that is the objective of AC processing.

III.1.4.   X-ray Diffraction and fluorescence XRD/XRF

The degrees of crystallinity of the activated carbon samples were determined by the X-ray diffraction method using X-ray diffraction "OLYMPUS BTX-716 Benchtop XRD" diffractometer equipped with Cu-Kα radiation (λ = 1.540598A°). The generator was operated at 40 kV voltage and 30 mA current. the samples were mounted on a sample holder and scanned from 0° to 60° (2θ angle range) at a scan rate of 2°/min.

The crystallinity index CI was calculated using the amorphous subtraction as the ratio between the area of the crystalline contribution and the total area (Park, Baker, Himmel, Parilla, & Johnson, 2010; Segal, Creely, Martin Jr, & Conrad, 1959):

$$Crystallinity\ index\ CI = \frac{Area\ of\ all\ the\ crystalline\ peaks}{Area\ of\ all\ crystalline\ and\ amorphous\ peaks}\ ....Eq\ 25$$

Figure II-6 show the XRD spectra of raw fiber, ACF_1, ACF_2, ACF_3, ACF4, and ACF_5, and the results of the crystallinity index CI are presented in Table II-5.
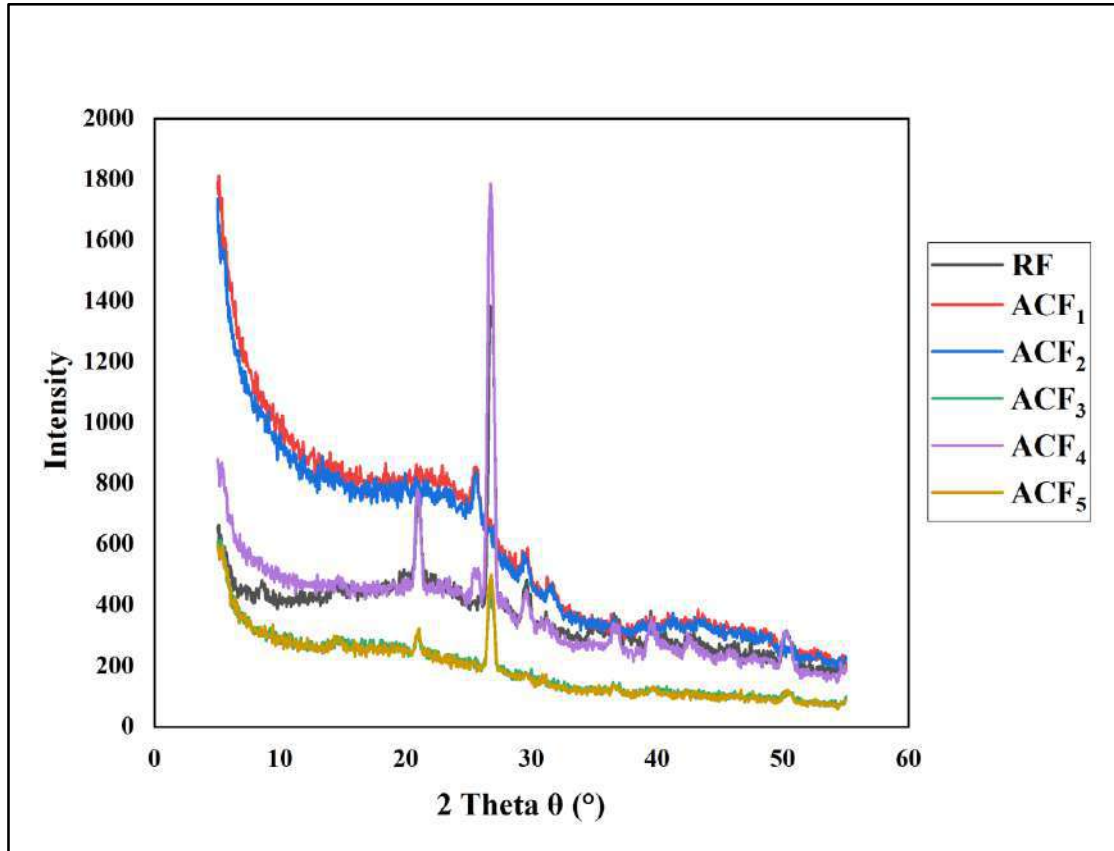
Figure II-6: The XRD spectra of raw fiber, ACF_1, ACF_2, ACF_3, ACF_4, and ACF_5.

Table II-5: The crystallinity index CI of each XRD spectra.

Samples	The crystallinity index CI
RF	31.86
ACF_1	7.25
ACF_2	8.25
ACF_3	22.47
ACF_4	27.71
ACF_5	21.18

From Figure II-6, it can be observed that the major crystalline peak for each sample occurs around $2\theta = 22°$, and $26°$, which represents the cellulose crystallographic plane (Galiwango, Rahman, Al-Marzouqi, Abu-Omar, & Khaleel, 2019). The crystallinity index (CI) was calculated for the different cellulose samples using amorphous subtraction (Park et al., 2010) and found to be 31.86% for raw fiber RF, which is the largest value compared to the other samples and is very close to the sample ACF_4 with (27.71%) indicate that it had almost identical diffraction patterns and relative crystallinities, and the samples with the smallest value are ACF_1, ACF_2 with (7.25%, 8.25%), and the rest of the samples for ACF_3 and ACF_5 with (22.47%, 21.18%) respectively, indicating the activated carbon samples had amorphous structure compared to the RF (Elseify et al., 2019). From the previous, we can conclude that date palm fibers before and after carbonization does not have the same crystallinities structure.
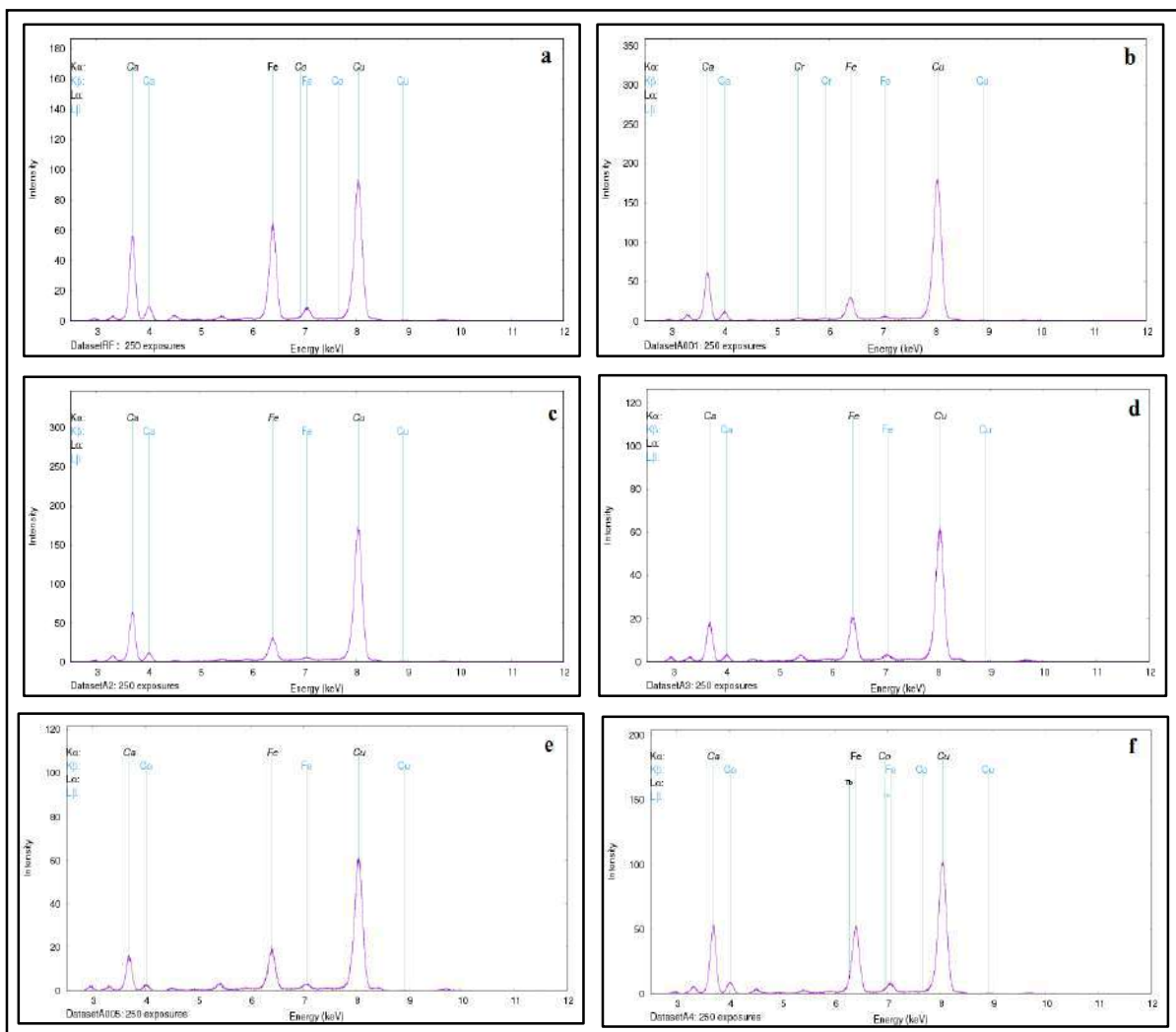
Image II-5: The XRF spectra of (a) raw fiber, (b) ACF_1, (c) ACF_2, (d) ACF_3, (e) ACF_4, and (f) ACF_5.

The raw fiber and activated carbon samples were subjected to XRF to analyze the chemical composition of elements present in the samples.

Image II-5 show the XRF spectra of (a) raw fiber, (b) ACF_1, (c) ACF_2, (d) ACF_3, (e) ACF_4, and (f) ACF_5. The raw fiber and the activated carbon samples consist of the common elements such as calcium (Ca), Iron (Fe), Copper (Cu) in major quantities while other minerals are present in trace amounts, a small amounts of Cobalt (Co) in raw fiber and ACF_5, Chromium (Cr) in ACF_1, and the existence of Terbium (Tb) only in ACF_5, this confirms the chemical analysis of samples.

III.2.   Chemical characterization

The chemical properties are all that is related to determining the functional groups of activated carbon, either by infrared imaging or by using Boham's method, in addition to determining its pH at zero points.

There is a variety of techniques for the surface chemistry characterization of activated carbons (Villacanas et al., 2006). However, the pH_{pzc} (carbon pH at its zero point of charge) indicates the acid or basic character of the carbon surface, while the surface chemistry characterization (acidity–basicity) of the activated carbon was performed with Boehm titration. Fourier Transform Infrared Spectroscopy (FT-IR) to identify its surface functional groups both qualitatively and quantitatively.

III.2.1.   Studies on point of charge

The pH nature of the AC samples was determined according to the ASTM D6851 method by mixing AC with deionized water with the pH measured by the pH meter after one day at 25°C.

The pH value required to give zero net surface charge (zero electric charge) is a convenient measure of the tendency of the AC surface to become either positively or negatively charged as a function of pH (Ahmed, 2016; González-García, 2018).

This value is designated as the point of zero charge of AC samples (pzc) (pH_{pzc}), this method was conducted to determine the pH_{pzc} of AC of date palm fiber, and it was measured as follows: 2 l of 0.1N NaCl was prepared and divided into 40 flasks each one containing 50 mL solutions. Then, their pH values were adjusted between 2 and 12 with the addition of 0.1 N solution of HCl or NaOH. pH of initial solutions was

measured with a pH meter and then noted as $pH_{initial}$. After the constant value of $pH_{initial}$ had been reached, 0.15 g of AC sample was added into each flask and then shaken. for 5 days at 25℃. After 5 days, pH of the solution was measured and noted as pH_{final}. Thus, the curve pHi - pH_f = f (pHi) was draw. The point of intersection between this curve and the line of equation x = 0 gives the pH at the point of zero charges of the active carbon considered.
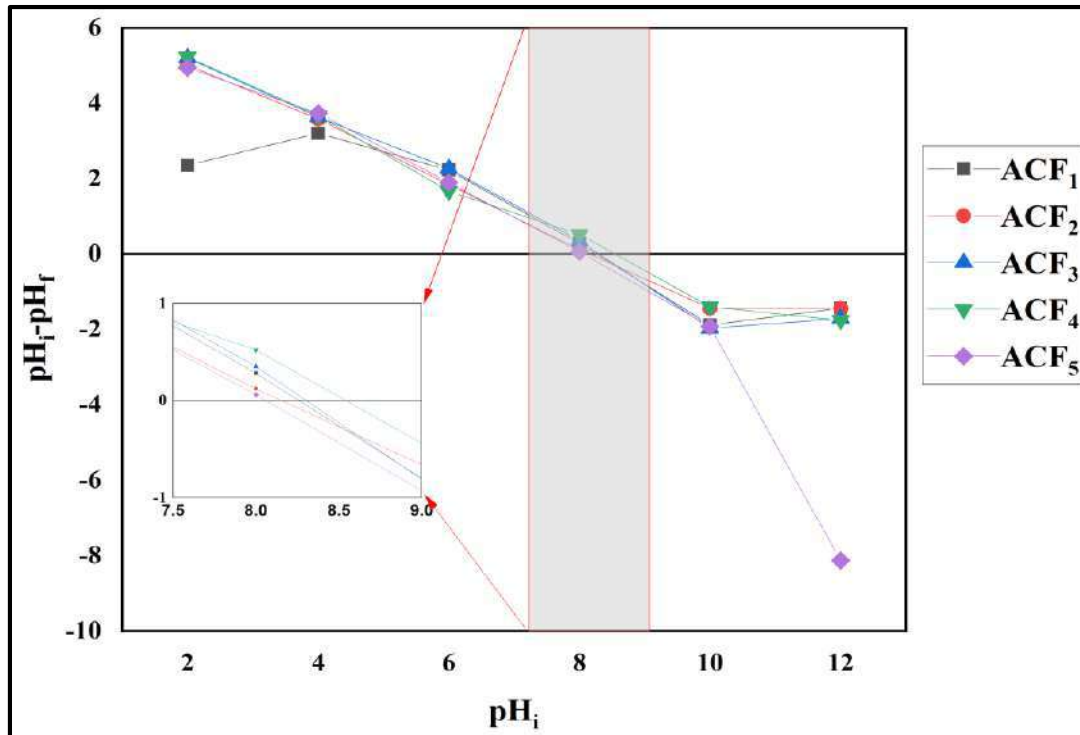
Figure II-7: The pH of the point of zero charge of ACs.

The significance of pH_{pzc} on a given AC surface is that the AC surface is positively charged when the pH is lower than the pH_{pzc} value (attracting anions). In comparison, the surface is negatively charged above pH_{pzc} (attracting cations/repelling anions). The pH_{pzc} of ACs of ACF_1, ACF_2, ACF_3, ACF_4 and ACF_5 samples were found to be 8.3, 8.1, 8.3, 8.5, and 8.0, respectively Table II-6. The pH of the solution when the ACs are added was 9.2, 9.7, 9.9, 9.7, and 9.5, respectively. As a result, the pH_{pzc} of activated carbon was lower than the pH solution, indicating that the AC surface was rich in negative charges. As a result, any sample in a slightly basic solution can be used to remove cationic contaminants.

Table II-6: pH nature and zero pH charge for activated carbon samples

Properties	Methods	ACF_1	ACF_2	ACF_3	ACF_4	ACF_5
pH nature	**The ASTM D6851 method**	9.15	9.68	9.87	9.46	9.70
pH_{pzc}		8.3	8.1	8.3	8.5	8

51

III.2.2. Determination of surface functional group

To determine the composition of active carbon in terms of acidic or basic surface groups, the Boehm method was used (Boehm, 1966). Using 0.1 N of $NaHCO_3$, Na_2CO_3 and NaOH, the acidic groups were found. As well as to neutralize the basic groups, a 0.1 N HCl was used (Depci, Kul, & Önal, 2012). For each sample, a mass of 0.5 g is added to a 25 ml of solutions prepared into a series of flasks at 25°C and then shaken for 72 h (Bamba et al., 2009). After filtration, the solutions are then dosed with HCl or NaOH at a concentration of 0.1 N in the presence of phenolphthalein as an indicator. NaHCO3 neutralizes the carboxylic groups (–COOH), Na_2CO_3 neutralizes the carboxylic groups (–COOH) and the lactone groups (–COO–) and NaOH neutralizes the carboxylic groups (–COOH), lactone (–COO–) and phenolic groups (–OH). The number of functional groups of the various acid functions is calculated by considering that $NaHCO_3$ neutralizes the carboxylic groups (–COOH). Based on the above method, the different acidic groups can be determined.

The functional groups on the surface of each AC were calculated by the Boehm titration Table II-7. The predominance of the acidic characteristics of the carboxyl, lactone, and phenolic functional groups was shown in the results described in Figure II-8. The AC obtained in general has a strong acidic character in range from 2.7 to 4, which is primarily due to the large number of groups of phenolic functions. the reduction in the duration of pyrolysis, the size of particle, the augmented in temperature of pyrolysis let the activated carbon become more acidic.

Table II-7: The functional groups on the surface of each AC

Sample		Functional groups (meq.g^{-1})				
		Carboxylic (-COOH)	Lactone (-COO-)	Phenolic (-OH)	Acidic	Basic
ACF$_1$	Boehm titration Methods	0.325	0.825	2.1	3.25	2.75
ACF$_2$		0.45	0.55	1.7	2.7	1.6
ACF$_3$		0.5	0.55	2.45	3.5	2.4
ACF$_4$		0.4	0.525	3.075	4	1.8
ACF$_5$		0.45	0.35	2.4	3.2	1.95
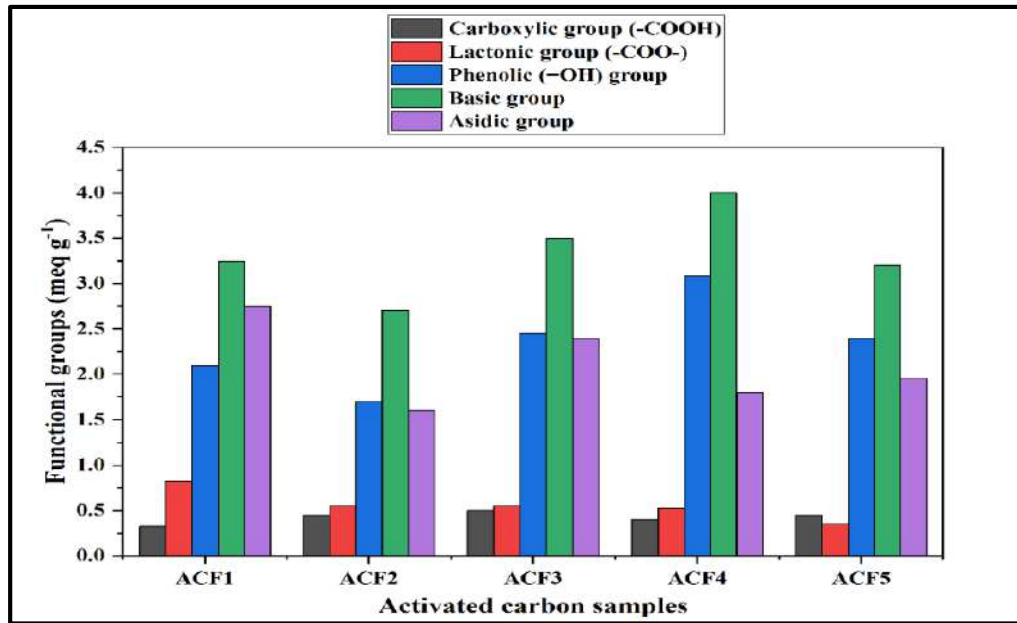
Figure II-8: The functional groups on the surface of activated carbons by Boehm titration.

III.2.3. FT-IR analysis

The chemical structures of ACs were analyzed by Attenuated Total Reflection-Fourier transform infrared (FTIR) spectrometer using Cary 600 series FTIR spectrometer (Agilent Technologies). The analysis was performed in a transmittance mode, the functional groups in the ACs in the range of 4000-600 cm^{-1} can be identified (Prahas, Kartika, Indraswati, & Ismadji, 2008; Reddy, Al Shoaibi, & Srinivasakannan, 2012).
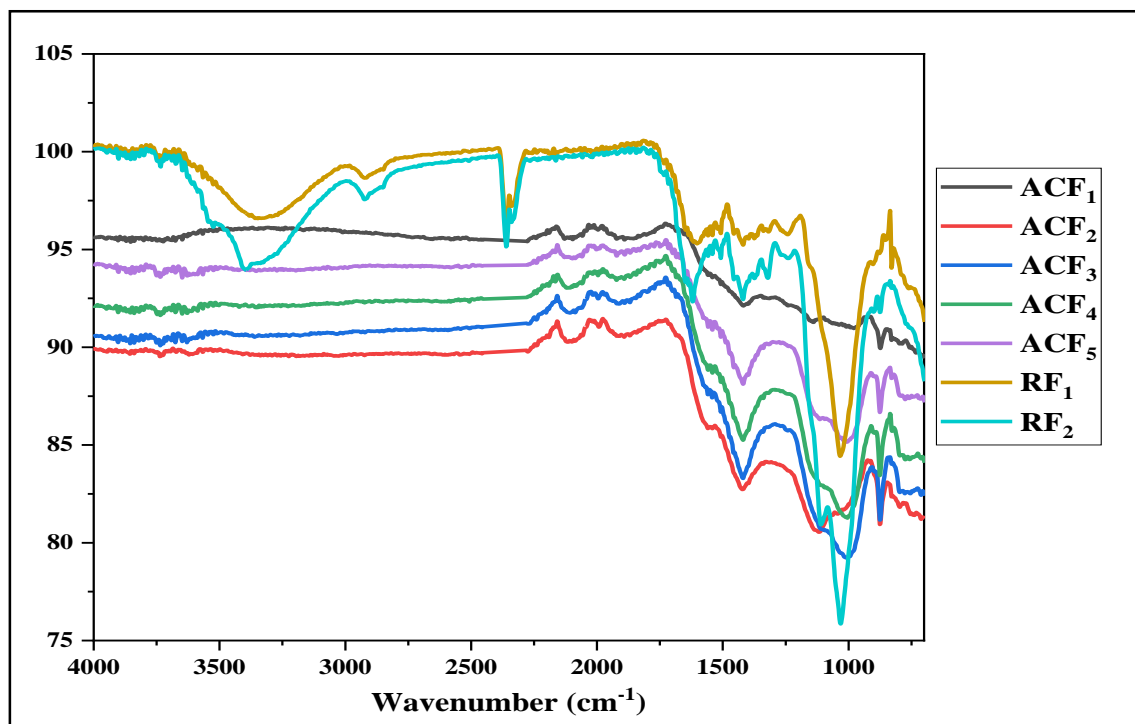
Image II-6: The FT-IR of raw fiber RF$_1$ and RF$_2$ and activated carbons samples

53

Image II-6 show the FT-IR spectra for raw fibers and ACF samples. The aim of the FTIR spectroscopy investigation was to classify the AC functional groups.

It should be noted that similar results from FTIR spectroscopy have been reported by (Galiwango et al., 2019; Riahi, Thayer, Mammou, Ammar, & Jaafoura, 2009). The absorption band detected in both types of raw fiber RF_1, RF_2, between 3524 and 3300 cm^{-1} was assigned to the hydroxyl (OH) group (Silva et al., 2021). The presence of the OH group was due to the adsorbed moisture content, cellulose and hemicelluloses in raw fiber (Yang, Yan, Chen, Lee, & Zheng, 2007). And the peak observed at 2924 cm^{-1} was allocated to the cellulose CH groups. The intensity of these RF (raw fiber) absorption bands was comparatively higher compared to that of ACF. The reduction in the intensity of this ACF peak was due to the vaporization of moisture during carbonization and activation (Keiluweit, Nico, Johnson, & Kleber, 2010).

Both samples, on the other hand, have the same peaks found. The absorption bands at 1619 and 1419 cm^{-1} were similar to (C=C) aromatic ring bonding and C-H alkene functional groups, respectively (Coates, 2006). The bands about 1321 and 1109 cm^{-1} were assigned to C=C-H in-plane bending (C-H deformation) and C-O ether bond stretching, respectively (Mohammed, Abdulhassan, & Al-Meshhdany, 2017). The peak around 1030 cm^{-1} is attributed to the C-O-C stretching vibration in the pyranose skeleton ring, the small peaks occurring in a replacement period between 760 and 600 cm^{-1} C-H deformation were possibly due to the presence of aromatic C-H in the date palm fiber and ACF's aromatic C-H out of plane bend (Benstoem et al., 2018).

After the carbonization and activation processes, the produced ACF samples showed different FT-IR spectra from the RF fiber. While various conditions of pyrolysis have been treated with the samples, it can be seen that, at most wavelengths, all ACs have similar absorption bands, suggesting their possession of similar functional groups other than ACF_1, where there is a small difference at about one peak.

The intensity of the beginning (Transmittance%) of the ACF's is lower than we had in RF's, where we note that the intensity of the OH stretching and cellulose C-H groups disappeared due to CO_2 activation that enabled the functional oxygen group to be removed (Benstoem et al., 2018), and we also observed that in terms of transmittance the other peaks were decreased. The ACs ACF_3, ACF_4, and ACF_5 that prepared from

RF_2 were found to generally have relatively strong absorption bands than the ACFs prepared from RF_1.

III.3.   Adsorption tests

When energy and material resources are extracted, processed, converted, and used, the related pollution impacts on our environment and even on our health often require that new and increasingly more efficient pollution control methods mast to be used (Huang, Bowers, Stinson, & Stephan, 1979).

We have to developing and demonstrating new and improved methodologies that will meet these needs both efficiently and economically, by developing an activated carbon process for the removal of pollutants containing wastewater.

Among the most dangerous pollutants we have chosen in our work are phenol and methylene blue.

III.3.1.   Adsorption procedure

III.3.1.1. Overview of used pollutants

III.3.1.1.1.   Phenol

Phenolic compounds, including chlorinated derivatives, represent omnipresent environmental pollutants. The appearance of simple phenolic compounds in water points to pollution stemming from industrial sources, such as manufacturers of dyes, drugs, antioxidants, pulp, and paper, or maybe the result of pesticide application. The presence of certain phenols in drinking water may have untoward effects even at ppb levels (Jeirani, Niu, & Soltan, 2017).

The toxicity and untoward organoleptic properties conferred by phenols have induced governmental agencies to limit their concentration in water for human consumption. The phenolic compounds are among the so-called priority pollutants defined by the U.S. Environmental Protection Agency and the European Community and should be of main concern in the detection of water and soil pollution (Rappoport, 2004).

Phenol shown in Image II-8 is the parent substance of a homologous series of compounds containing a hydroxyl group bound directly to the aromatic ring. Phenol, or PhOH in shorthand notation, belongs to the family of alcohols due to the presence of the OH group and it is in fact the simplest aromatic member of this family. The hydroxyl group of phenol determines its acidity whereas the benzene ring

Image II-7: Phenol structure

characterizes its basicity. Thus, it is formally the enol form of the carbonyl group (Rappoport, 2004). Physico-chemical properties of phenol show in table below:

Table II-8: Physico-chemical properties of phenol

Properties	
Chemical formula	C_6H_6O
Molar mass	94.113 g.mol^{-1}
Appearance	Transparent crystalline solid
Odor	Sweet and tarry
Density	1.07 g.cm^{-3}
Melting point	40.5 °C (104.9 °F; 313.6 K)
Boiling point	181.7 °C (359.1 °F; 454.8 K)
Solubility in water	8.3 g/100 mL (20 °C)
Vapor pressure	0.4 mmHg (20 °C)
Acidity (pK_a)	9.95 (in water), 18.0 (in DMSO), 29.1 (in acetonitrile).
Conjugate base	Phenoxide
UV-vis (λ_{max})	270.75 nm

III.3.1.1.2. Methylene blue

Methylene blue was first prepared in 1876, by Heinrich Caro. It is on the World Health Organization's List of Essential Medicines, it is the first synthetic drug, and had already a 120-year history in several areas of medicine, also known as methylthioninium chloride, is a salt used as a medication and dye (Schirmer, Adler, Pickhardt, & Mandelkow, 2011).

Image II-8: Methylene blue structure

Methylene blue is a formal derivative of phenothiazine a tricyclic. It is a dark green powder that yields a blue solution in water. The hydrated form has 3 molecules of water per unit of methylene blue, it has a pH of 6 in water (10g/l) at 25 °C (77 °F).

Image II-9: The various concentrations in order to create a calibration curve

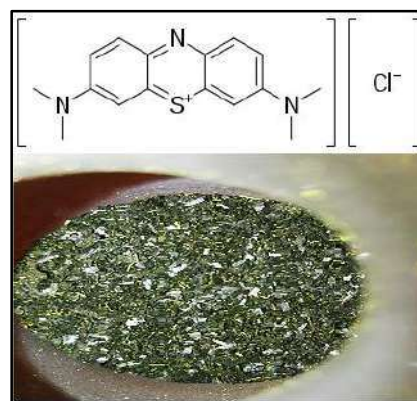Characteristics of methylene blue (Zaini, Ngiik, Kamaruddin, Setapar, & Yunus, 2014) mentioned in table below:

Table II-9: Physico-chemical properties of methylene blue

Properties	
Chemical formula	$C_{16}H_{18}ClN_3S$
IUPAC name	3,7-bis(Dimethylamino)- phenothiazin-5-ium chloride
Molar mass	319.85 g.mol^{-1}
Colour index number	52015
Wavelength, λ	663 nm
Solubility in water	1/25 g.ml^{-1}

III.3.1.2. Calibration curve

Preparation of the stock solution: it was prepared by dissolving 0.5 g of the solid (phenol and methylene blue powder) in 500 ml of distilled water separately. So that we have two stock solutions, phenol, and methylene blue with a concentration of 1000 ppm (mg.l^{-1}).

In order to create a titration curve for phenol and methylene blue, we prepared solutions of different concentrations from diluting the stock solution, we passed the solutions of phenol and methylene blue of concentrations (5, 10, 15, 20, 40, 60 ppm) and (3, 5, 10, 15, 20, 25, 30 ppm) respectively through the UV-Visible spectrophotometer (Spectro Scan 80DV) measuring the UV-Vis absorbance intensity at λ_{max}= 270 nm.
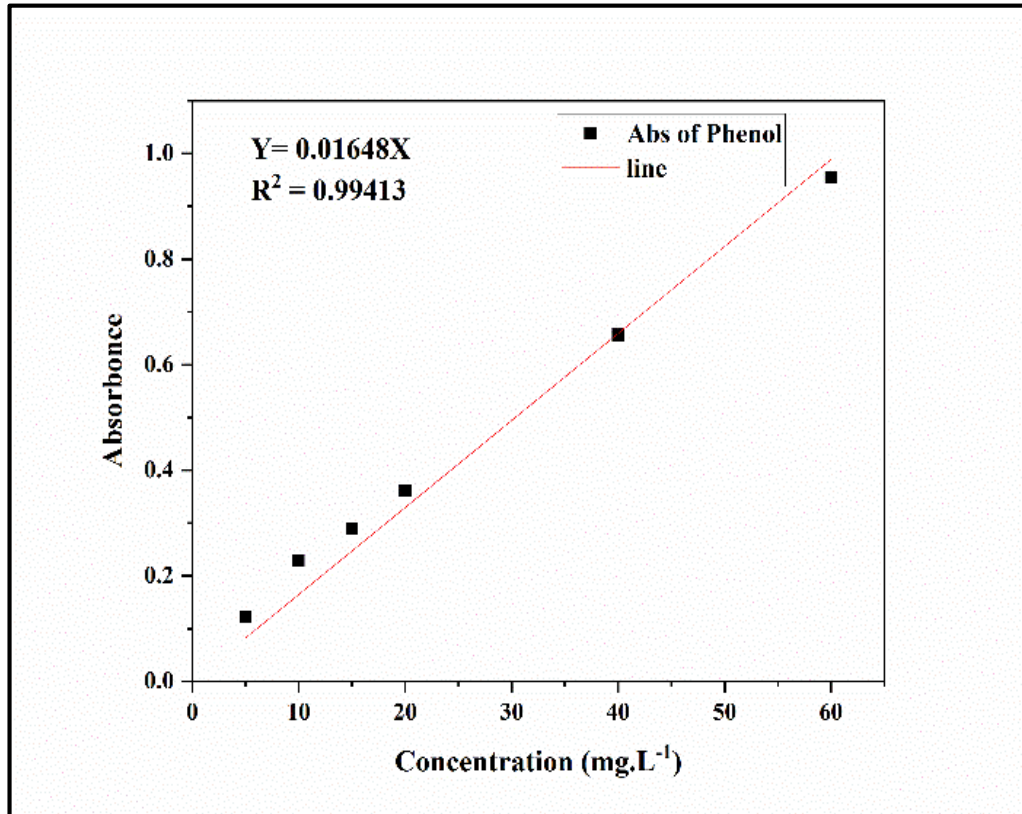
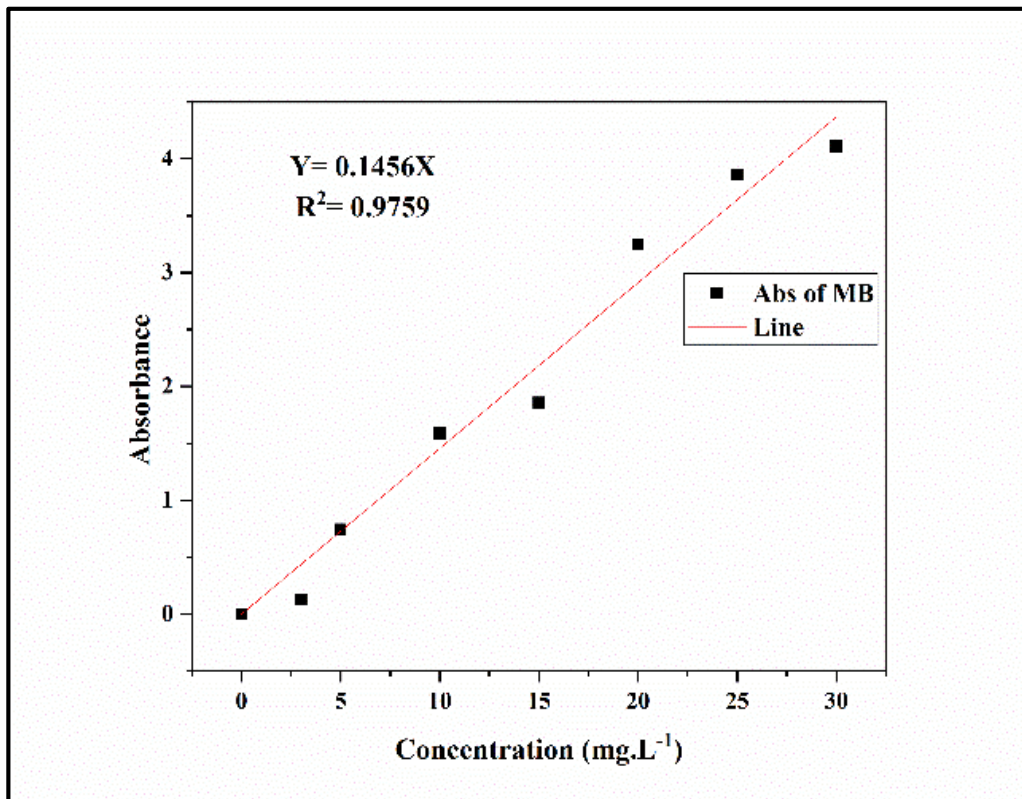Figure II-9: The calibration curve of Phenol.

Figure II-10: The calibration curve of Methylene blue.

The experimental data reported in Figure II-9 and Figure II-10, indicate a linear relationship between absorbance and concentration with a correlation coefficient $R^2 = 0.99413$ of Phenol and $R^2 = 0.9759$ of Methylene blue.

The phenol and Methylene blue concentration is determined from the following equations:

$$C_e = \frac{Abs}{0.01648} \ for \ Phenol........Eq\ 26 \quad and \quad C_e = \frac{Abs}{0.1456} \ for\ MB\ ....Eq\ 27$$

With: Y is Absorbance and X is the equilibrium concentration.

III.3.1.3. Adsorbate preparation

All working solutions were prepared by diluting the stock solution with deionized water. Phenol and Methylene blue adsorption measurements were carried out to determine the adsorption capacity by ACF samples at 25 °C, by measuring the UV-Vis absorbance intensity for solutions with unknown concentrations after the absorption process is completed (at $\lambda_{max} = 270$ nm for Phenol $\lambda_{max} = 662$ nm for Methylene blue) using UV-Vis spectrophotometer (SpectroScan 80DV).

In general, the principle is adding a specific mass of each ACF sample into well-closed flasks containing a specific volume of stock solution diluting with different concentrations. All the flasks are shaken for specific time with a shaker to ensure even mixing of the ACF with the target solution (Phenol or Methylene blue). About 5ml of each solution is taken using a filtered syringe from each flask. Then, the solution is scanned by UV-Vis spectrophotometer. The concentrations of the solutions are obtained by comparing the absorbance's intensity to the calibration curve.

We have 5 samples ACF_1, ACF_2, ACF_3, ACF_4 and ACF_5, and two stock solutions Phenol and MB 1000 ppm= 1000 mg. l^{-1}. Factors affecting the adsorption process such as mass, initial concentration, time and temperature are manipulated to comprehensively characterize activated carbon.

The amount of Phenol adsorbed by ACF was calculated by the following equation (Rahman et al., 2017):

$$q_t = \frac{(C_0 - C_e)V}{m} \quad ....Eq\ 28$$

Where C_o and C_e are the liquid–phase concentrations (mg.l^{-1}) of phenol at initial and at equilibrium, respectively. V is the volume (l) of the solution and m is the mass (g) of dry adsorbent used.

$$\%Removal\ of\ phenol = \frac{C_0 - C_t}{C_0} \times 100\% \quad ....Eq\ 29$$

Where C_o is the initial concentration (mg.l^{-1}) and C_t is the concentration at time t. The amount of adsorption at equilibrium, q_e (mg.g^{-1}).

1. **Mass effect**

We prepared a solution with a fixed concentration (C_0= 50 mg.l^{-1} of phenol) and (C_0= 20 mg.l^{-1} of MB) with different mass of adsorbent (m= 10, 20, 30, 40, 50, 60 mg) for time 3h, 600 rpm of agitation at 25°C
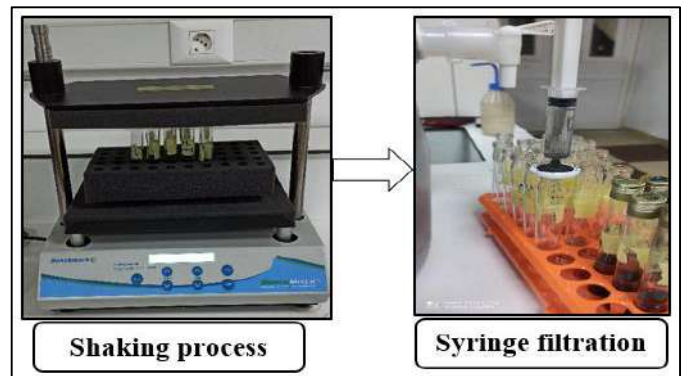
Image II-10: Adsorption process for mass determination

✓ Phenol: 5 samples x 6 mass = 30 samples.

✓ MB: 5 samples x 6 mass = 30 samples.
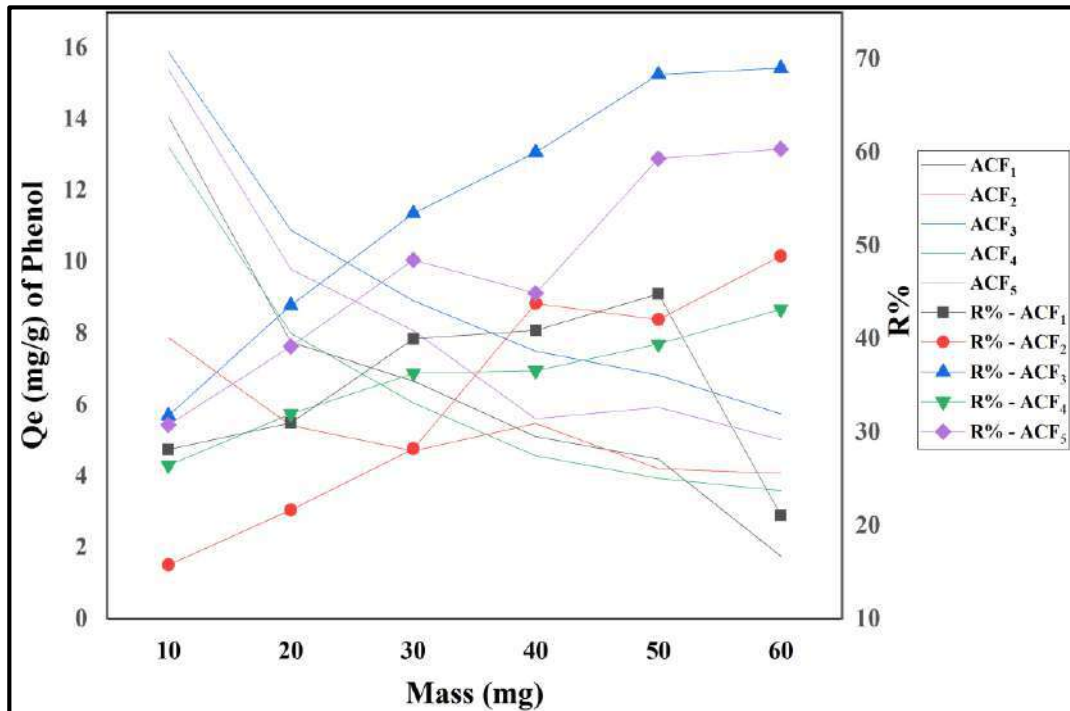
Figure II-11: Effect of mass on phenol adsorption

60
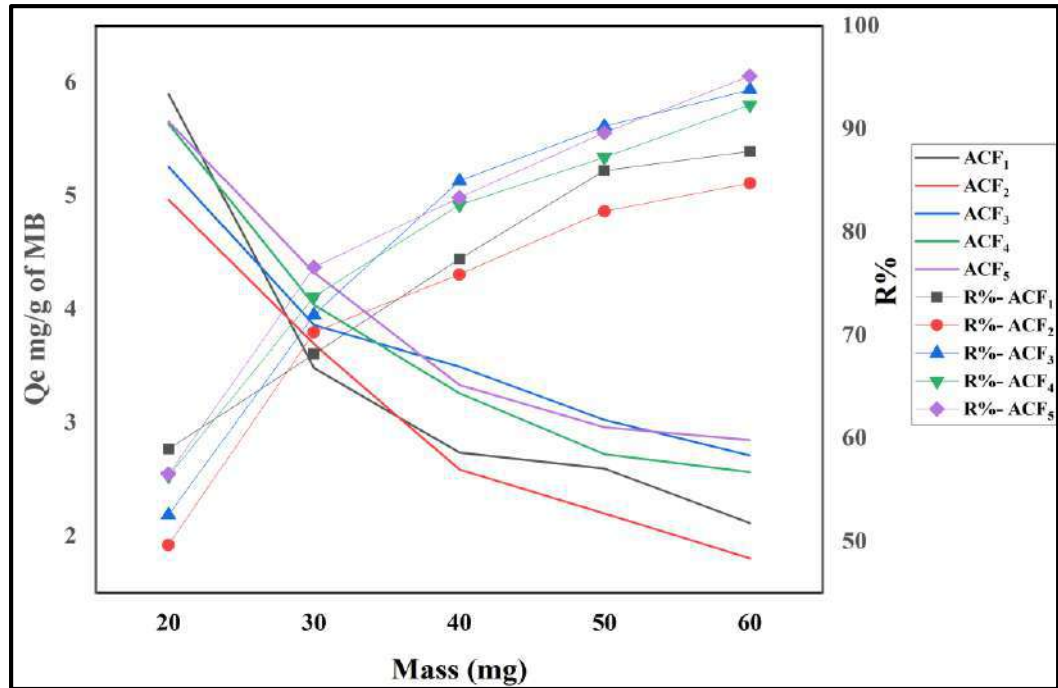
Figure II-12: Mass effect on the Adsorption of Methylene Blue.

From above two Figure II-11 and Figure II-12, we notice the following:

✓ For phenol, the optimal mass for best adsorption is 40 mg in all samples.

✓ As for methylene blue, the ideal mass for the best adsorption is different from one sample to another, for ACF_1 sample the ideal mass is 50 mg, and for ACF_2 sample it is 30 mg and 60 mg for the rest of the samples.

✓ This difference in mass is due to the physical properties of the pollutants and the adsorbent, pore size and diameters, etc., because each adsorbent has a limited adsorption capacity.

2. <u>Initial concentration effect</u>

We have prepared solutions (C_0= 20, 40, 60, 80, 100 mg.l^{-1} of phenol) and (C_0= 3, 5, 10, 15, 20 mg.l^{-1} of MB) with the optimal mass for each sample, for 3h, 600 rpm of agitation at 25°C.

✓ Phenol: 5 samples x 5 concentrations = 25 samples

✓ MB: 5 samples x 5 concentrations = 25 samples
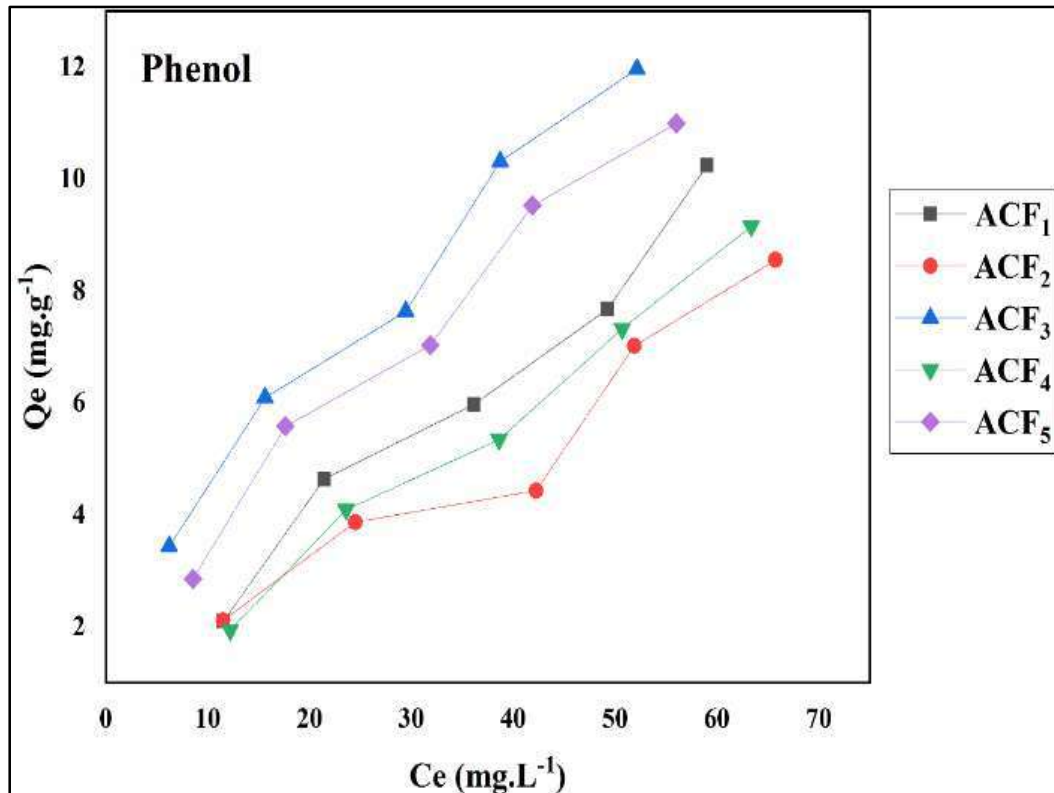
Figure II-13: The initial concentration effect of removal Phenol.
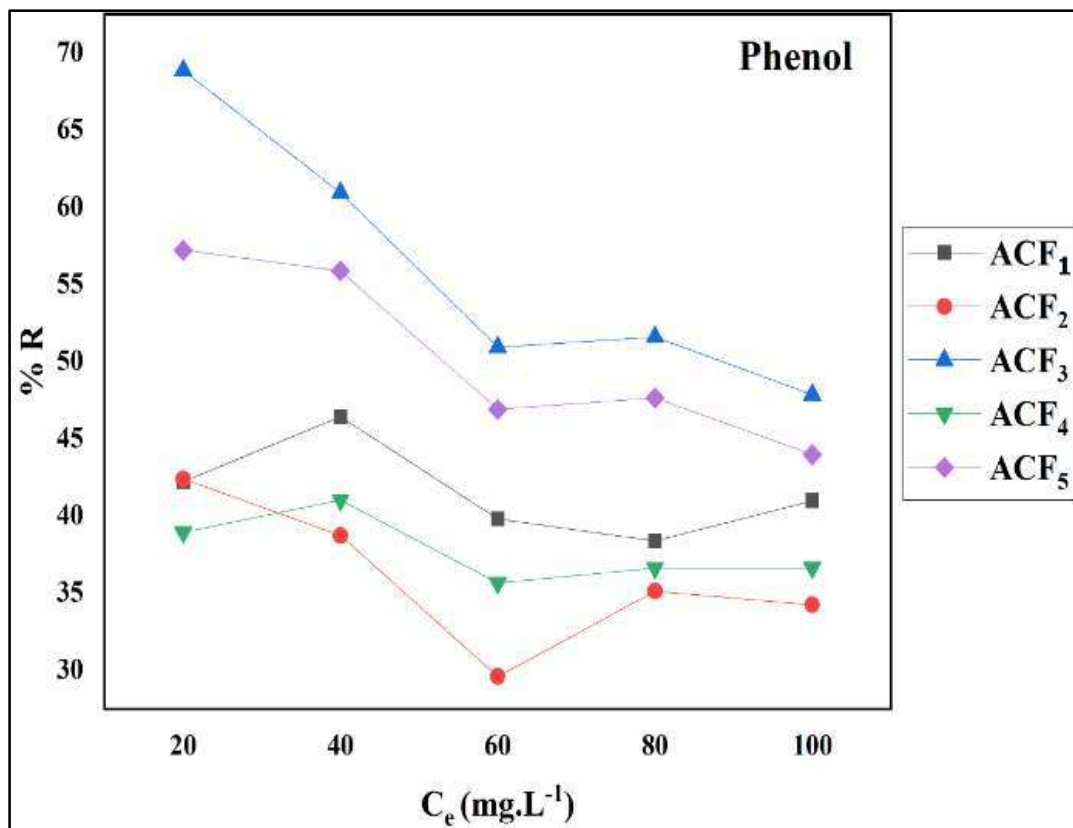
Figure II-14: the yield of removal Phenol.

62

The effects of initial phenol concentrations on the removal of phenols have been studied and their removal percentage shown in Figure II-13 and Figure II-14, respectively. Experiments were performed at varying initial phenol concentrations of 20-100 mg.l^{-1}, 40 mg of ACF and 600 rpm of agitation at 25°C. As can be shown, when the initial phenol concentration increased from 20 to 100 mg.l^{-1}, removal of phenol of ACF$_1$, ACF$_2$, ACF$_3$, ACF$_4$ and ACF$_5$ decreased from 42.98%, 42.38%, 68.84%, 38.93% and 57.20% to 40.98%, 34.23%, 47.84%, 36.63% and 43.97%, respectively, and the uptake capacity increased from 2.11, 2.12, 3.44, 1.95, and 2.86 mg.g^{-1} to 10.24, 8.56, 11.96, 9.16, and 10.99 mg.g^{-1}, respectively, after adsorption time of 180 min. The increase in the amount of adsorbed phenol at equilibrium (q$_e$) with an increase in phenol concentration is attributable to a higher availability of phenol molecules in the adsorption solution and a higher interaction between the adsorbent and the adsorbate at a higher phenol concentration, which could be due to an increase in the driving force of the phenol molecules towards the adsorbent (Afshina, Rashtbaria, Shirmardic, Vosoughib, & Hamzehzadeha, 2019).

ACF$_3$ was found to have the highest phenol adsorption capacity, followed by ACF$_5$, ACF$_1$, ACF$_4$ and ACF$_2$ for the concentration range tested in this study, with the pores diameter calculated in this study for ACF$_1$, ACF$_2$, ACF$_3$, ACF$_4$ and ACF$_5$ being 1.92, 2.11, 1.89, 1.93, and 2.10 (nm) respectively. The difference in this value for these adsorbents and the smaller of specific surface area (166.29 m^2.g^{-1}) and higher pores diameter (2.11 nm) explains the higher adsorption capacities of phenol for ACF$_3$ compared to the other ACs.

The effects of initial Methylene blue concentrations on the removal of Methylene blue have been studied and their removal percentage shown in Figure II-15 and Figure II-16, respectively.

Experiments were performed at varying initial MB concentrations of 3-20 mg.l^{-1}, with 50, 30 mg of ACF$_1$ and ACF$_2$ respectively and 60 mg for reset samples with 600 rpm of agitation at 25°C.

As can be shown, when the initial MB concentration increased from 3 to 20 mg.l^{-1}, removal of phenol of ACF$_1$, ACF$_2$, ACF$_3$, ACF$_4$ and ACF$_5$ decreased from 94.02%, 95.28%, 99.77%, 97.21% and 99.77% to 39.19%, 40.35%, 84.55%, 65.42% and 75.90%, respectively, and the uptake capacity increased from 0.56, 0.95, 0.50, 0.49,

and 0.50 mg.g^{-1} to 1.57, 2.69, 2.82, 2.18, and 2.53 mg.g^{-1}, respectively, after adsorption time of 180 min. The increase in the amount of adsorbed Methylene blue at equilibrium (q_e) with an increase in Methylene blue concentration attributable to a higher availability of Methylene blue molecules in the adsorption solution and a higher interaction between the adsorbent and the adsorbate at higher concentration of Methylene blue, which could be due to an increase in the driving force of the Methylene blue molecules towards the adsorbent.
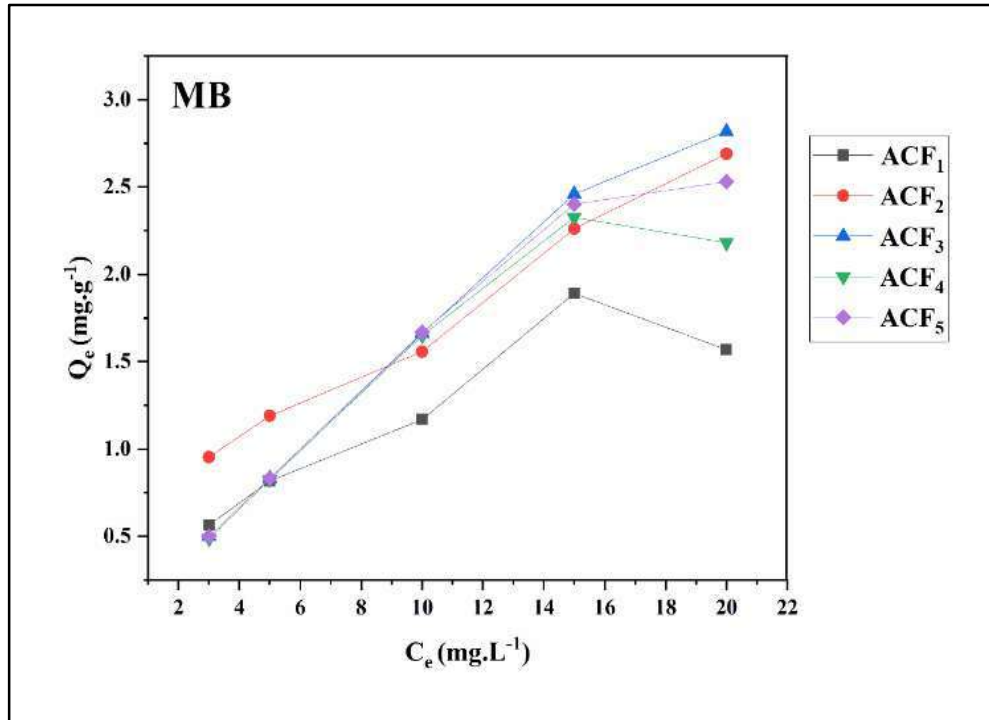
Figure II-15: The initial concentration effect and the removal ratio of Methylene blue.
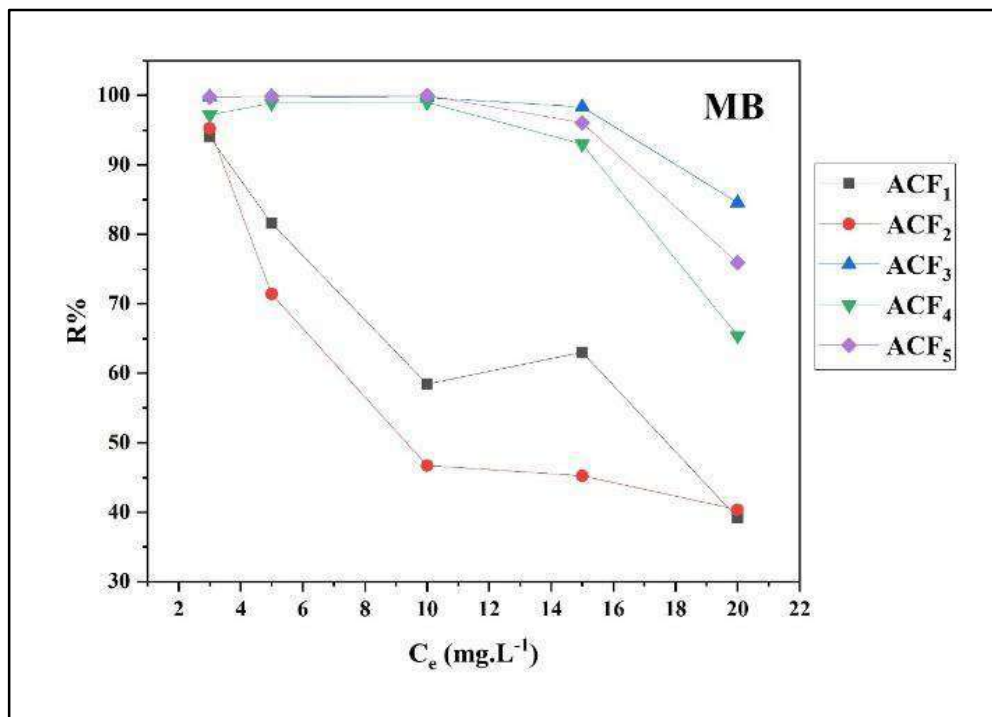
Figure II-16: The removal ratio of Methylene blue.

ACF$_3$ was found to have the highest MB adsorption capacity, followed by ACF$_2$, ACF$_5$, ACF$_4$ and ACF$_1$ for the concentration range tested in this study, the specific surface area for ACF$_1$, ACF$_2$, ACF$_3$, ACF$_4$ and ACF$_5$ is 278.22, 313.40, 166.29, 168.13, 205.53 (m^2.g^{-1}) and the pores diameter is 1.92, 2.11, 1.89, 1.93, and 2.10 (nm) respectively.

The difference in this value for these adsorbents and the smaller of specific surface area (166.29 m^2.g^{-1}) and higher pores diameter (1.93 nm) compared to other samples are the reason for the higher MB adsorption capacity for ACF$_3$. The fact that all adsorbents have a limited number of active sites, which would have been saturated above a certain concentration, can explain the decrease in the percentage removal.

The classification of adsorption isotherms of both Phenol and MB is L4-curve (the normal), according to (Giles et al., 1974) this class implies that the slope gradually falls with an increase in concentration, and with the gradual covering of the surface, it becomes more difficult to find vacant sites.

We also noted that the largest removal of Phenol and MB was in the low concentrations and that the best adsorption of phenol was at a concentration of 20 ppm, while for methylene blue at a concentration of 15 ppm.

65

3. **Time effect**

We have prepared solutions (C_0= 20 mg.l^{-1} of Phenol and C_0= 15 mg.l^{-1} of MB) with the optimal mass for each sample, and 600 rpm of agitation at 25°C, for times (t= 5, 10, 20, 40, 60, 80, 100, 120, 150, 180 min).

- ✓ Phenol: 5 samples x 10 Times = 50 samples
- ✓ MB: 5 samples x 10 Times = 50 samples.

Equilibrium time is one of the most important parameters in the design of wastewater treatment systems. These experiments have been carried out at variations of time of contact (0–180 min). After every contact time, the sample was removed and filtered immediately and the filtrate was analyzed.

Figure II-17 and Figure II-18 show the plot of the amount of phenol and MB adsorbed versus time onto ACF$_1$, ACF$_2$, ACF$_3$, ACF$_4$, and ACF$_5$ activated carbon at 25°C respectively.
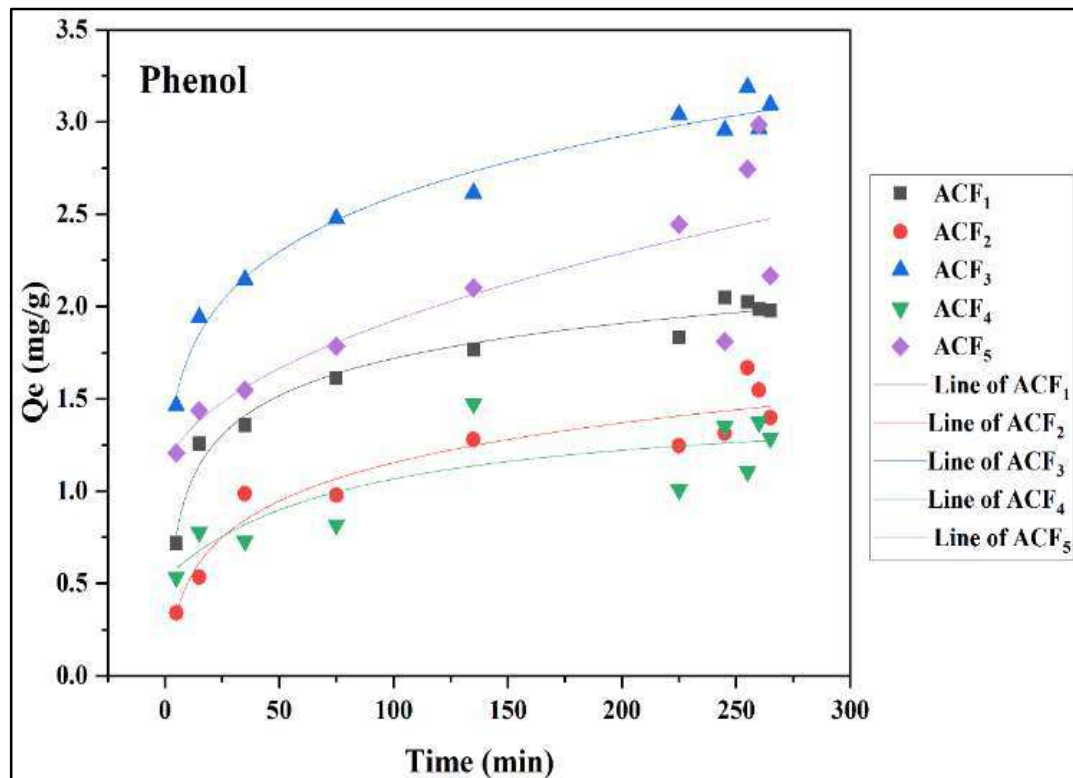
Figure II-17: Time effect on Phenol Adsorption.
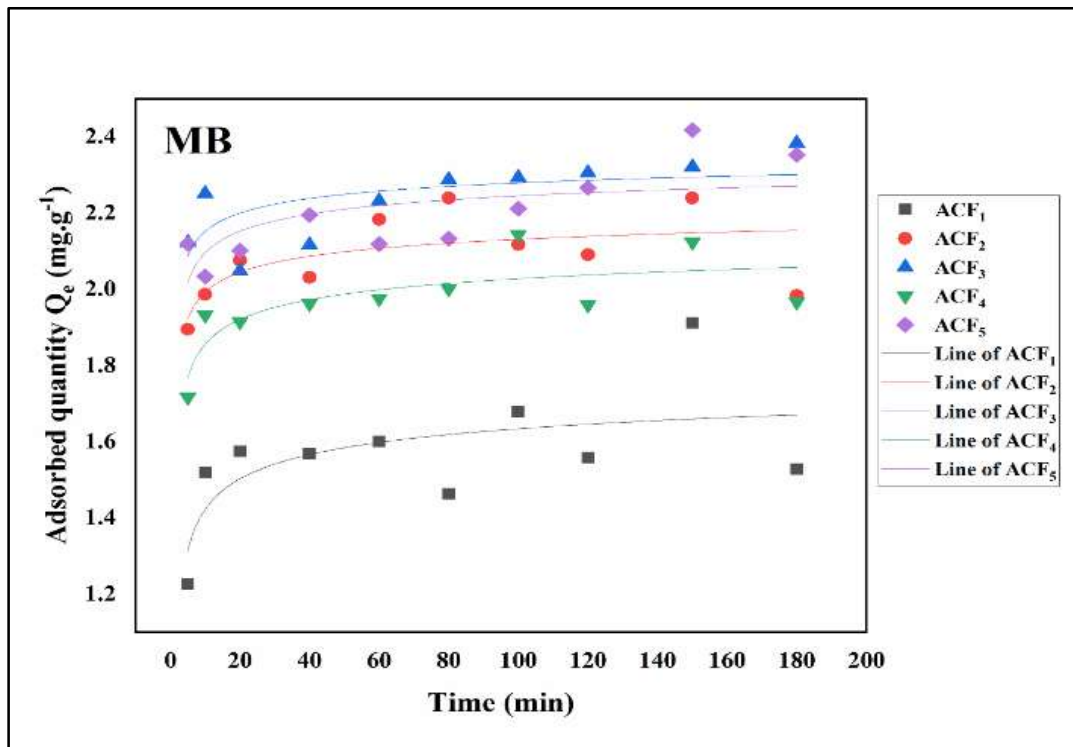
Figure II-18: Time effect on MB Adsorption.

The result showed that the adsorption of both phenol and methylene blue initially increases with increasing the contact time and then the adsorption capacity is almost constant, adsorption reaches equilibrium. The time taken to reach the equilibrium was 150 min for Phenol and 40 min for MB (Mashhadi, Javadian, Ghasemi, Saleh, & Gupta, 2016).

It is observed also that ACF_3 presents higher adsorption than other samples, especially in the initial time. The adsorption curves for all samples reach equilibrium after a certain time, which differ among them (Ioannou & Simitzis, 2009).

The adsorption capacity increases according to the order:

- ✓ For Phenol: $ACF_3 > ACF_5 > ACF_1 > ACF_2 > ACF_4$.
- ✓ For MB: $ACF_3 > ACF_5 > ACF_2 > ACF_4 > ACF_1$.

4. <u>Temperature effect</u>

We have prepared solutions (C_0= 20 mg l^{-1} of Phenol and C_0= 15 mg l^{-1} of MB) with the optimal mass for each sample, and 600 rpm of agitation at 25°C, for times (t= 180 min), with different temperature (T= 20, 35, 45 °C).

- ✓ Phenol: 5 samples x 6 temperatures = 30 samples
- ✓ MB: 5 samples 6 temperatures = 30 samples
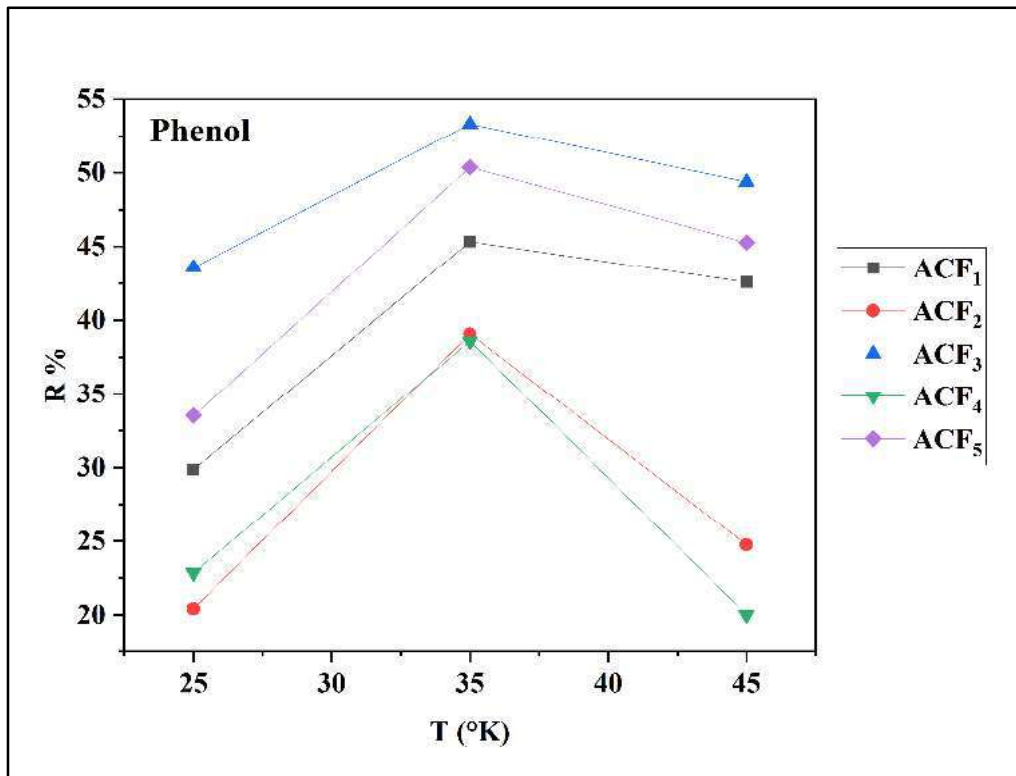
Figure II-19: Temperature effect on Phenol Adsorption.
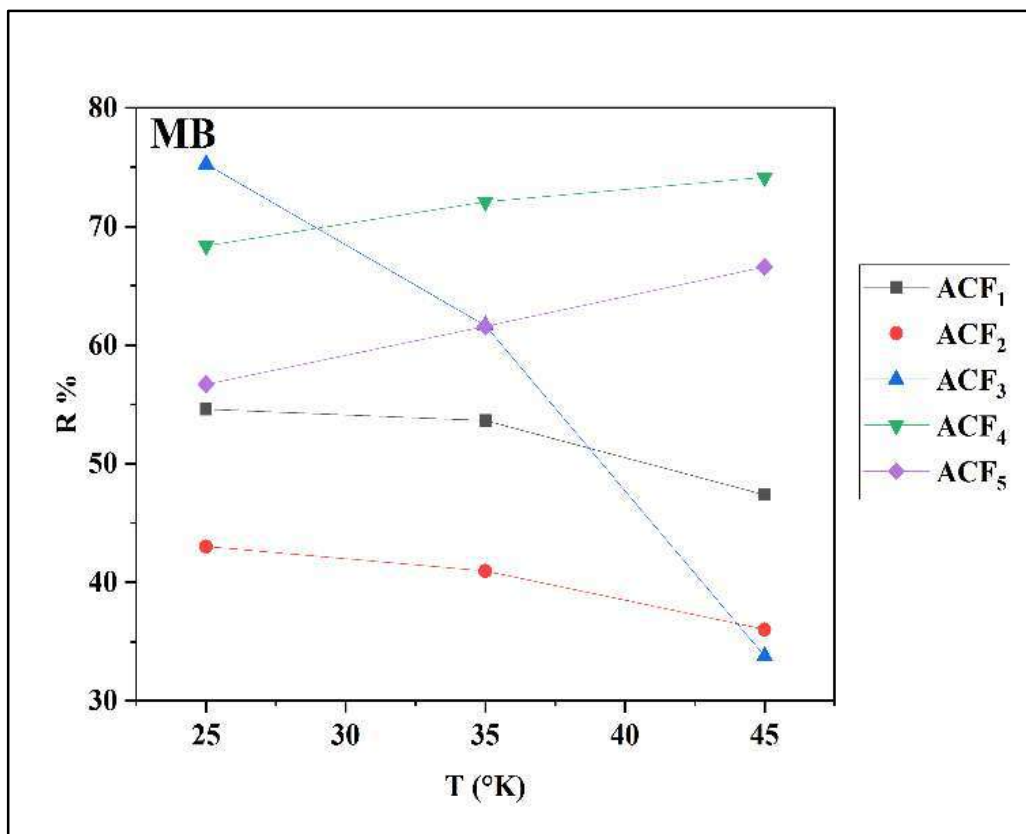
Figure II-20: Temperature effect on MB Adsorption.

The effect of temperature on Phenol and MB adsorption was investigated in the range of 25–45 °C. Illustrated in Figure II-19 and Figure II-20 respectively.

Through Figure II-19 we notice at the temperature of 25 °C the percentage removal of phenol on Activated carbons of ACF_1, ACF_2, ACF_3, ACF_4, and ACF_5 is 29.88, 20.42, 22.85, 43.58, and 20.00 % respectively, and increases when the temperature increases to 35 C to be 45.33, 39.06, 53.30, 38.58, 33.52 % respectively. And beyond the temperature of 35 °C, the percentage removal decreases with an increase in temperature. Thus, the optimum temperature was selected to be 35 °C for the best Phenol adsorption.

The observations are explained in terms of the relatively more efficient packing of phenol molecules in carbon pores when present in a liquid state at higher temperatures.

Figure II-20 shows that the percentage removal of methylene blue varies from one sample to another. for the samples, ACF_1, ACF_2, and ACF_3 the percentage removal of methylene blue decreased from 54.60, 43.02, and 75.26 % to 47.37, 36.03, and 33.78 98.69 % respectively, while it is increased as for the samples ACF_4 and ACF_5 from 68.38, 56.69 % to 74.16, 66.60 % respectively when the temperature was increased from 25 °C to 45 °C

The temperature has two major effects on the adsorption process. Firstly, the increasing temperature is known to enhance the diffusion rate of adsorbate molecules across the external boundary layer and in the internal pores of adsorbent particles, owing to the decrease in the viscosity of the solution. In addition, temperature alteration will differ the equilibrium capacity of the adsorbent for a particular adsorbate (increase the tendency of disaggregation) (Foo & Hameed, 2010).

The reason for the increase of the adsorption capacity with an increase in temperatures is generally dependent on the reaction between adsorbate and adsorption. For phenol, is probably because decreased retarding forces acting on the phenol ions increased the mobility of ions, thereby increasing the sorptive capacity of the adsorbent. But, the diffusion of phenol into pores of the activated carbon is not the only rate-controlling step so; the diffusion process could be ignored with adequate contact time (Foo & Hameed, 2010; Shehu, Danbature, Magaji, Yakubu, & Balarak, 2021). While as for MB, the results are attributed to the increased mobility of MB ions with increasing temperature. With increasing reaction temperature in solution, the amount of non-protonated functional groups on the adsorbent increases due to the increase in the dissociation constant of the protonated hydroxyl groups. Increasing the temperature

is known to increase the rate of diffusion of the adsorbate molecules across the external boundary layer and in the internal pores of the adsorbent particle, owing to the decrease in the viscosity of the dye solution (Anbarasan, Dhadhala, Kalicharan, & Arivalagan, 2021; Chandola, Thathola, & Bisht, 2021).

On another side, the decrease in adsorption with the increase in temperature, from 25 °C to 45 °C, points towards the possibility of physical adsorption and suggested weak adsorption between phenol and MB with activated carbon sites. Since adsorption is an exothermic process, it would be expected that an increase in temperature would result in decreased adsorption capacity. As a result, the increase in temperature led to a decrease in adsorption performance indicating the exothermic nature of the adsorption reaction (Chandola et al., 2021).

III.3.2.   Adsorption models

The relationship between adsorbate molecules and adsorbent surface isotherms can be defined by adsorption isotherms. which are important in predictive modeling the procedures for designing the adsorption system because the adsorption capacity of a quantitative adsorbent could be described, and it helps in making the selection of appropriate adsorbents and determination of adsorbent dosage feasible. Several isotherm models are available (Anbarasan et al., 2021).

To balance the experimental results, two types of isothermal models (Langmuir and Freundlich) were fitted. Their correlation with our adsorption process was judged by the values of the correlation coefficient (R^2).

The Langmuir model is based on the assumption that maximum adsorption corresponds to a saturated monolayer of solute molecules on a homogenous surface with all active sites being equivalent and with the same energy. The Langmuir model assumes dynamic equivalent and no interaction between adsorbates in the plane of the surface (Al-Haidary, Zanganah, Al-Azawi, Khalili, & Al-Dujaili, 2011; Anbarasan et al., 2021).

Langmuir plot for the adsorption of phenol and MB on to ACF_1, ACF_2, ACF_3, ACF_4 and ACF_5 activated carbon at 25℃ are shown in Figure II-22 and Figure II-21, respectively. The results obtained for the Langmuir isotherm equations of phenol and MB are listed in Table II-10.

The parameters such as the R_L, the adsorption equilibrium constant, which is related to adsorption free energy and corresponds to the affinity between the adsorbent surface and the adsorbate, are given by the Langmuir model. As well as the maximum adsorption capacity (q_{max}) that is combined with the amount of phenol adsorbed to complete a monolayer, full coverage is achieved when all existing sites have been filled.
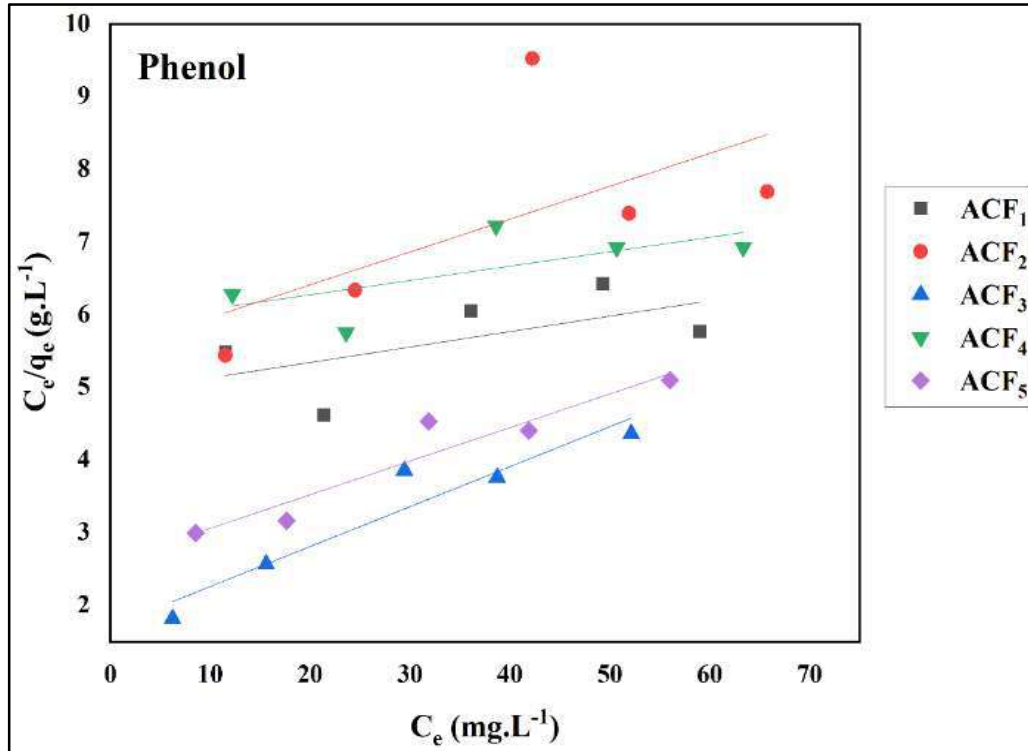

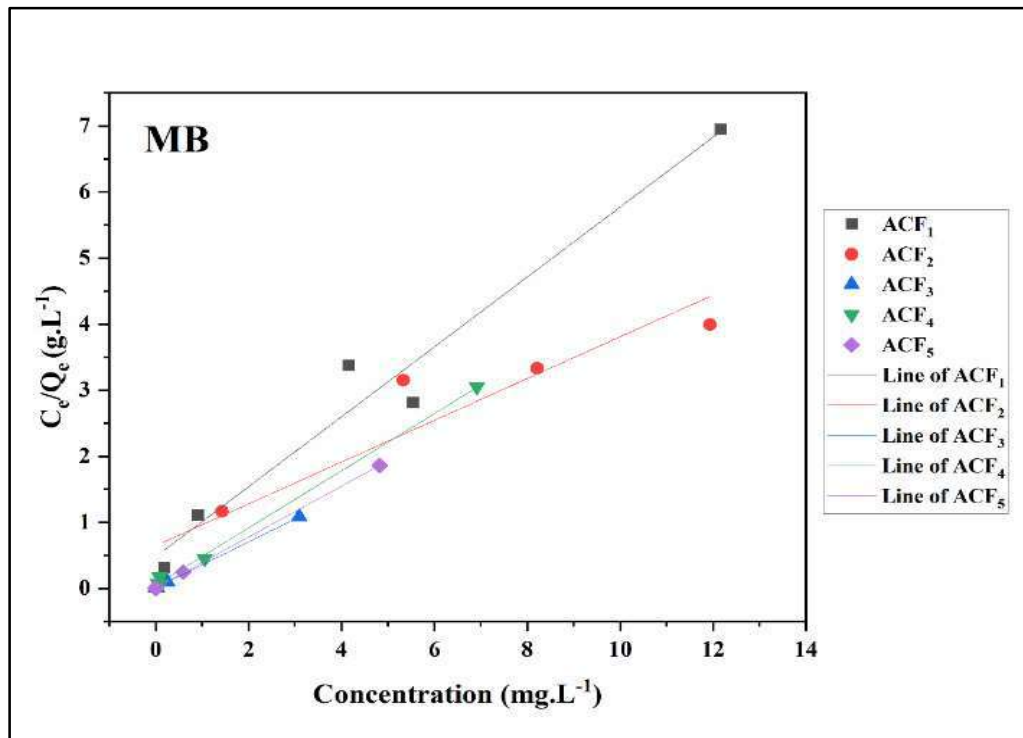Figure II-22: Langmuir plot for the adsorption of phenol onto activated carbons at 25℃.

Figure II-21: Langmuir plot for the adsorption of MB onto activated carbons at 25℃.

71

Table II-10: Parameters obtained from Langmuir isothermal of phenol and MB onto ACF_1, ACF_2, ACF_3, ACF_4 and ACF_5 activated carbon at 25℃.

Adsorbent	Langmuir isothermal constants							
	Phenol				MB			
	q_{max} (mg.g^{-1})	b (l.mg^{-1})	R_L	R^2	q_{max} (mg.g^{-1})	b (l.mg^{-1})	R_L	R^2
ACF_1	44.64	0.004	0.70	0.92	1.89	1.10	0.044	0.96
ACF_2	20.79	0.008	0.54	0.98	3.16	0.49	0.093	0.89
ACF_3	1.75	0.361	0.03	0.99	2.88	36.15	0.001	1.00
ACF_4	6.14	0.032	0.24	0.90	2.31	8.67	0.006	1.00
ACF_5	20.83	0.018	0.36	0.99	2.60	45.79	0.001	1.00

The values of q_{max} Langmuir model of ACF_1, ACF_2, ACF_3, ACF_4, and ACF_5 were found to be (for Phenol: 44.64, 20.79, 1.75, 6.14, and 20.83 mg.g^{-1}, respectively and for MB 1.89, 3.16, 2.88, 2.31, and 2.60 mg.g^{-1}, respectively, we note that the equilibrium adsorption capacity obtained for Phenol is clearly higher than MB. In the present experiment, factors (R_L) were found to be for Phenol: 0.70, 0.54, 0.03, 0.24, and 0.36, respectively and for MB 0.044, 0.093, 0.001, 0.006, and 0.001, respectively. All the R_L values indicate that the adsorption was favorable.

The Freundlich model is described by a formula assuming heterogeneous multilayer adsorption on heterogeneous surfaces with the interaction between the adsorbates molecules and that adsorption capacity increases with the analytic concentration (Al-Haidary et al., 2011; Anbarasan et al., 2021).

Freundlich plot for the adsorption of phenol and MB onto ACF_1, ACF_2, ACF_3, ACF_4 and ACF_5 activated carbon at 25℃ are shown in Figure II-23 and Figure II-24, respectively.

The results obtained for the Freundlich isotherm equations of phenol and MB are listed in Table II-11.

In general, the Freundlich n-value of an effective adsorbent is between 1 and 10. It was found that the value of n was for Phenol: 1.12, 1.31, 1.73, 1.10 and 1.43, respectively and for MB: 3.38, 4.12, 4.03, 4.00, and 8.24, respectively. The values of n > 1 represent favorable adsorption conditions, indicating the favorable adsorption of phenol and MB onto ACF's.

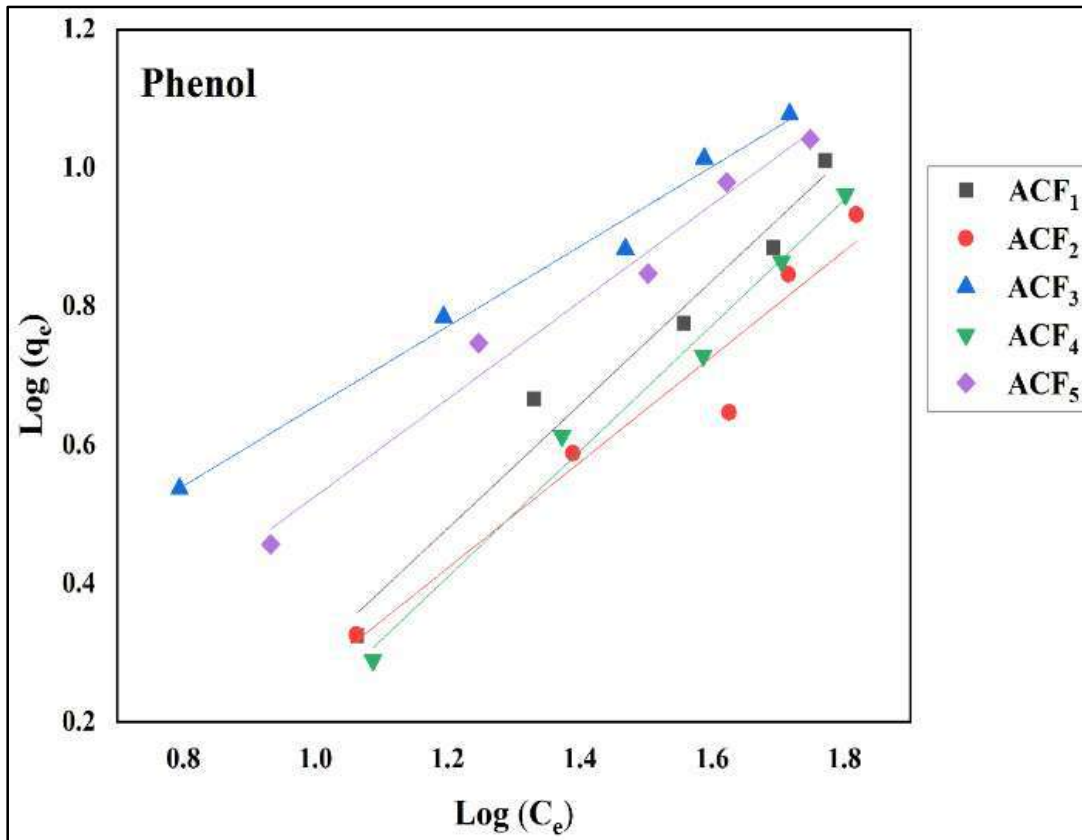Figure II-23: : Freundlich plot for the adsorption of phenol onto ACF$_1$, ACF$_2$, ACF$_3$, ACF$_4$ and ACF$_5$ activated carbon at 25℃.
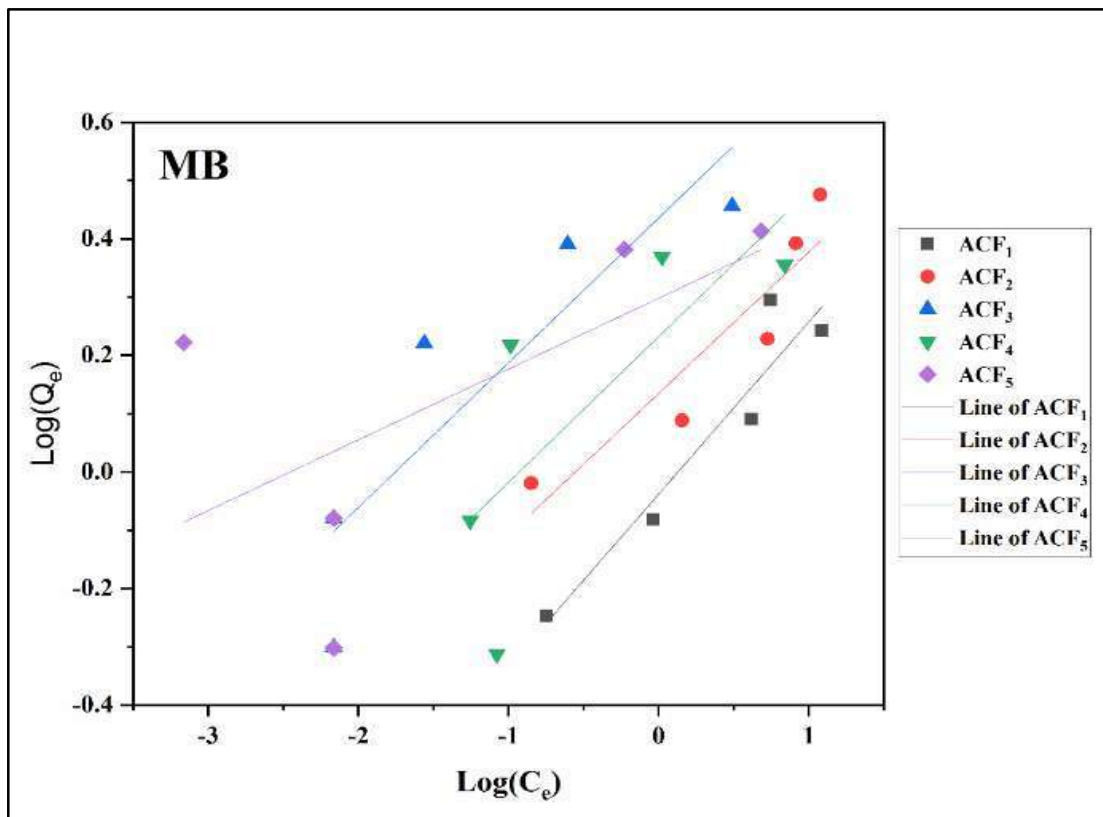

Figure II-24: Freundlich plot for the adsorption of MB onto ACF$_1$, ACF$_2$, ACF$_3$, ACF$_4$ and ACF$_5$ activated carbon at 25℃

Table II-11: Parameters obtained from Frenudlich isothermal of phenol and MB onto ACF₁, ACF₂, ACF₃, ACF₄ and ACF₅ activated carbon at 25℃.

Adsorbent	Freundlich isothermal					
	Phenol			MB		
	n	$K_f[(mg.g^{-1})\,(l.mg^{-1})^{1/n}]$	R^2	n	$K_f[(mg.g^{-1})\,(l.mg^{-1})^{1/n}]$	R^2
ACF₁	1.12	0.26	0.97	3.38	0.92	0.91
ACF₂	1.31	0.32	0.94	4.12	1.36	0.86
ACF₃	1.73	1.20	0.99	4.03	2.73	0.78
ACF₄	1.10	0.21	0.99	4.00	1.71	0.56
ACF₅	1.43	0.67	0.98	8.24	1.99	0.39

These results indicated that both the Langmuir and Freundlich isotherm models can adequately describe the adsorption data. The applicability of the two isotherm models to the investigated systems implies that both monolayer adsorption (i.e., only a limited number of surface sites are adsorbing sites for the phenol molecule) and heterogeneous surface conditions exist under the experimental conditions studied.

III.3.3.   Adsorption kinetics

In order to analyze the rate of adsorption and possible adsorption mechanism of phenol and MB onto activated carbons samples, the pseudo-first-order and pseudo-second-order models were applied to adsorption data.

➢ **The pseudo-first-order mode**

The pseudo-first-order plots for the adsorption of phenol and MB onto ACF₁, ACF₂, ACF₃, ACF₄ and ACF₅ activated carbon at 25℃ are shown in Figure II-25 and Figure II-26, respectively, and their constants are given in Table II-12.

Table II-12: Pseudo-first-order adsorption constants of phenol and MB onto activated carbons at 25°C.

model	Pseudo-First order							
Pollutant	Phenol				MB			
Parameters	$Q_{e,exp}$ (mg.g⁻¹)	$Q_{e,cal}$ (mg.g⁻¹)	k_1 (min⁻¹)	R^2	$Q_{e,exp}$ (mg.g⁻¹)	$Q_{e,cal}$ (mg.g⁻¹)	k_1 (min⁻¹)	R^2
ACF₁	2.28	0.99	-0.53	0.94	1.91	1.00	-2.17	0.74
ACF₂	2.00	1.00	-0.14	0.81	1.34	0.89	-1.36	0.81
ACF₃	3.37	0.99	0.87	0.96	2.86	0.99	-2.82	0.73
ACF₄	1.73	0.99	-0.77	0.73	2.57	0.90	1.52	0.57
ACF₅	2.45	0.99	-0.56	0.65	3.00	0.99	-1.28	0.70
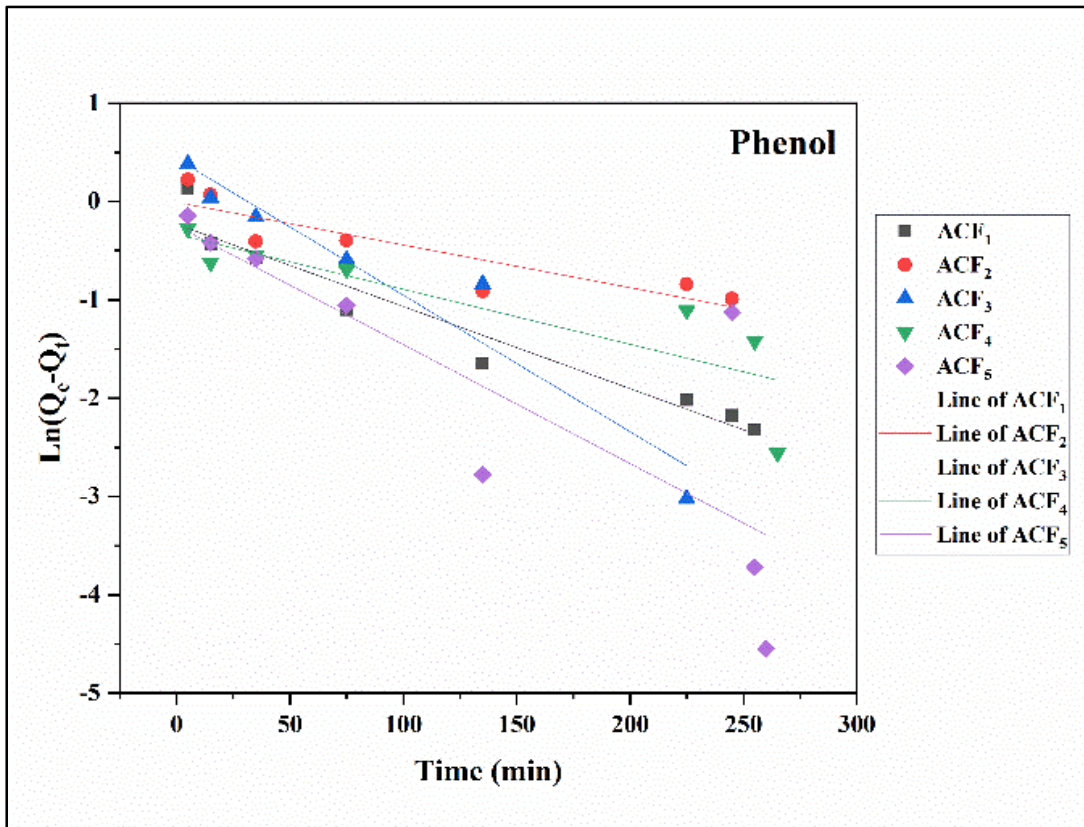
Figure II-25: Pseudo- first- order plot for the adsorption of phenol onto ACF₁, ACF₂, ACF₃, ACF₄ and ACF₅ activated carbon at 25℃.
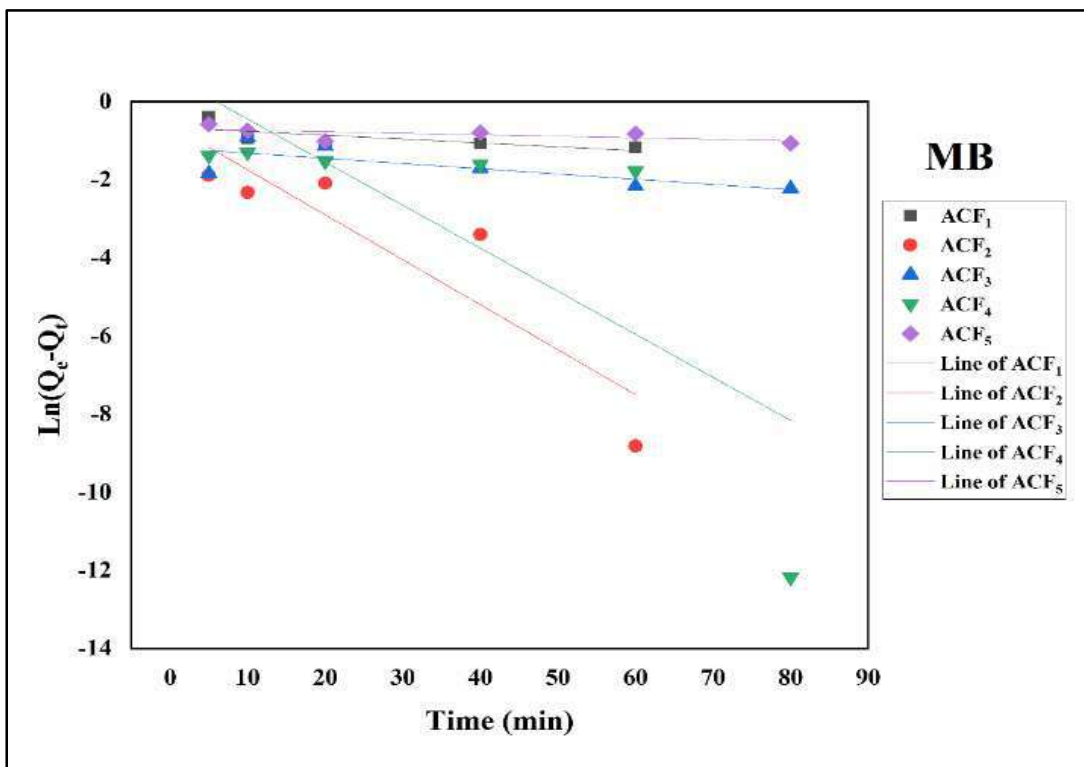
Figure II-26: Pseudo- first- order plot for the adsorption of MB onto ACF₁, ACF₂, ACF₃, ACF₄ and ACF₅ activated carbon at 25℃.

Based on Table II-12, the correlation coefficient R^2 of ACF$_1$, ACF$_2$, ACF$_3$, ACF$_4$ and ACF$_5$ was found to be for Phenol 0.94, 0.81, 0.96, 0.73, and 0.65 respectively. And for MB 0.74, 0.81, 0.73, 0.57, and 0.70 respectively. It should be noted that these are undesirable low values, and the values of calculated adsorption capacities ($Q_{e,cal}$, calculated) were far lower than experimental ones ($Q_{e,exp}$, experimental), where it is estimated at about a third, suggesting that the adsorption process did not fit the pseudo-first-order model.

➢ **The pseudo-second-order model**

The pseudo-second-order plots for the adsorption of phenol and MB onto ACF$_1$, ACF$_2$, ACF$_3$, ACF$_4$ and ACF$_5$ activated carbon at 25℃ are shown in Figure II-27 and Figure II-28, respectively, and their constants are given in Table II-13.
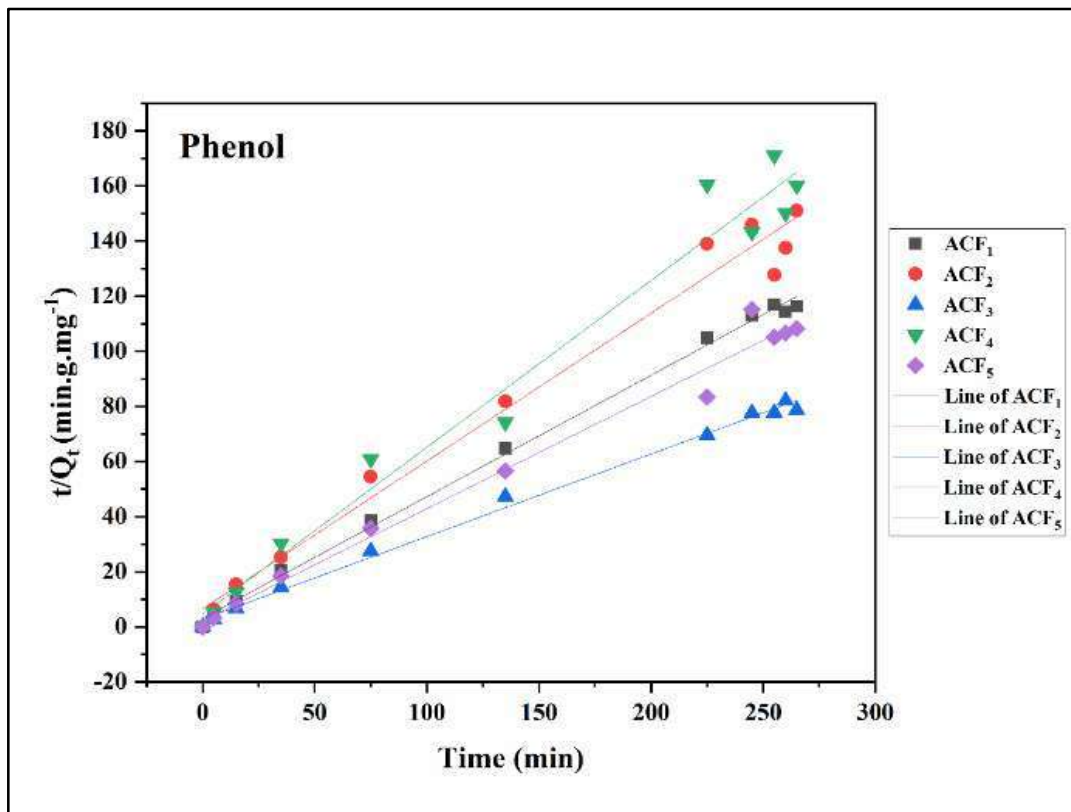
Figure II-27: Pseudo-second order plot for the adsorption of phenol and MB onto ACF$_1$, ACF$_2$, ACF$_3$, ACF$_4$ and ACF$_5$ activated carbon at 25℃.
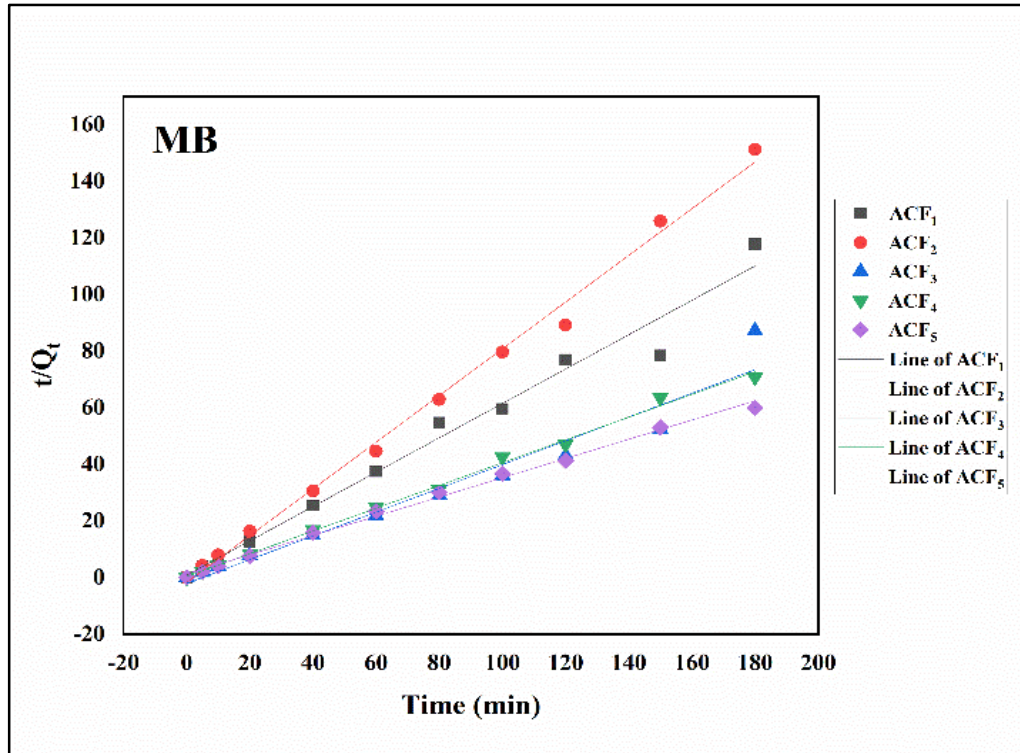
Figure II-28: Pseudo-second order plot for the adsorption of MB onto ACF$_1$, ACF$_2$, ACF$_3$, ACF$_4$ and ACF$_5$ activated carbon at 25℃.

Table II-13: Pseudo-second-order adsorption constants of phenol and MB onto activated carbons at 25°C.

model	Pseudo-second order							
Pollutant	**Phenol**				**MB**			
Parameters	$Q_{e,exp}$ (mg.g^{-1})	$Q_{e,cal}$ (mg.g^{-1})	K_2 (g.mg^{-1}.min^{-1})	R^2	$Q_{e,exp}$ (mg.g^{-1})	$Q_{e,cal}$ (mg.g^{-1})	K_2 (g.mg^{-1}.min^{-1})	R^2
ACF$_1$	2.28	2.27	0.06	1.00	1.91	1.65	0.33	0.98
ACF$_2$	2.00	1.86	0.04	0.98	1.34	2.08	-0.46	0.99
ACF$_3$	3.37	3.33	0.03	1.00	2.86	2.38	0.15	1.00
ACF$_4$	1.73	1.65	0.08	0.98	2.57	2.03	0.75	1.00
ACF$_5$	2.45	2.45	0.08	0.99	3.00	2.38	0.11	1.00

Based on Table II-13, the correlation coefficient R^2 of ACF$_1$, ACF$_2$, ACF$_3$, ACF$_4$ and ACF$_5$ was found to be for Phenol 1.00, 0.98, 1.00, 0.98, and 0.99 respectively. And for MB 0.98, 0.99, 1.00, 1.00, and 1.00 respectively. It should be noted that they are desirable excellent values. The difference between the values of calculated adsorption capacities ($Q_{e,cal}$, calculated) and the experimental ones ($Q_{e,exp}$, experimental) is not very large, where they are almost equal, suggesting that the adsorption process did fit the pseudo-second-order model.

The work indicated that the pseudo-first-order model is not suitable for the adsorption of both phenol and methylene blue, while the pseudo-second-order model showed results indicating its association with their adsorption.

> **Thermodynamic adsorption**

Figure II-29 and Figure II-30 illustrate the adsorption thermodynamic plot for the adsorption of phenol and MB onto ACF_1, ACF_2, ACF_3, ACF_4, and ACF_5 activated carbon respectively, and their parameters listed in the Table II-14 .

Figure II-29: Adsorption thermodynamic plot for the adsorption of phenol onto ACF_1, ACF_2, ACF_3, ACF_4 and ACF_5 activated carbon.
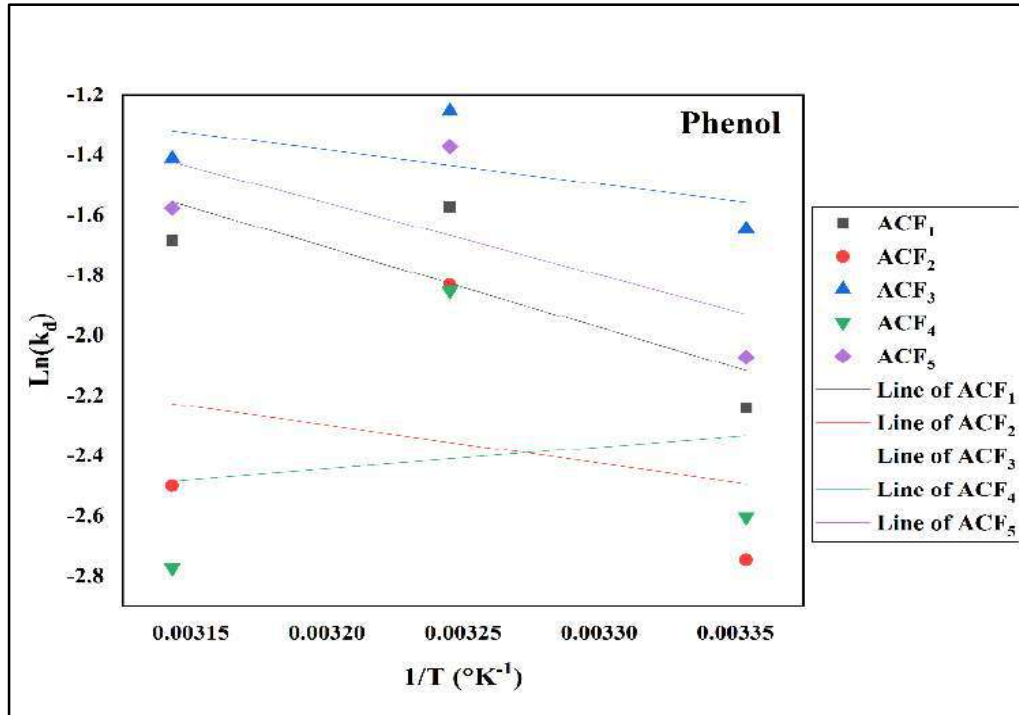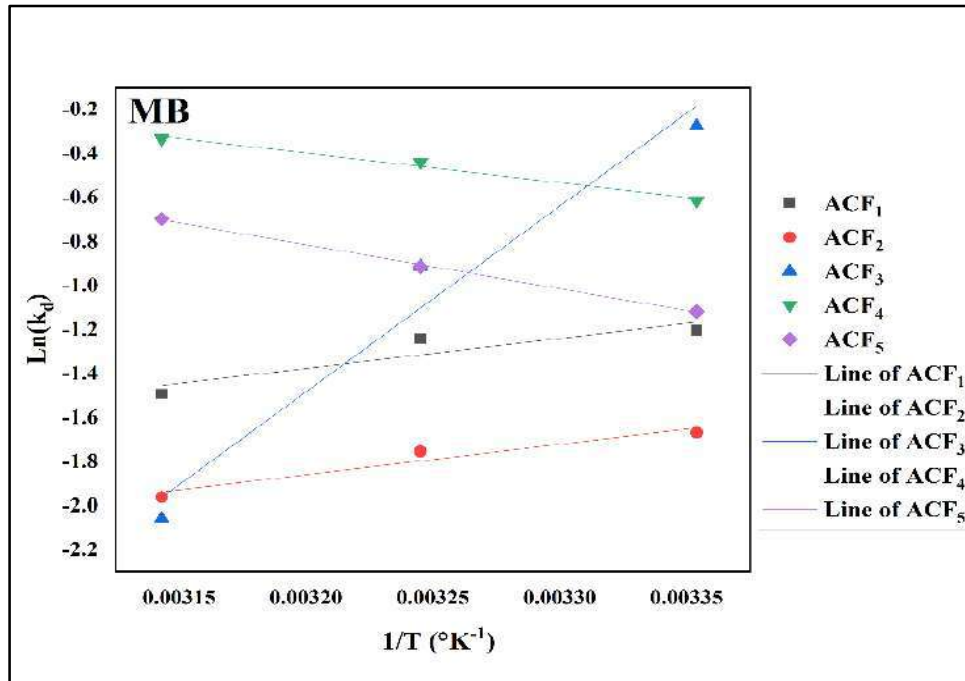

Figure II-30: Adsorption thermodynamic plot for the adsorption of MB onto ACF_1, ACF_2, ACF_3, ACF_4 and ACF_5 activated carbon.

Table II-14: Adsorption thermodynamic constants for the adsorption of phenol and MB onto activated carbons.

	T (K)	K_d (L.g^{-1})	Phenol ΔH° (KJ. mol^{-1})	ΔS° (KJ. mol^{-1})	ΔG° (KJ. mol^{-1})	K_d (L.g^{-1})	Methylene blue ΔH° (KJ. mol^{-1})	ΔS° (KJ. mol^{-1})	ΔG° (KJ. mol^{-1})
ACF$_1$	298.15	0.11			5.25	0.23			3.46
	308.15	0.21	22.17	0.06	4.68	0.27	-1.44	-0.02	3.62
	318.15	0.19			4.11	0.23			3.79
ACF$_2$	298.15	0.06			6.18	0.19			4.08
	308.15	0.16	10.47	0.01	6.04	0.17	-11.50	-0.05	4.60
	318.15	0.08			5.89	0.14			5.13
ACF$_3$	298.15	0.19			3.86	0.76			0.45
	308.15	0.29	9.42	0.02	3.67	0.40	-70.16	-0.24	2.82
	318.15	0.24			3.49	0.13			5.19
ACF$_4$	298.15	0.07			5.78	0.54			1.50
	308.15	0.16	-5.96	-0.04	6.18	0.65	11.18	0.03	1.17
	318.15	0.06			6.57	0.72			0.85
ACF$_5$	298.15	0.13			18.28	0.33			2.78
	308.15	0.25	-0.05	-0.06	18.89	0.40	16.59	0.05	2.32
	318.15	0.21			19.51	0.50			1.85

Thermodynamic parameters are important in adsorption studies; they provide a better understanding of the effect of temperature on the adsorption process. They include standard enthalpy change (ΔH°), Standard entropy change (ΔS°) and standard free energy change (ΔG°) ([Anbarasan et al., 2021](#)).

The negative values of (ΔH°) obtained in the adsorption indicate that the adsorption process was exothermic in nature whereas it was endothermic in the positive values. Positive values of (ΔS°) indicate an increase in randomness at the solid-solution interface during the adsorptions process. This indirectly shows the affinity of the adsorbents towards the adsorbate molecule, while the negative values indicate a decrease in randomness. Negative (ΔG°) values indicate that the adsorption was spontaneous in nature and was non-spontaneous in positive values.

Whereas, the increasing in (ΔG°) values with increasing temperature. It is suggested that at higher temperature, more driving forces are leading to higher adsorption update. While the decreasing in values of (ΔG°) with increasing temperature. It suggests that at higher temperature the driving forces are less resulting in lower adsorption update

Through both the figure and the table, we notice different results from one sample to another, and this is due to the nature and composition of the active sites and the

characteristics of the pores of each sample in addition to the type of absorbent and how to interact with it.

As for the adsorption of phenol, we note that the adsorption onto ACF_1, ACF_2, ACF_3 have positive values of ($\Delta H°$) and ($\Delta G°$) and ($\Delta S°$), that indicate it is an endothermic and non-spontaneous in nature with an increase in randomness respectively. As for the sample ACF_4 and ACF_5 has a negative value of ($\Delta H°$) and ($\Delta S°$) with positive values ($\Delta G°$), which indicate that their adsorption is endothermic with decrease randomness and still non-spontaneous in nature.

For the adsorption of methylene blue, the adsorption onto ACF_1, ACF_2, and ACF_3 has a negative value of ($\Delta H°$) and ($\Delta S°$) and positive ($\Delta G°$) values that indicate it is an exothermic with a decrease in randomness and it is non-spontaneous in nature respectively. As for ACF_4 and ACF_5 it is exactly the opposite. The adsorption is endothermic with increase randomness and still non-spontaneous. generally, the thermodynamic adsorption data indicated that the adsorption was physical.

IV. Application

Our society has grown and today relies on the massive use of fossil resources (coal, gas, and oil). However, the rapid development of emerging countries and the growing energy needs of all, pose two major problems that are the management of energy stocks and global warming(Belhachemi, 2001; Largeot, 2009).

Electrochemical charge storage at an electrical double layer formed at an electrode-electrolyte interface (electrochemical double-layer capacitors, EDLC) is currently under extensive investigation owing to their high power capabilities than other existing electrical energy storage devices (Misnon, Zain, & Jose, 2019).

The need for electrical energy has led to a rapid increase in research on energy storage systems, particularly batteries and supercapacitors. These two systems are, in fact, complementary, the batteries having high energy densities and the supercapacitors being able to deliver high power densities. Currently, among the different types of supercapacitors, those whose electrodes are based on activated carbon, called carbon/carbon supercapacitors, are the most successful systems; they are produced in large numbers and used in various applications requiring power peaks (starting

vehicles, saving memory, the emergency opening of doors, etc.) (Belhachemi, 2001; Largeot, 2009).

Carbons nanomaterials or nanostructures of all forms, viz. activated carbons (ACs), graphite, graphene, carbon nanotubes (CNTs), carbon nanofibers, carbon aerogels, and carbon quantum dots, are the commercial choice for EDLCs because (i) their higher electrical conductivity (among other materials of large surface area) enable fast charging and discharging and high power density (PD) thereby, (ii) long cycle stability, and (iii) cost practicality. Although graphene and CNTs offer much superior electrical conductivity and surface area than the other forms of carbon, ACs are currently used for the commercialization of supercapacitors (SCs) due to their renewability and ease of processability, and lower cost, tunable surface area to enable the optimum electrode-electrolyte interface, tailor ability of pore distribution by controlling the synthetic conditions, and acceptable electrical conductivity (Misnon et al., 2019).

The supercapacitor consists of two porous electrodes, generally made of activated carbon and impregnated with electrolyte, which are separated by an insulating and porous membrane (to ensure ionic conduction).

Activated carbon prepared from a low-cost material, has a relative conductivity, good temperature stability, and corrosion; while NCT has high conductivity and a big specific surface. they are, therefore, materials of choice in supercapacitors. So the objective of this part is the preparation of electrodes using the activated carbon from the date palm fiber with CNT and compared in terms of energy density and power density.

IV.1.   Electrode preparation steps

We go through several processes in order to prepare the electrode, which is grinding and sifting, then activating and drying, passing through the preparation of the colloidal solution for forming the active substance in order to complete the preparation of an electrode and then characterize it.

Activated carbon (AC) is a typical material for supercapacitor electrode fabrication and operates in the electrochemical double layer mechanism. Biomass-derived carbon is an attractive precursor of AC synthesis due to its renewable and cost-efficient properties.

1) Crashing and sifting

In order to ensure that the colloidal solution is formed, we must ensure that the samples are well crushed and the same size, so we use the grinding device (Broyeur à Billes Haut énergie Avec Refroidissement circulation) and then the sifting device (Tamiseuse à vibrations AS 200 control).

- ✓ The crashing is done for 10 min with 20 balls under-speed 500 tr.s^{-1} at 21°C.
- ✓ The sifting took place for 15 min with a 40 µm sieve small one.
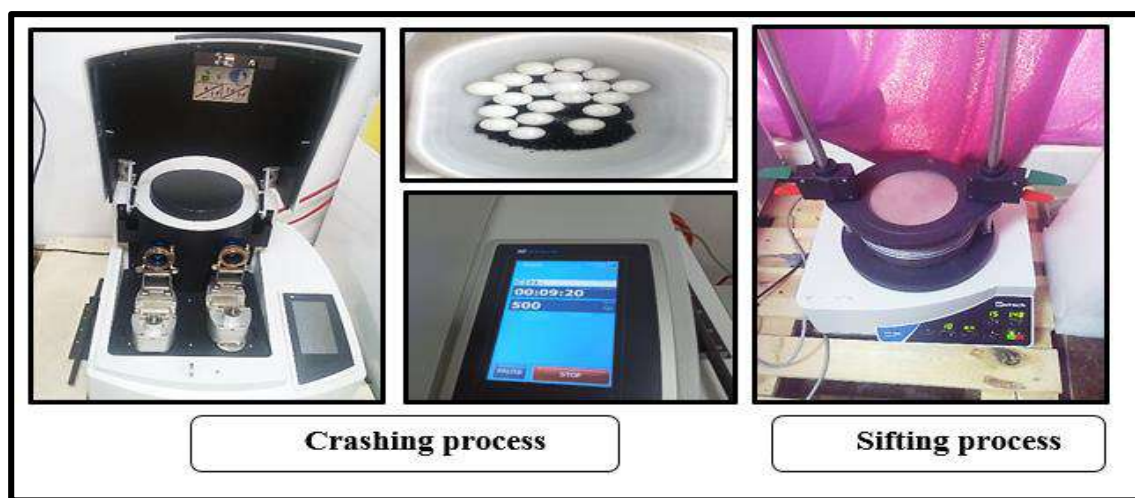
Image II-11: Crashing and sifting process

2) Activating and drying

- In order to improve the reactive activity, in particular the adsorption capacity of activated carbon (AC), the AC will first be acid-treated with HNO_3.

- 1 g of AC was added to 50 ml of 6M HNO_3 solution with stirring 130 rpm for 1 hour at 80 °C in incubator device (IKA® KS 3000 ic control), in order to introduce negative groups on its surface.
- The product was washed with distilled water until nature pH obtained, and then was recovered by means of a filtration system using centrifuge device (ROTINA 380 R) **Error! Reference source not found.** for 20 min with 3500 rpm, and dried in an oven (memmert oven) at 60 °C for one day.
- The product obtained was mark as ACFH ($ACFH_1$, $ACFH_2$, $ACFH_3$, $ACFH_4$, and $ACFH_5$).

Image II-12: Acidification process

3) The colloidal solution preparation

After the acidification process, different colloidal solutions with a concentration of $2mg.ml^{-1}$ are prepared with the following compositions and ratios:

- MWCNT (10mg in 5ml of distilled water),
- $ACFH_1$ (10mg in 5ml of distilled water),
- $ACFH_2$ (10mg in 5ml of distilled water),
- $ACFH_3$ (10mg in 5ml of distilled water),
- $ACFH_4$ (10mg in 5ml of distilled water),
- $ACFH_5$ (10mg in 5ml of distilled water),
- $MWCNT/ACFH_1$ (5mg MWCNT and 5mg of $ACFH_1$ in 5ml of distilled water),
- $MWCNT/ACFH_2$ (5mg MWCNT and 5mg of $ACFH_2$ in 5ml of distilled water),
- $MWCNT/ACFH_3$ (5mg MWCNT and 5mg of $ACFH_3$ in 5ml of distilled water),
- $MWCNT/ACFH_4$ (5mg MWCNT and 5mg of $ACFH_4$ in 5ml of distilled water),
- $MWCNT/ACFH_5$ (5mg NTC and 5mg of $ACFH_5$ in 5ml of distilled water),

- The solutions of the mixture are kept in a relatively cold ultrasonic bath until the solutions become colloidal solutions.

Image II-13: The colloidal solution preparation

Note: The colloidal solution preparation was applied in all the products but only MWCNT/ACFH$_1$, MWCNT/ACFH$_2$, and MWCNT have been successful in the experiment, because the aforementioned samples are light compared to the samples in which the colloidal solution did not form.

4) The active material forming

- 1 ml of the colloid solution is deposited by flow drop on a surface of 1 cm^2 of glass and dried in an oven at 40 °C, to obtain 2 mg.cm^{-2} of the active material.

We must ensure that the active material contacts the carrier (aluminum) and is homogeneous along the surface to eventually have a successful electrode.

Image II-14: The electrodes prepartion

- It is noteworthy that the only valid electrodes are MWCNT, MWCNT/ACFH$_1$ and MWCNT/ACFH$_2$.

- Then we proceed to the characterization of the obtained electrodes using a VoltaLab 40 (Dynamic Potentiostat PGZ301).

IV.2.   Electrodes Characterization

Image II-15: The VoltaLab instrumentation

VoltaLab instrumentation: is ideal for DC and AC electrochemical analysis applications in the areas of corrosion, pitting testing, battery testing, fuel cells, electroplating, electro catalysis, nanomaterial's, coatings and sensor development and includes a series of potentiostats and current/ voltage amplifiers (SAS, 2005).

Three-Electrode Setup: To conduct an experiment, one requires three electrodes.

- **The reference electrode:** is a half cell with a known reduction potential. Its only role is to act as reference in measuring and controlling the working electrode's potential and at no point does it pass any current.

- **The auxiliary electrode:** acts as the other half of the cell, it must have a known potential with which to gauge the potential of the working electrode; furthermore, it must balance the charge added or removed by the working electrode.

- **The working electrode:** which makes contact with the analyte, must apply the desired potential in a controlled way and facilitate the transfer of charge to and from the analyte (Marken, Neudeck, & Bond, 2010).

Image II-16: The three-Electrode Setup

Because it is extremely difficult for an electrode to maintain a constant potential while passing current to counter redox events at the working electrode. The auxiliary electrode passes all the current needed to balance the current observed at the working electrode. To achieve this current, the auxiliary will often swing to extreme potentials at the edges of the solvent window, where it oxidizes or reduces the solvent or supporting electrolyte. These electrodes, the working, reference, and auxiliary make up the modern three-electrode system.

The cyclic voltammetry and galvanostatic charge/discharge types of electrochemical analyses award the most reliable results to evaluate usefulness of the examined materials as electrodes for supercapacitors.

IV.2.1.   Cyclic voltammetry

Voltammetry experiments investigate the half-cell reactivity of an analyte. Cyclic voltammetry (CV) is a type of potentiodynamic electrochemical measurement and it is the study of current as a function of applied potential.

In a cyclic voltammetry experiment, the working electrode potential is ramped linearly versus time. Unlike in linear sweep voltammetry, after the set potential is reached in a CV experiment, the working electrode's potential is ramped in the opposite direction to return to the initial potential. These cycles of ramps in potential may be repeated as many times as needed. The current at the working electrode is plotted versus the applied voltage (that is, the working electrode's potential) to give curves $I = f(E)$ are called cyclic voltammogram trace (Largeot, 2009; Marken et al., 2010).

The shape of the curves depends on the speed of potential variation (nature of driving force) and on whether the solution is stirred or quiescent (mass transfer). Most experiments control the potential (volts) of an electrode in contact with the analyte while measuring the resulting current (amperes).

Cyclic voltammetry is generally used to study the electrochemical properties of an analyte in solution or of a molecule that is adsorbed onto the electrode.

The cyclic voltammetry detection tests were carried out in a three-electrode cell: a reference electrode Calomel B20B110 (Hg_2Cl_2), counter-electrode with platinum Disc B35M150 and the working electrodes which are MWCNT/ACFH$_1$, MWCNT/ACFH$_2$, and MWCNT using VoltaLab 40 (Dynamic Potentiostat PGZ301).

The cyclic voltammetry measurements are made in an aqueous solution of 0.1M H_2SO_4 with a different scanning speeds of 5, 10, 20, 30, 40, 60, 80, 100, 120 mV/s; the active surface is $1cm^2$. Figure depicts the cyclic voltammograms of the carbon electrode.
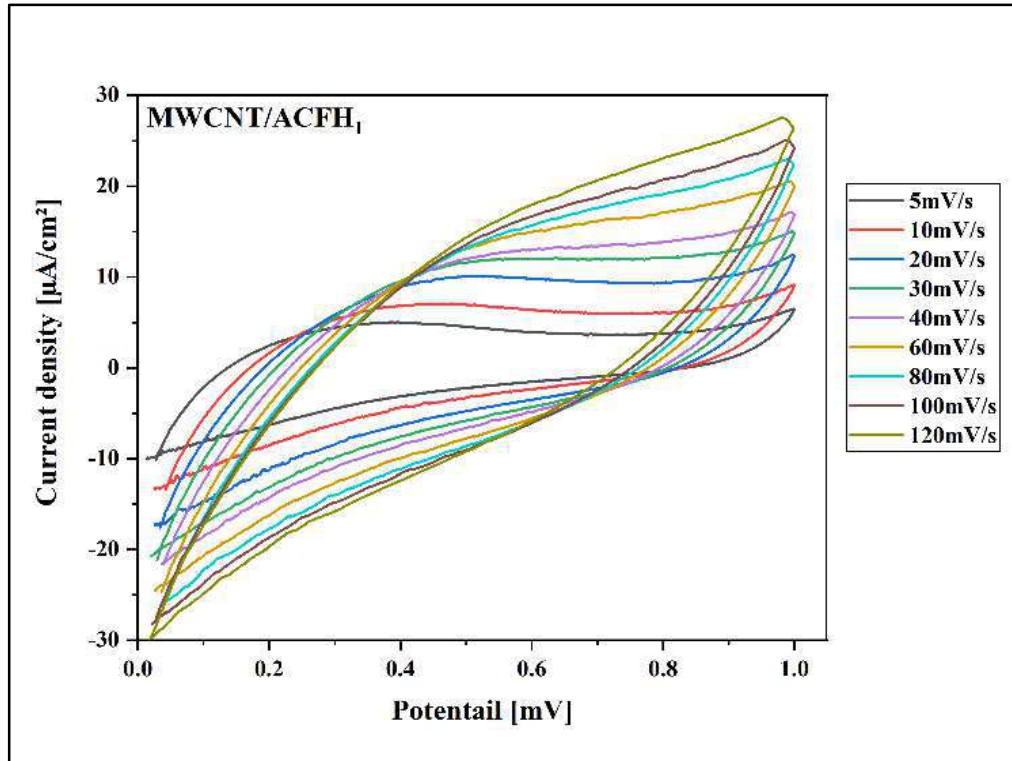
Figure II-31: The CV curves of MWCNT/ACFH$_1$ at the potential window of 0-1 mV and scan rate range of 5–120 mV/s.
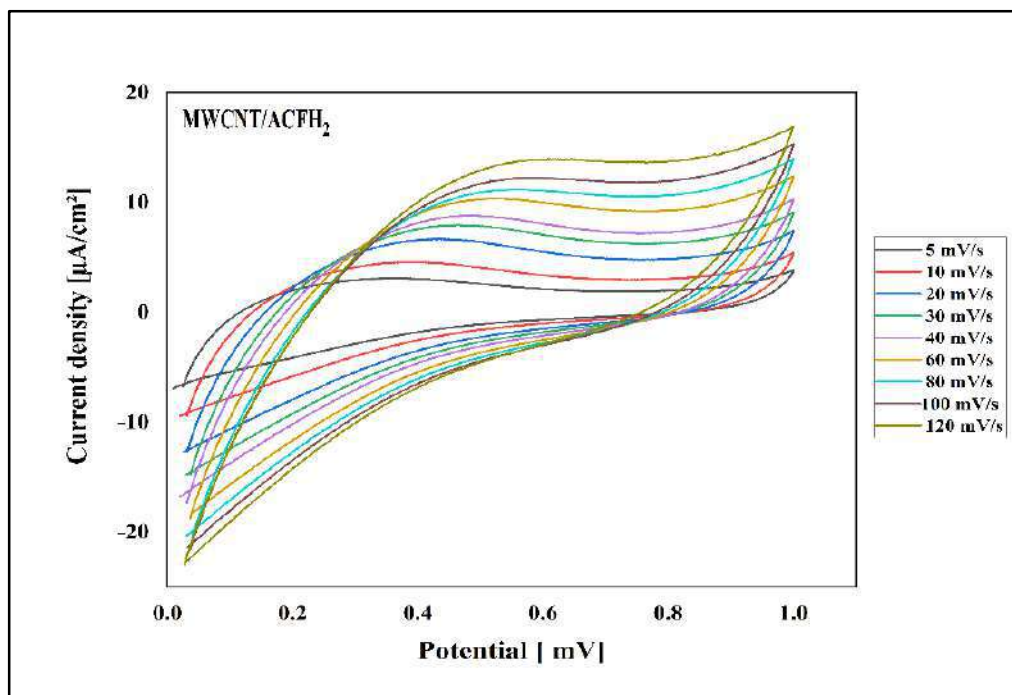
Figure II-32: The CV curves of MWCNT/ACFH$_2$ at the potential window of 0-1 mV and scan rate range of 5–120 mV/s.
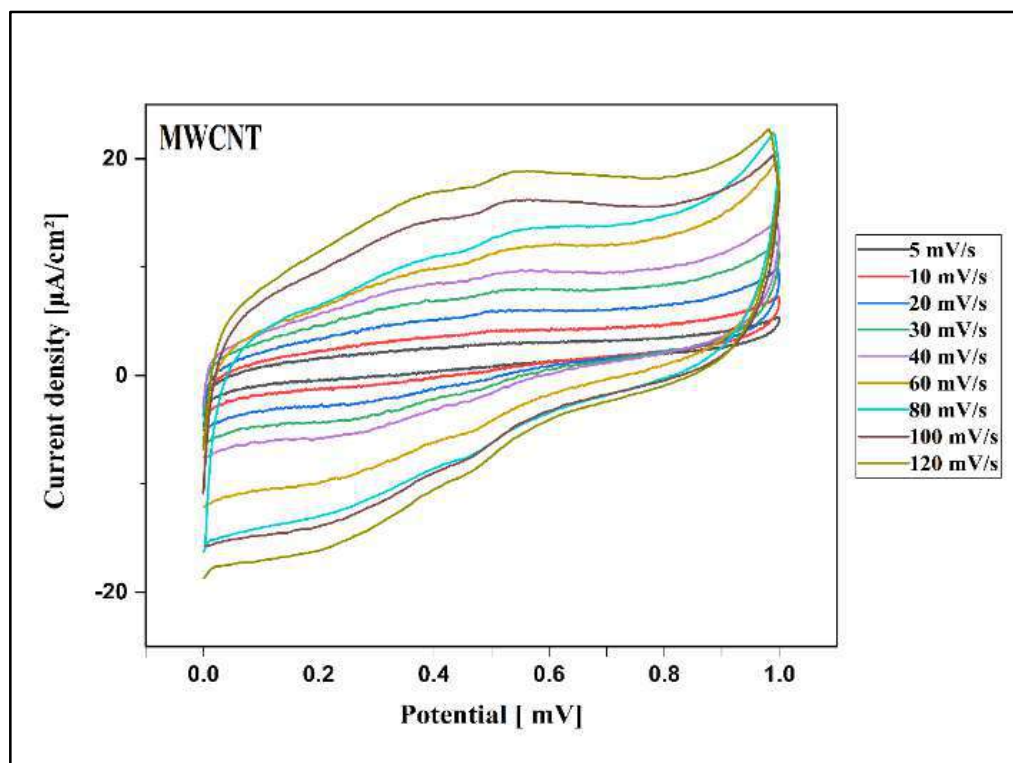
Figure II-33: The CV curves of MWCNT at the potential window of 0-1 mV and scan rate range of 5–120 mV/s.

Figure II-31, Figure II-32 and Figure II-33 shows the CV curves of MWCNT/ACFH$_1$, MWCNT/ACFH$_2$, and MWCNT at the potential window of 0 to 1 mV according to the potential sweep rate range of 5–120 mV.s^{-1} respectively.

Generally, all the electrodes demonstrate a quasi-rectangular CV curve. This near rectangular curve suggested an ideal capacitor and that the electrodes have a rapid charge and discharge mechanism. However, the curves contained a small slant, this slope of the charging curve results from the charging resistance of the electrode, or more precisely from the time constant of the capacitive electrode.

Furthermore, the rectangular shape of the CV curves remains unchanged at a high scan rate, proving the high-rate performance of the electrodes. This is due to the porous structure of ACFs and MWCNT, which provide many paths for transporting electrolyte ions into the bulk electrode. The lower the resistance the more the cyclic voltammogram approaches a rectangular shape.

In the EDLC mechanism, there is only ion absorption and desorption took place on the interface of electrodes. Since the presence of pores improves the surface area of electrode, the ion movement process can be enhanced for better EDLC performance.
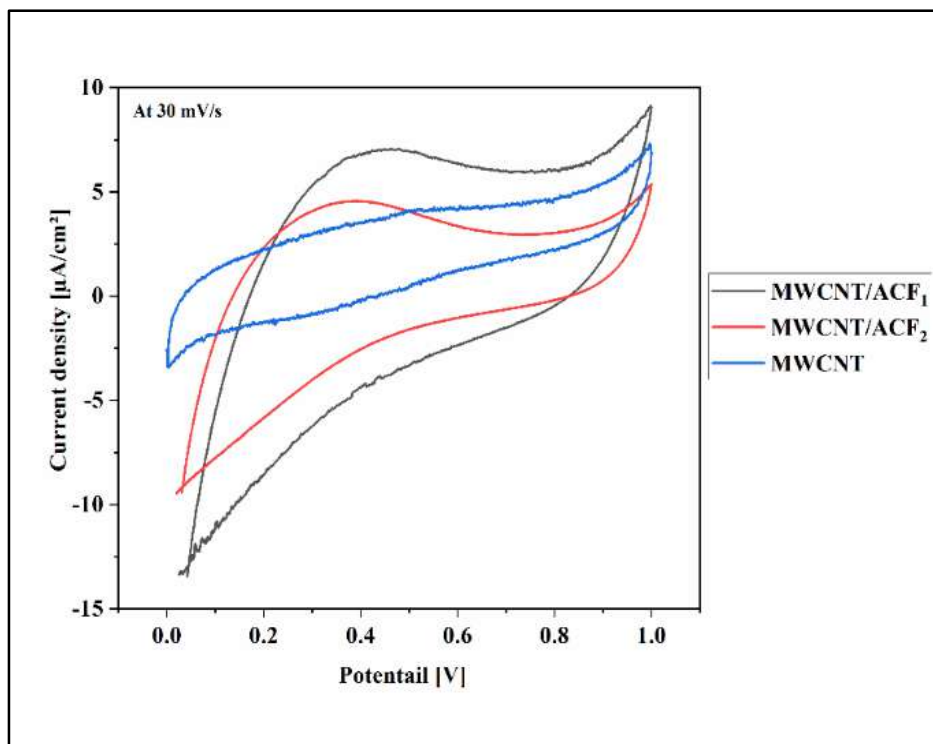
Figure II-34: The CV curves of MWCNT/ACFH1, MWCNT/ACFH2, and MWCNT at the potential window of 0-1 mV and scan rate 30 mV/s.

The comparison of CV curves for all the electrodes at scan rate of 30 mV.s^{-1} is compared in Figure II-34. MWCNT has the most rectangular shape of the CV curve as compared with other electrodes. This condition describes that there is mainly an EDLC mechanism that takes place in MWCNT electrode, and the current is quite stable with the rise of voltage. In contrast, MWCNT/ACFH$_1$ and MWCNT/ACFH$_2$ have a slightly distorted rectangular curve, suggesting that a minimum redox reaction take places in MWCNT/ACFH$_1$ and MWCNT/ACFH$_2$ electrode.

IV.2.1.   Charge-discharge galvanostatic

Galvanostatic cycling involves applying a constant current across a supercapacitor and measuring the potential response of the electrode or cell. This technique is widely used to study the cycle life of a supercapacitor. It also makes it possible to calculate the capacitance as well as the equivalent series resistance RS of the cell. System degradation can be estimated by the increase in RS after cycling (Dinh, 2014; Largeot, 2009).

A constant current is applied to the terminals of the supercapacitor between two potential terminals. The potential response of the cell and the electrodes is then recorded. The representative electrical circuit of a supercapacitor is the series

association of a capacitor and a resistor. Determination of the optimum operating potential is crucial for maximizing the life time of cells. Each electrolyte behaves differently, therefore, it is analyzed individually using GCD technique (Misnon et al., 2019).
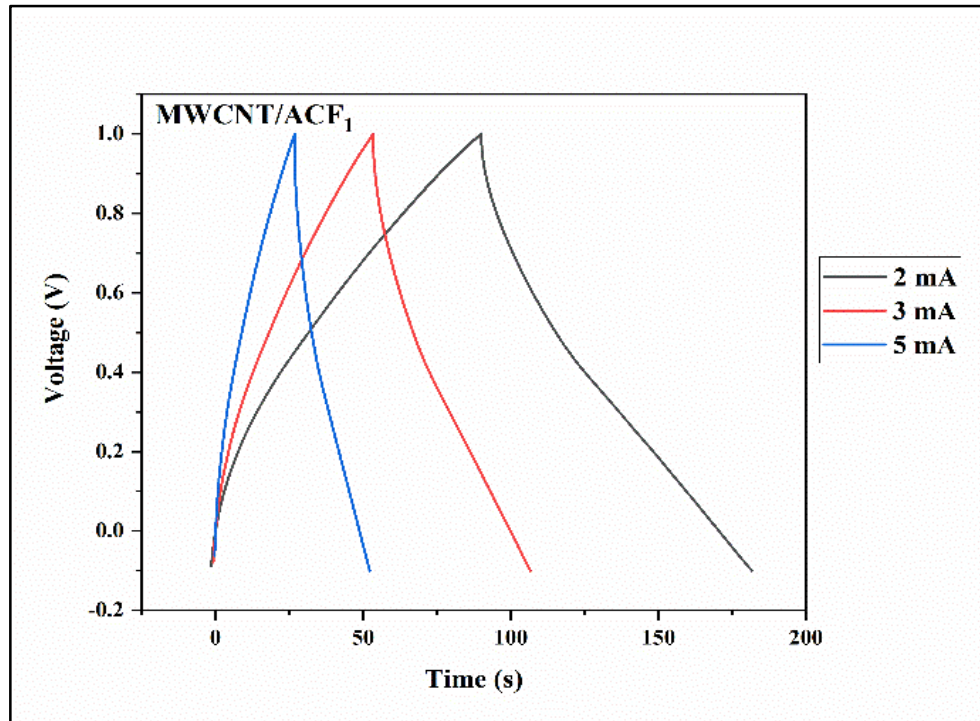
Figure II-35: GCD curve of MWCNT/ACFH$_1$ in 0.1M H$_2$SO$_4$ electrolyte at the potential window from 0 to 1 V.
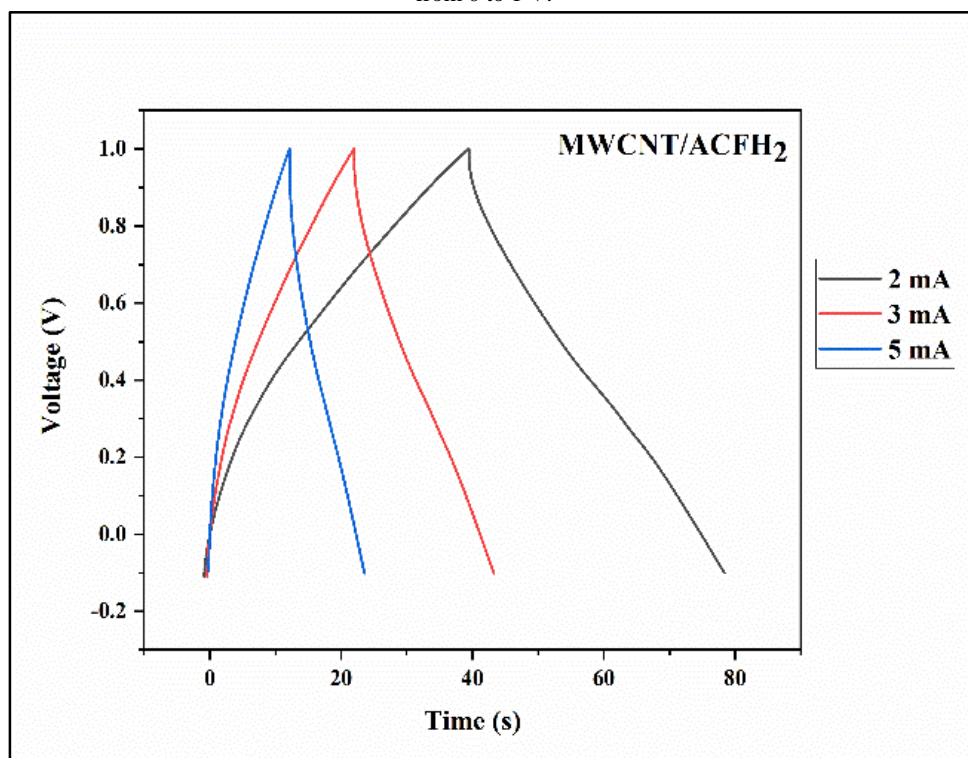
Figure II-36: GCD curve of MWCNT/ACFH$_2$ in 0.1M H$_2$SO$_4$ electrolyte at the potential window from 0 to 1 V.

90
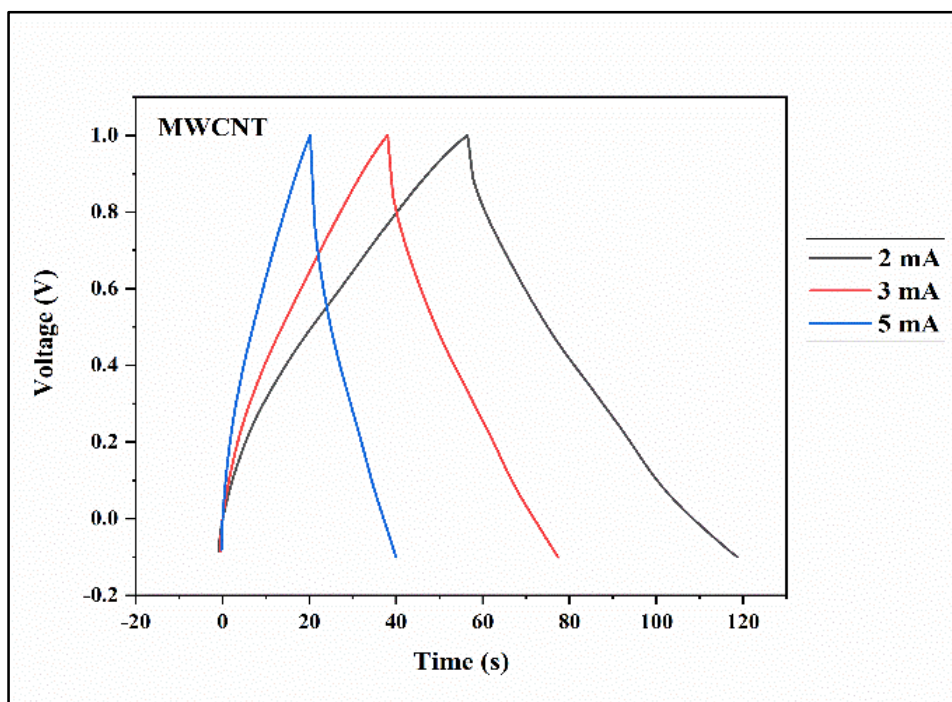
Figure II-37: GCD curve of MWCNT in 0.1M H_2SO_4 electrolyte at the potential window from 0 to 1 V.

The GCD curves of MWCNT/ACFH$_1$, MWCNT/ACFH$_2$, and MWCNT at the potential range of $-$ 1.0 to 1.0 V in 1 M H_2SO_4 electrolyte at a three current 2, 3, and 5 mA are shown in Figure II-35, Figure II-36, and Figure II-37 respectively.
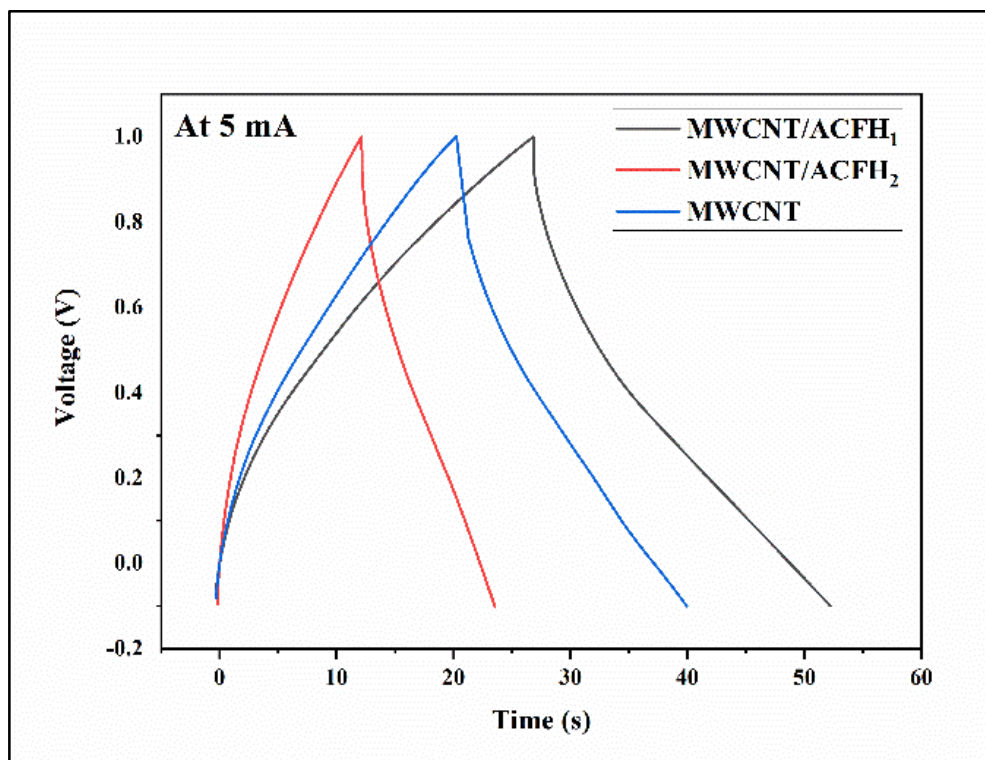
Figure II-38: Galvanostatic charge/discharge curves with a current load of 5 mA in 1 M H_2SO_4
electrolyte for MWCNT/ACFH$_1$, MWCNT/ACFH$_2$, and MWCNT electrodes.

Generally, all electrodes display a triangular shape of GCD curve. This represents the ideal charging and discharging mechanism of the electrodes, which are indicative of good capacitive behavior, high electrochemical stability, rapid charge reversibility and long cycle life, which indicating that EDLC mechanism occurs during the reaction (Misnon et al., 2019; Misnon, Zain, Lei, Vijayan, & Jose, 2020).

For GCD analysis, The specific capacity C_S of the electrodes was measured from the GCD graphs using the following equation (Misnon et al., 2020):

$$C_S = \frac{i\,t_d}{mV}\, ...Eq\ 30$$

The energy density (E_D) and the power density (P_D) was calculated using the following equations (Misnon et al., 2019):

$$E_D = \frac{1}{2}C_S V^2 ....Eq\ 31$$

$$P_D = \frac{E_D \times 3600}{t_d}........Eq\ 32$$

Where:

- C_S: The Specific capacity (F.g^{-1});
- i: The current (A);
- t_d: The discharge time required for each applied current;
- m: Mass-loading (g);
- V: Potential window (V);
- E_D: Energy density (Wh.kg^{-1});
- P_D: Power density (W.kg^{-1}).
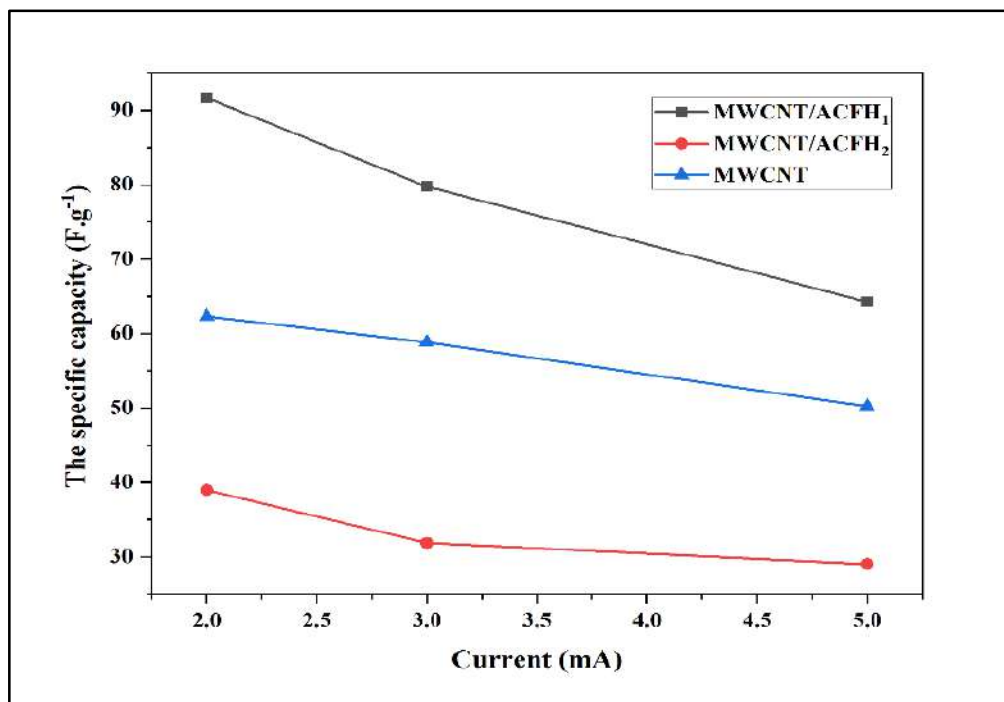
Figure II-39: Specific capacitance versus current plots of electrodes

The variation of specific capacitance as a function of current of electrodes is presented in Figure II-39. Higher specific capacitance was observed at a lower current in all the studied electrodes. The C_S decreases when current increase. The C_S values are ranging from 91.64 to 64.25 $F.g^{-1}$ for MWCNT/ACFH$_1$, 38.99 to 29.05 $F.g^{-1}$ for MWCNT/ACFH$_2$ and 62.30 to 50.22 $F.g^{-1}$ for MWCNT, the high C_s value was by MWCNT/ACFH$_1$ this is contributed by high S_{BET} and well-developed pore structure and the low C_s value was by MWCNT/ACFH$_2$, Low specific capacitance at higher current is due to lack of time for electrolyte ions to adsorb and desorb on the surface of the electrode (Bhoyate et al., 2017).

At the same time, the mesopore structure allows more ions to diffuse into porous active material, maximizing the charge-discharge process. As a result, more EDLC mechanism takes place and leads to enhancement of C_S of electrodes. These results are contributed by good physicochemical properties of ACF and MWCNT:

- Good carbon crystallinity for charge transport,
- Presence of functional group for adsorption capacity,
- Well-developed porosity structure for electrolyte ion diffusion (Misnon et al., 2020).

High S_{BET} provides more active sites for more electrolyte accumulation on the electrode–electrolyte surface, but from the Table II-3 we note that ACF$_2$ has a higher

surface area than ACF_1, which leads to the following arrangement for the electeodes: the surface area of $MWCNT/ACFH_2$ is greater than the surface area of $MWCNT/ACFH_1$ is greater than the surface area of MWCNT. But $MWCNT/ACFH_1$ showed the best results, which indicating that there is an ideal surface area for the electrodes, which should neither be more than nor less than the ideal surface area.

Therefore, the conductivity and surface area must be balanced in order to have an excellent supercapacitor.
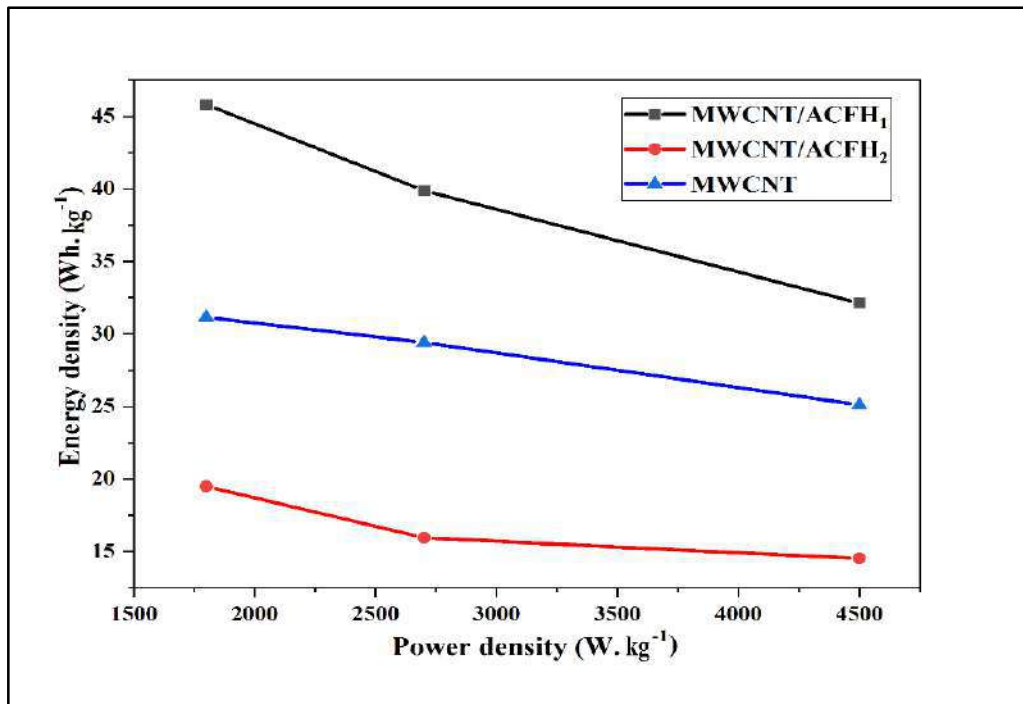
Figure II-40: Ragone plot for $MWCNT/ACFH_1$, $MWCNT/ACFH_2$, and MWCNT electrodes.

The specific power (P_D) and specific energy (E_D) for all of the cells, calculated from GCD curves using Eqs. (31) and (32), respectively, are shown as Ragone plots in Figure II-40 . demonstrate that the performance of electrodes in electrolyte, a decreasing in the specific energy with increasing specific power for all cells according to the trend ($MWCNT/ACFH_1$> MWCNT> $MWCNT/ACFH_2$). It can be clearly seen that the maximum specific energy and specific power were produced by the $MWCNT/ACFH_1$ cell, with values of 45.82 $Wh.kg^{-1}$ and 1800 $W.kg^{-1}$, respectively. These results fall within the typical range of specific energy and power density for supercapacitors, observed high energy and power density could enable its potential use for fast-charge supercapacitor batteries.

IV.2.2.　　　Morphology

Images Image II-18, Image II-19, and Image II-20 show SEM images of electrodes MWCNT/ACF$_1$, MWCNT/ACF$_2$, and MWCNT with Mag 1.00 kx and 5.00 kx respectively.

In general, samples MWCNT/ACF$_1$ and MWCNT/ACF$_2$ have similar surface shapes, characterized by the appearance of grooves forming a sponge-like surface and perfectly interconnected pores. While the figure of MWCNT shows a surface shape similar to the aforementioned figures, but with the presence of smooth, flat surfaces that reduce the presence of pores. Where the MWCNT/ACF$_1$ shows the presence of more pores than the MWCNT/ACF$_2$, and MWCNT, due to merging the samples together.
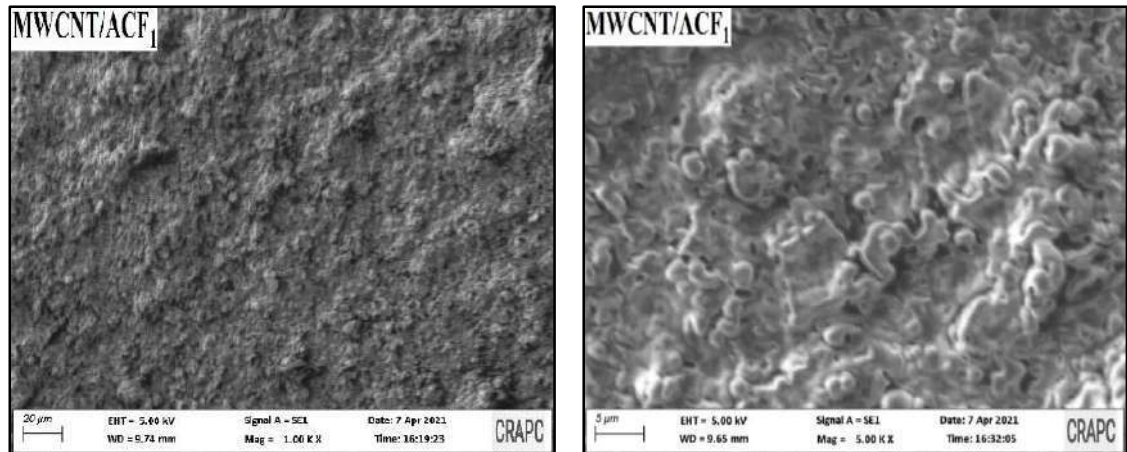
Image II-17: SEM images of electrode MWCNT/ACF$_1$ with Mag 1 and 5 kx.
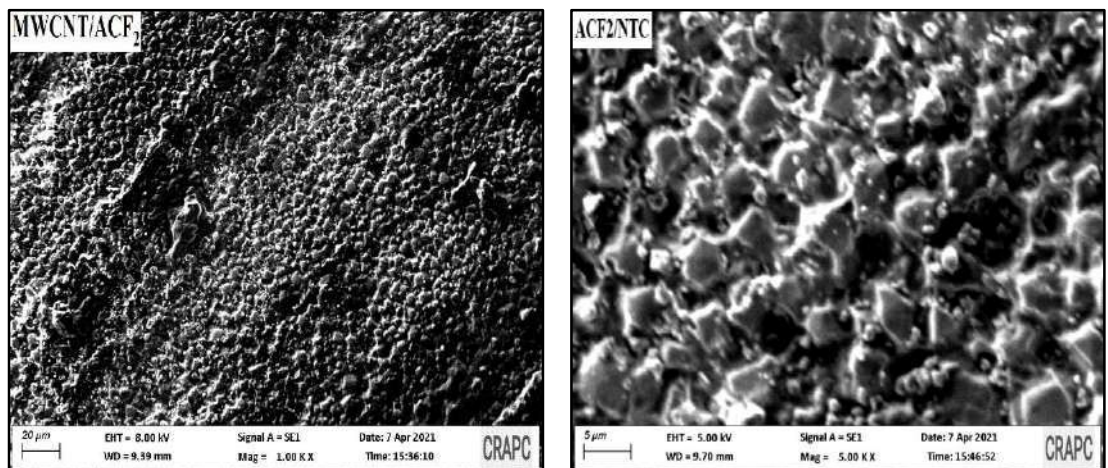
Image II-18: SEM images of electrode MWCNT/ACF$_2$ with Mag 1 and 5 kx.
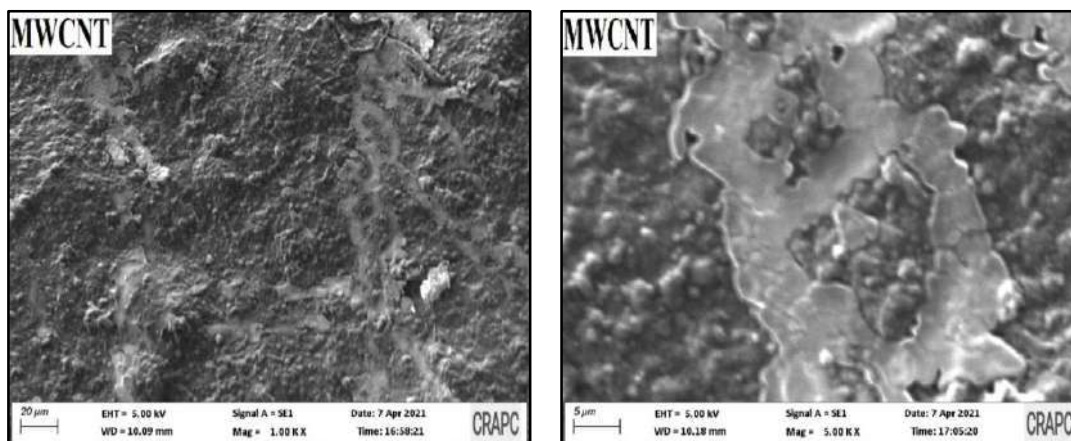
Image II-19: SEM images of electrode MWCNT with Mag 1 and 5 kx.

V. Conclusion of experimental parity

Over the course of four years 2018-2021 of experimental work, I started with the preparation of activated carbon (primary treatment, pyrolysis and physical activation) and then characterization of activated carbon samples (physical and chemical characterization and adsorption properties) to the preparation of supercapacitors as an applied example of activated carbon for energy storage

The overall results of the experimental work are as follows:

✓ Date palm fibers are suitable for the preparation of successful activated charcoal with excellent surface area and best properties, it can be effectively utilized as a raw material for ACF production.

✓ From the physical characterization, we note that:

- the highest burn-off was 95.73 wt% for the ACF_2 which means that it has the largest surface area and pores volume compared to other activated carbons.

- From the N_2 adsorption-desorption isotherm at 77K we found a clear different structures of samples, while the higher amount of nitrogen adsorbed is for ACF_2 sample, and with BET surface area 313.40 $m^2.g^{-1}$, and pores diameter 1.93 nm.

- Well-developed micropore structures with different morphologies of palm date fiber after activation processes were found by the SEM image, which is compatible with the pore size distribution curve.

- The D-R isotherm showed that the adsorption type is chemisorption.

- XRD showed activated carbon samples have an amorphous structure more than a crystalline structure, while XRF indicate that The raw fiber and the activated carbon samples consist of the common elements such as calcium (Ca), Iron (Fe), Copper (Cu).

✓ From the chemical characterization, we note the following:

- The pH_{zpc} and Boehm titration have also shown the richness in negative charges and a strong acidic character respectively of ACs.

- FTIR study of both RF's and ACF's was carried out and found the common functional groups are: C= C acetone, C-H of (CH$_3$band) alkane, C-O ether, C-O-C, aromatic C-H.

✓ The adsorption tests include (Adsorption isotherms, models, and kinetic) so we mention the most important results:

- The removal of phenol and MB from aqueous solution using ACF's prepared from date palm fiber has been investigated quite effectively.

- The maximum adsorption capacity of phenol and MB onto ACF's was observed for ACF$_3$ 11.96, and 2.82 mg.g^{-1} respectively, the difference in this value for these adsorbents and the smaller of specific surface area (166.29 m^2.g^{-1}) and higher pores diameter (2.11 nm) explains the higher adsorption capacities of phenol and MB for ACF$_3$ compared to the other ACs.

- The samples showed that the highest percentage of adsorption was at low phenol and MB concentration.

- The equilibrium adsorption data were satisfactorily fitted to Langmuir and Freundlich isotherms.

- The adsorption process is compatible with a pseudo-second-order model, while did not fit for a pseudo-first-order model.

✓ As concluded overall, ACF$_2$ is the one that has the most adsorption value in the gas phases, unlike the liquid phases, while ACF$_3$ has the largest adsorption value in the liquid phases over the gas phases. ACF$_2$ is larger in the surface area compared to ACF$_3$, unlike the pore diameter, ACF$_3$ has the largest pores in diameter compared to ACF$_2$, all these confirm that the structural properties have an effect on the selectivity of the adsorption phases.

✓ From the application part:

- We used activated carbon to prepare supercapacitors for energy storage, and the experiment was successful for both samples ACF_1 and ACF_2.

- It is also mast be noting that the best electrode is $MWNTC/ACF_1$ according to the characterization based on cyclic voltammetry, charge-discharge galvanostatic and SEM.

General Conclusion

General Conclusion

The world today focuses on two very important biggest concerns: environmental protection and energy storage, these concerns we try to analyze and find solutions for in our work, so the objective is to make activated carbon a compromise of environmental protection and energy storage.

The study focuses on the exploitation of date palm fibers (Ghars) from the oases of Ouargla - Algeria in order to prepare activated charcoal by physical activation using CO_2 as an activating agent with the change in the factors of pyrolysis temperature, pyrolysis time, and the size of the sample.

- We obtained samples of activated carbon in record time and with cheap cost, with a surface area and pore diameter ranging from 166.29 to 313.40 $m^2.g^{-1}$ and 1.89 to 2,11 nm, considered as one of the best adsorbents containing many mesopores and few micropores.
- The lower the temperature and duration of pyrolysis and the larger the sample size, the burn-off increase.
- The maximum nitrogen adsorption capacity was recorded at around 150 $cm^3.g^{-1}$. The lower the pyrolysis temperature, and the greater the duration of pyrolysis, and the larger the particle size, the quantity of adsorbed increase.
- 313.40 $m^2.g^{-1}$ was recorded as the largest specific surface area. The BET surface area increased with the decrease in the pyrolysis temperature and the increase in the duration of pyrolysis and the granularity of samples.
- SEM images of the raw materials and AC samples showed that the processes of carbonization (pyrolysis) and physical activation caused the development of porosity and a large surface area for adsorption.
- XRD showed activated carbon samples have an amorphous structure more than a crystalline structure, while XRF indicated that The raw fiber and the activated carbon samples consist of the common elements such as calcium (Ca), Iron (Fe), Copper (Cu).
- The pH_{PZC} of the activated carbon was lower than that of the solution pH, indicating that the AC surface was rich in negative charges, this means that the samples are suitable for a basic solution to remove cationic contaminants.
- The Boehm titration shown a strong acidic character of all activated carbons.

- The FTIR spectrum of both RF and ACF showed the following common functional groups: C= C acetone, C-H of (CH3band) alkane, C-O ether, C-O-C, aromatic C-H, except OH function, due to moisture in the raw materials (RF) after the washing process

The effect of mass, initial concentration, time, and temperature on the adsorption capacity of phenol and methylene blue on activated carbon ACF_1, ACF_2, ACF_3, ACF_4, and ACF_5 were studied.

- The classification of adsorption isotherms of both Phenol and MB is L4-curve according to Giles et al. which implies that the slope gradually falls with an increase in concentration, and with the gradual covering of the surface, so it becomes more difficult to find vacant sites.
- The largest removal of Phenol and MB was in the low concentrations at 20 ppm and 15 ppm respectively.
- The Langmuir and Freundlich isotherms were studied on all samples while both were well fit.
- The two models have applied: a pseudo-first-order model and a pseudo-second-order model on the adsorption of phenol and methylene blue, which corresponded to a pseudo-second-order model more.
- The thermodynamic adsorption plot and its parameters indicate that phenol adsorption mostly indicates that the adsorption was exothermic with an increase in randomness and was spontaneous in nature, while MB adsorption mostly indicates that the adsorption was exothermic with a decrease in randomness and was non-spontaneous in nature. generally, the thermodynamic adsorption data indicated that the adsorption was physical.

Date palm fiber is not only targeted as a raw material for its just cheapness but also in order to protect the environment from huge quantities without using it and investing it in the preparation of activated carbon that helps us in all fields, besides purification of water or gases on the one hand and energy storage on the other hand.

The application part was related to the investment of activated carbon prepared for the preparation of supercapacitors to find a solution for energy storage.

The supercapacitors for energy storage were prepared using the prepared activated carbon and was successful. The results indicated that the activated carbon is suitable

for preparing good supercapacitors with the greatest specific capacity of 91.64 $F.g^{-1}$ and the largest charging and discharging time of 100 s, while the lower CS was of 29.05 $F.g^{-1}$, and the maximum specific energy and specific power were produced with values of 45.82 $Wh.kg^{-1}$ and 1800 $W.kg^{-1}$, respectively.

By the end of this humble work, I suggest as perspectives the following points:

1. The Exploitation of the experimental results in order to develop a semi-pilot unit based essentially on modeling and optimization.
2. Enlarging the fields of application especially in agriculture and electronics by using electrodes as a specific sensor material for the detection of certain potential pollutants and as capacitors for energy storage (Batteries for example).

Nowadays, the use of renewable energy sources seems to be an unavoidable global trend. Given the large volume of biomass in arid and semi-arid areas, concerted efforts must be made to better exploit this abundant economic potential.

Bibliographies

Abdallah, M. (2018). Adsorption du bleu de méthylène par charbon actif. university of Eloued

Afshina, S., Rashtbaria, Y., Shirmardic, M., Vosoughib, M., & Hamzehzadeha, A. (2019). Adsorption of Basic Violet 16 dye from aqueous solution onto mucilaginous seeds of Salvia sclarea: kinetics and isotherms studies. Desalination and water treatment, 161, 365-375. doi:https://doi.org/10.5004/dwt.2019.24265

Ahmed, M. J. (2016). Preparation of activated carbons from date (Phoenix dactylifera L.) palm stones and application for wastewater treatments: Review. Process Safety and Environmental Protection, 102, 168-182. doi:https://doi.org/10.1016/j.psep.2016.03.010

Al-Haidary, A. M. A., Zanganah, F. H. H., Al-Azawi, S. R. F., Khalili, F. I., & Al-Dujaili, A. H. (2011). A study on using date palm fibers and leaf base of palm as adsorbents for Pb (II) ions from its aqueous solution. Water, Air, & Soil Pollution, 214(1-4), 73-82. doi:https://doi.org/10.1007/s11270-010-0405-1

Al-Kaabi, K., Al-Khanbashi, A., & Hammami, A. (2004). Natural fiber reinforced composites from date palm fibres.

Al-Oqla, F. M., & Sapuan, S. M. (2014). Natural fiber reinforced polymer composites in industrial applications: feasibility of date palm fibers for sustainable automotive industry. Journal of Cleaner Production, 66, 347-354.

Al-Swaidan, H. M., & Ahmad, A. (2011, 2011). Synthesis and characterization of activated carbon from Saudi Arabian dates tree's fronds wastes.

Alhijazi, M., Zeeshan, Q., Safaei, B., Asmael, M., & Qin, Z. (2020). Recent developments in palm fibers composites: a review. Journal of Polymers and the Environment, 1-26. doi:https://doi.org/10.1007/s10924-020-01842-4

Alwared, A. I., Al-Hubboubi, S. K. A., & Dawood, D. S. (2016). Effect of Date Palm Leaf Fiber on Mechanical Properties of Concrete. Association of Arab Universities Journal of Engineering Sciences, 23(2), 49-66.

Anbarasan, V., Dhadhala, S., Kalicharan, A. A., & Arivalagan, K. (2021). Equilibrium Modelling, Thermodynamic and Kinetic Studies on the Bio Sorption of Malachite Green Dye By a Low Cost Effective Adenanthera Pavonina Leaves Activated Carbon. Sch Int J Chem Mater Sci, 4(7), 196-203.

Atheba, G. P. (2009). Traitement des eaux par action combinée de la photocatalyse solaire et de l'adsorption sur charbon actif: conception et réalisation du procédé. Université Paul Verlaine, Metz,

Bamba, D., Dongui, B., Trokourey, A., Zoro, G. E., Athéba, G. P., Robert, D., & Wéber, J. V. (2009). Etudes comparées des méthodes de préparation du charbon actif, suivies d'un test de dépollution d'une eau contaminée au diuron. J. Soc. Ouest-Afr. Chim, 028, 41 - 52.

Bansal, R. C., & Goyal, M. (2005). Activated carbon adsorption: Taylor Francis

Bibliographies

Bechki, M. K., & Lounas, A. (2019). Préparation et caracterisation du charbon actif à partir des noyaux du palmier dattier et des coquilles des noix. Université Kasdi Merbah – Ouargla,

Belaid, O. (2017). L'utilisation de charbon actif préparé à partir des noyaux dattes locales dans l'epuration des eaux usées urbaines. Influence de la variété des dattes. Université Kasdi Merbah – Ouargla,

Belaid, O., Bebba, A. A., Sekirifa, M. L., Baameur, L., & Al-Dujaili, A. H. (2017). Preparation and characterization of chemically activated carbons from different varieties of date stones. Desalin. Water Treat, 65, 267-273. doi:https://doi.org/10.5004/dwt.2017.20285

Belhachemi, F. (2001). Modélisation et caractérisation des supercondensateurs à couche double électrique utilisés en électronique de puissance.

Benstoem, F., Becker, G., Firk, J., Kaless, M., Wuest, D., Pinnekamp, J., & Kruse, A. (2018). Elimination of micropollutants by activated carbon produced from fibers taken from wastewater screenings using hydrothermal carbonization. Journal of environmental management, 211, 278-286. doi:https://doi.org/10.1016/j.jenvman.2018.01.065

Bernal, V., Giraldo, L., & Moreno-Piraján, J. C. (2018). Physicochemical properties of activated carbon: their effect on the adsorption of pharmaceutical compounds and adsorbate–adsorbent interactions. C—Journal of Carbon Research, 4(4), 62.

Bhoyate, S., Ranaweera, C. K., Zhang, C., Morey, T., Hyatt, M., Kahol, P. K., . . . Gupta, R. K. (2017). Eco-friendly and high performance supercapacitors for elevated temperature applications using recycled tea leaves. Global Challenges, 1(8), 1700063.

Binette, M.-J. (2000). Nouveaux matériaux nanocomposites dérivés des polysilicates lamellaires: University of Ottawa (Canada).

Boehm, H. P. (1966). Chemical Identification of Surface Groups. In D. D. Eley, H. Pines, & P. B. Weisz (Eds.), Advances in Catalysis (Vol. 16, pp. 179-274): Academic Press.

Boudrahem, F., Yahiaoui, I., Saidi, S., Yahiaoui, K., Kaabache, L., Zennache, M., & Aissani-Benissad, F. (2019). Adsorption of pharmaceutical residues on adsorbents prepared from olive stones using mixture design of experiments model. Water Science & Technology, 1-12. doi:https://doi.org/10.2166/wst.2019.346

Bouguedoura, N., Bennaceur, M., Babahani, S., & Benziouche, S. E. (2015). Date palm status and perspective in Algeria. In Date palm genetic resources and utilization (Vol. 1, pp. 125-168): Springer.

Boulkrah, H. (2008). Etude comparative de l'adsorption des ions plomb sur différents adsorbants. Université du 20 août 1955 Skikda,

Boumediri, H., Bezazi, A., Del Pino, G. G., Haddad, A., Scarpa, F., & Dufresne, A. (2019). Extraction and characterization of vascular bundle and fiber strand from date palm rachis as potential bio-reinforcement in composite. Carbohydrate polymers, 222, 114997. doi:https://doi.org/10.1016/j.carbpol.2019.114997

Bibliographies

Boutadara, K., Ben Ali, L., & Kalloum, S. (2017). Valorisation des déchets ligno-cellulosiques, issus du palmier dattier, en charbon actif. (master). Université Ahmed Draia-ADRAR,

Bragg, W. H., & Bragg, W. L. (1913). The reflection of X-rays by crystals. Proceedings of the Royal Society of London. Series A, Containing Papers of a Mathematical and Physical Character, 88(605), 428-438.

Brunauer, S., Emmett, P. H., & Teller, E. (1938). Adsorption of gases in multimolecular layers. Journal of the American chemical society, 60(2), 309-319. doi:https://doi.org/10.1021/ja01269a023

Byrne, C. E., & Nagle, D. C. (1997). Carbonized wood monoliths—Characterization. Carbon, 35(2), 267-273. doi:https://doi.org/10.1016/S0008-6223(96)00135-2

Chandola, D., Thathola, P., & Bisht, A. (2021). Removal of phenol from aqueous solution using biochar produced from Araucaria Columnaris Bark.

Chien, S. H., & Clayton, W. R. (1980). Application of Elovich equation to the kinetics of phosphate release and sorption in soils. Soil Science Society of America Journal, 44(2), 265-268.

Coates, J. (2006). Interpretation of infrared spectra, a practical approach. Encyclopedia of analytical chemistry: applications, theory and instrumentation. doi:https://doi.org/10.1002/9780470027318.a5606

Crini, G., Lichtfouse, E., Wilson, L. D., & Morin-Crini, N. (2018). Adsorption-oriented processes using conventional and non-conventional adsorbents for wastewater treatment. Green adsorbents for pollutant removal, 18, 23-71. doi:https://doi.org/10.1007/978-3-319-92111-2_2

Daifullah, A. A. M., Yakout, S. M., & Elreefy, S. A. (2007). Adsorption of fluoride in aqueous solutions using KMnO4-modified activated carbon derived from steam pyrolysis of rice straw. Journal of hazardous materials, 147(1-2), 633-643.

Daoud, M., & Benturki, O. (2014). Activation d'un charbon à base de noyaux de jujubes et application à l'environnement. Adsorption d'un colorant de textile. Revue des Energies Renouvelables SIENR Ghardaïa, 14, 155-162.

Dehghani-Sanij, A. R., Tharumalingam, E., Dusseault, M. B., & Fraser, R. (2019). Study of energy storage systems and environmental challenges of batteries. Renewable and Sustainable Energy Reviews, 104, 192-208.

Depci, T., Kul, A. R., & Önal, Y. (2012). Competitive adsorption of lead and zinc from aqueous solution on activated carbon prepared from Van apple pulp: Study in single-and multi-solute systems. Chemical Engineering Journal, 200, 224-236.

Dinh, T. T. M. (2014). Développement de filières technologiques pour la réalisation de micro-supercondensateurs intégrés sur silicium.

Dixit, S., & Yadav, V. L. (2019). Synthesis of green thermally resistant composite: A review. Indian Journal of Chemical Technology (IJCT), 26(6), 494-503.

Djidel, T. (2011). Etude de la préparation d'un charbon actif a partir des grain d'olives et application sur des rejets industriels. Université des Sciences et de la Technologie Med-Boudif d'Oran,

Dubinin, N. P. (1947). Work of Soviet biologists: theoretical genetics. Science, 105(2718), 109-112. doi:https://doi.org/10.1126/science.105.2718.109

Bibliographies

Elena-Fernandez, I. (2002). Etude de la carbonisation et l'activation de précurseurs végétaux durs et mous. (3).

Elseify, L. A., Midani, M., Shihata, L. A., & El-Mously, H. (2019). Review on cellulosic fibers extracted from date palms (Phoenix Dactylifera L.) and their applications. Cellulose, 26(4), 2209-2232.

Faouzia, B. (2014). Elimination des colorants cationiques par des charbons actifs synthétisés à partir des résidus de l'agriculture, mémoire de magister. Université Ferhat Abbas Setif-1, Algérie,

Foo, K. Y., & Hameed, B. H. (2010). An overview of dye removal via activated carbon adsorption process. Desalination and water treatment, 19(1-3), 255-274. doi:https://doi.org/10.5004/dwt.2010.1214

Galiwango, E., Rahman, N. S. A., Al-Marzouqi, A. H., Abu-Omar, M. M., & Khaleel, A. A. (2019). Isolation and characterization of cellulose and α-cellulose from date palm biomass waste. Heliyon, 5(12), e02937. doi:DOI:https://doi.org/10.1016/j.heliyon.2019.e02937

Giles, C. H., Smith, D., & Huitson, A. (1974). A general treatment and classification of the solute adsorption isotherm. I. Theoretical. Journal of Colloid and Interface Science, 47(3), 755-765. doi:https://doi.org/10.1016/0021-9797(74)90252-5

González-García, P. (2018). Activated carbon from lignocellulosics precursors: A review of the synthesis methods, characterization techniques and applications. Renewable and Sustainable Energy Reviews, 82, 1393-1414. doi:https://doi.org/10.1016/j.rser.2017.04.117

Herschel, W. (1800). Experiments on the refrangibility of the invisible rays of the sun. Philosophical Transactions of the Royal Society of London(90), 284-292.

Holmes, R. J. (1991). Chemical modification of activated carbon adsorbents.

Ioannou, Z., & Simitzis, J. (2009). Adsorption kinetics of phenol and 3-nitrophenol from aqueous solutions on conventional and novel carbons. Journal of hazardous materials, 171(1-3), 954-964.

Jeirani, Z., Niu, C. H., & Soltan, J. (2017). Adsorption of emerging pollutants on activated carbon. Reviews in Chemical Engineering, 33(5), 491-522.

Keiluweit, M., Nico, P. S., Johnson, M. G., & Kleber, M. (2010). Dynamic molecular structure of plant biomass-derived black carbon (biochar). Environmental science & technology, 44(4), 1247-1253. doi:https://doi.org/10.1021/es9031419

Kim, Y. S., Yang, S. J., Lim, H. J., Kim, T., & Park, C. R. (2012). A simple method for determining the neutralization point in Boehm titration regardless of the CO2 effect. Carbon, 50(9), 3315-3323.

Koller, E. (2001). Génie chimique: Dunod.

Langmuir, I. (1918). The adsorption of gases on plane surfaces of glass, mica and platinum. Journal of the American chemical society, 40(9), 1361-1403.

Largeot, C. (2009). Développement de supercondensateurs carbone/carbone: relation entre la taille des ions de l'électrolyte et la taille des pores de la matière active. Université de Toulouse, Université Toulouse III-Paul Sabatier,

Bibliographies

Leinekugel-le-Cocq, D. (2004). Contribution à la modélisation dynamique simplifiée d'un procédé d'adsorption modulée en pression (PSA). Université Claude Bernard-Lyon 1,

Liu, K., Zakharova, N., Adeyilola, A., & Zeng, L. (2021). Experimental Study on the Pore Shape Damage of Shale Samples during the Crushing Process. Energy & Fuels, 35(3), 2183-2191.

Marken, F., Neudeck, A., & Bond, A. M. (2010). Cyclic voltammetry. In Electroanalytical methods (pp. 57-106): Springer.

Marsh, H., & Reinoso, F. R. (2006). Activated carbon: Elsevier.

Mashhadi, S., Javadian, H., Ghasemi, M., Saleh, T. A., & Gupta, V. K. (2016). Microwave-induced H2SO4 activation of activated carbon derived from rice agricultural wastes for sorption of methylene blue from aqueous solution. Desalination and water treatment, 57(44), 21091-21104.

Menéndez-Díaza, J. A., & Martín-Gullón, I. (2006). Types of carbon adsorbents and their production. Interface science and technology, 7, 1-47.

Mimouni, Y., Siboukeur, O., & Bayoussef, Z. (2014). Fructose-rich syrup from Ghars cultivar dates (Phoenix dactylifera L.). Emirates Journal of Food and Agriculture, 963-969.

Misnon, I. I., Zain, N. K. M., & Jose, R. (2019). Conversion of oil palm kernel shell biomass to activated carbon for supercapacitor electrode application. Waste and Biomass Valorization, 10(6), 1731-1740.

Misnon, I. I., Zain, N. K. M., Lei, T. S., Vijayan, B. L., & Jose, R. (2020). Activated carbon with graphitic content from stinky bean seedpod biowaste as supercapacitive electrode material. Ionics, 26(8), 4081-4093.

Mohammed, A. K., Abdulhassan, A. A., & Al-Meshhdany, W. Y. (2017). Biosorption of Chromium ions from Aqueous Solutions by using Date Palm Fibers. Iraqi Journal of Biotechnology, 16(4), 8-14. doi:https://doi.org/10.4172/2157-7064.1000194

Nzihou, A. (2020). Handbook on characterization of biomass, biowaste and related by-products: Springer Nature.

Ooi, C. H., Cheah, W. K., Sim, Y. L., Pung, S. Y., & Yeoh, F. Y. (2017). Conversion and characterization of activated carbon fiber derived from palm empty fruit bunch waste and its kinetic study on urea adsorption. J Environ Manage, 197, 199-205. doi:https://doi.org/10.1016/j.jenvman.2017.03.083

Owaid, M. N., Al-Saeedi, S. S., & Al-Assaffii, I. A. A. (2014). Impact palm date fibers (fibrillum) and sawdust extract on mycelial growth rate of four species of Pleurotus. Tikrit Journal for Agricultural Sciences, 14, 1-7.

Park, S., Baker, J. O., Himmel, M. E., Parilla, P. A., & Johnson, D. K. (2010). Cellulose crystallinity index: measurement techniques and their impact on interpreting cellulase performance. Biotechnology for biofuels, 3(1), 1-10.

Poudres, S. e. T. d. (2018). Le phénomène d'adsorption physique   Retrieved from https://nte.mines-albi.fr/STP/co/uc_AdsorptionPhysique.html

Prahas, D., Kartika, Y., Indraswati, N., & Ismadji, S. (2008). Activated carbon from jackfruit peel waste by H3PO4 chemical activation: Pore structure and surface

chemistry characterization. Chemical Engineering Journal, 140(1-3), 32-42. doi:https://doi.org/10.1016/j.cej.2007.08.032

Rahman, M. W., Ali, M. Y., Saha, I., Al Raihan, M., Moniruzzaman, M., Alam, M. J., . . . Khan, M. M. R. (2017). Date palm fiber as a potential low-cost adsorbent to uptake chromium (VI) from industrial wastewater. Desalination and Water Treatment, 88, 169-178. doi:10.5004/dwt.2017.21402

Rappoport, Z. (2004). The chemistry of phenols: John Wiley & Sons.

Reddy, K. S. K., Al Shoaibi, A., & Srinivasakannan, C. (2012). A comparison of microstructure and adsorption characteristics of activated carbons by CO2 and H3PO4 activation from date palm pits. New Carbon Materials, 27(5), 344-351. doi:https://doi.org/10.1016/S1872-5805(12)60020-1

Reffas, A., Bernardet, V., David, B., Reinert, L., Lehocine, M. B., Dubois, M., . . . Duclaux, L. (2010). Carbons prepared from coffee grounds by H3PO4 activation: Characterization and adsorption of methylene blue and Nylosan Red N-2RBL. Journal of hazardous materials, 175(1-3), 779-788.

Riahi, K., Thayer, B. B., Mammou, A. B., Ammar, A. B., & Jaafoura, M. H. (2009). Biosorption characteristics of phosphates from aqueous solution onto Phoenix dactylifera L. date palm fibers. Journal of hazardous materials, 170(2-3), 511-519. doi:https://doi.org/10.1016/j.jhazmat.2009.05.004

Rim Baccar Ep Yangui, Montserrat Sarrà Adroguer, Paqui Blánquez Cano, & Bouzid., J. (2014). Removal of water pollutants by adsorption on activated carbon prepared from olive-waste cakes and by biological treatment using ligninolytic fungi. Universitat Autònoma de Barcelona,

Rouquerol, F., Rouquerol, J., & Sing, K. (1999). Adsorption by powders and porous solids: principles, methodology and applications. London: Academic press.

SAS, R. A. (2005). VoltaLab Electrochemical Research Equipment. 1-36.

Schirmer, R. H., Adler, H., Pickhardt, M., & Mandelkow, E. (2011). Lest we forget you—methylene blue…. Neurobiology of aging, 32(12), 2325-e2327.

Segal, L., Creely, J., Jr., Martin Jr, A. E., & Conrad, C. M. (1959). An empirical method for estimating the degree of crystallinity of native cellulose using the X-ray diffractometer. Textile research journal, 29(10), 786-794.

Sekirifa, M. L. (2013). Étude des propriétés adsorbantes des charbons activés issus des noyaux de dattes. Application au traitement d‴ effluent aqueux. Thèse de doctorat, Université de Mokhtar, Annaba,

Sekirifa, M. L., & Hadj-Mahammed, M. (2005). Etude comparative de la capacité adsorbante d'un charbon actif issu de noyaux de dattes et un charbon actif commercial. Sciences & Technologie. B, Sciences de l'ingénieur, 55-59.

Sekirifa, M. L., Hadj-Mahammed, M., Pallier, S., Baameur, L., Richard, D., & Al-Dujaili, A. H. (2013). Preparation and characterization of an activated carbon from a date stones variety by physical activation with carbon dioxide. Journal of Analytical and Applied Pyrolysis, 99, 155-160. doi:https://doi.org/10.1016/j.jaap.2012.10.007

Sekirifa, M. L., Pallier, S., Hadj-Mahammed, M., Richard, D., Baameur, L., & Al-Dujaili, A. H. (2013). Measurement of the Performance of an Agricultural

Residue-based Activated Carbon Aiming at the Removal of 4-chlophenol from Aqueous Solutions. Energy Procedia, 36, 94-103. doi:https://doi.org/10.1016/j.egypro.2013.07.012

Shaarani, F. W., & Hameed, B. H. (2010). Batch adsorption of 2, 4-dichlorophenol onto activated carbon derived from agricultural waste. Desalination, 255(1-3), 159-164.

Shackley, M. S. (2010). X-ray fluorescence spectrometry (XRF) in geoarchaeology: Springer.

Shehu, Z., Danbature, W. L., Magaji, B., Yakubu, Y. S., & Balarak, D. (2021). Adsorption of Phenol from Wastewater using Copper Oxide Supported on Activated Carbon Obtained from Coal: Thermodynamics and Kinetics Studies. Chemical Science & Engineering Research.

Silva, M. C., Spessato, L., Silva, T. L., Lopes, G. K. P., Zanella, H. G., Yokoyama, J. T. C., . . . Almeida, V. C. (2021). H3PO4–activated carbon fibers of high surface area from banana tree pseudo-stem fibers: Adsorption studies of methylene blue dye in batch and fixed bed systems. Journal of Molecular Liquids, 324, 114771.

Sing, K. S. W. (1985). Reporting physisorption data for gas/solid systems with special reference to the determination of surface area and porosity (Recommendations 1984). Pure and applied chemistry, 57(4), 603-619. doi:https://doi.org/10.1351/pac198557040603

SING, K. S. W., EVERETT, D. H., HAUL, R. A. W., MOSCOU, L., PIEROTTI, R. A., ROUQUEROL, J., & SIEMIENIEWSKA, T. (1985). REPORTING PHYSISORPTION DATA FOR GAS/SOLID SYSTEMS with Special Reference to the Determination of Surface Area and Porosity. Pure and Applied Chemistry (IUPAC), 57, 603-619.

Soubeyrand, E. (2012). Adsorption et séparation de gaz en mode dynamique sur des matériaux hybrides. (PHD). Aix-Marseille,

Sun, L.-M., Meunier, F., & Baron, G. (2005). Adsorption: Procédés et applications. Techniques de l'ingénieur. Technologies de l'eau, 2(J2731).

Suryanarayana, C., & Norton, M. G. (1998). X-ray diffraction: a practical approach: Springer Science & Business Media.

Tan, I. A. W., Ahmad, A. L., & Hameed, B. H. (2009). Adsorption isotherms, kinetics, thermodynamics and desorption studies of 2, 4, 6-trichlorophenol on oil palm empty fruit bunch-based activated carbon. Journal of hazardous materials, 164(2-3), 473-482.

Trifi, I. M. (2012). Étude de l'élimination du chrome VI par adsorption sur l'alumine activée par dialyse ionique croisée. (Thèse de Doctorat).

UNESCO. (2020). World: World Water Development Report 2020 - Water and Climate Change.

Vargas, A. M. M., Cazetta, A. L., Garcia, C. A., Moraes, J. C. G., Nogami, E. M., Lenzi, E., . . . Almeida, V. C. (2011). Preparation and characterization of activated carbon from a new raw lignocellulosic material: Flamboyant (Delonix regia) pods. Journal of environmental management, 92(1), 178-184. doi:https://doi.org/10.1016/j.jenvman.2010.09.013

Villacanas, F., Pereira, M. F., Orfao, J. J., & Figueiredo, J. L. (2006). Adsorption of simple aromatic compounds on activated carbons. J Colloid Interface Sci, 293(1), 128-136. doi:10.1016/j.jcis.2005.06.032

Yang, H., Yan, R., Chen, H., Lee, D. H., & Zheng, C. (2007). Characteristics of hemicellulose, cellulose and lignin pyrolysis. Fuel, 86(12-13), 1781-1788. doi:https://doi.org/10.1016/j.fuel.2006.12.013

Zaini, M. A. A., Ngiik, T. C., Kamaruddin, M. J., Setapar, S. H. M., & Yunus, M. A. C. (2014). Zinc chloride-activated waste carbon powder for decolourization of methylene blue. Jurnal Teknologi, 67(2).